NACA RM A50C30

NACA

RESEARCH MEMORANDUM

WIND-TUNNEL TESTS OF A 0.16-SCALE MODEL OF THE X-3 AIRPLANE AT HIGH SUBSONIC SPEEDS.- ADDITIONAL STABILITY AND CONTROL CHARACTERISTICS AND THE AERODYNAMIC EFFECTS OF EXTERNAL STORES AND RAM JETS

By Joseph W. Cleary and Jack A. Mellenthin

Ames Aeronautical Laboratory
Moffett Field, Calif.

NATIONAL ADVISORY COMMITTEE
FOR AERONAUTICS

WASHINGTON

June 13, 1950
Declassified April 15, 1958

NATIONAL ADVISORY COMMITTEE FOR AERONAUTICS

RESEARCH MEMORANDUM

WIND-TUNNEL TESTS OF A 0.16-SCALE MODEL OF THE X-3 AIRPLANE AT HIGH SUBSONIC SPEEDS.- ADDITIONAL STABILITY AND CONTROL CHARACTERISTICS AND THE AERODYNAMIC EFFECTS OF EXTERNAL STORES AND RAM JETS

By Joseph W. Cleary and Jack A. Mellenthin

SUMMARY

Additional wind-tunnel tests of the 0.16-scale model of the X-3 airplane have been made at low and high subsonic Mach numbers to investigate the lateral- and longitudinal-stability and -control characteristics. The X-3 is a research airplane incorporating a low-aspect-ratio wing and tail with sharp leading and trailing edges and is designed for supersonic speeds.

The results of the tests show a stable variation of all-moving-tail incidence with Mach number for Mach numbers less than about 0.85. Deflecting the wing leading-edge flaps, in general, reduced the Mach number range for this stick-fixed static stability and increased the negative tail incidence required to trim the airplane in level flight.

For Mach numbers less than about 0.85, deflecting the leading-edge flaps increased the maximum lift-drag ratio and reduced the drag at lift coefficients greater than about 0.2.

Tests of the model equipped with airbrakes indicated generally satisfactory longitudinal-stability characteristics with a single or double brake mounted forward of the wing at fuselage station 41.00 inches.

Adding fuel tanks or ram jets to the wing tips or adding fuel tanks beneath the wing appeared to be aerodynamically feasible inasmuch as the lateral- or longitudinal-stability and -control characteristics were not excessively affected. Although the wing-tip tanks reduced the lift coefficient for balance, they increased the lift-curve slope and the static-longitudinal stability. The underwing tanks reduced the longitudinal stability in the region of 0.2 lift coefficient. Both tank installations increased the drag coefficient at zero lift about 0.003 at the lower Mach numbers, but the tip tanks produced less drag than the

underwing tanks at lift coefficients above about 0.2 and Mach numbers less than 0.85. The principal effect of the wing-tip ram jets was to increase the lift-curve slope and to reduce the lift coefficient for balance.

The normal force imposed on the wing tips by the tip tanks or by the ram jets increased approximately linearly with angle of attack up to the wing stall.

At an angle of attack of 6° and a Mach number of 0.925, the aileron retained approximately 80 percent of its low-speed effectiveness.

INTRODUCTION

Preliminary wind-tunnel tests of the 0.16-scale model of the X-3 airplane (reference 1) indicated that the stabilizing fins of the jettisonable nose had an unfavorable effect on the longitudinal-stability characteristics. For this reason, the nose fins were eliminated and plans for a jettisonable nose as a means of pilot escape were abandoned.

The high-speed wind-tunnel tests were later resumed on this basis to furnish additional basic force and moment data on the model. The additional investigation included a determination of the effects of simulated air scoops, airbrakes, external stores, and wing-tip ram jets on the longitudinal and lateral characteristics of the model. Measurements were made of the normal force and the pitching moment transmitted to the model wing tip by a fuel tank and a typical ram jet. The results are presented in this report with a limited analysis of the stability and control characteristics.

The tests were requested by the U. S. Air Force and were made in the Ames 16-foot high-speed wind tunnel.

COEFFICIENTS AND SYMBOLS

Pitching moments, yawing moments, and rolling moments were computed with respect to mutually perpendicular axes that passed through the center of gravity. One axis coincided with the fuselage reference line while another was parallel to the wing 75-percent-chord line and normal to the plane of symmetry. The center of gravity was assumed to lie on the fuselage reference line and above the 15-percent point of the wing mean aerodynamic chord. This is the system of reference axes used in reference 1.

The horizontal-tail hinge moments were computed with respect to a lateral axis passing through the 25-percent point of the mean aerodynamic

chord of the exposed tail. Tip-tank and ram-jet pitching moments were computed with respect to a lateral axis passing through the 15-percent point of the wing mean aerodynamic chord.

The coefficients and symbols used in this report are defined as follows:

C_C cross-wind-force coefficient $\left(\frac{\text{cross-wind force}}{qS}\right)$

C_D drag coefficient $\left(\frac{\text{drag}}{qS}\right)$

C_L lift coefficient $\left(\frac{\text{lift}}{qS}\right)$

C_{N_R} ram-jet normal-force coefficient $\left(\frac{\text{ram-jet normal force}}{qS_R}\right)$

C_{N_T} tip-tank normal-force coefficient $\left(\frac{\text{tip-tank normal force}}{qS_T}\right)$

C_{h_t} horizontal-tail hinge-moment coefficient $\left(\frac{\text{horizontal-tail hinge moment}}{qS_t\bar{c}_t}\right)$

C_l rolling-moment coefficient $\left(\frac{\text{rolling moment}}{qSb}\right)$

C_m pitching-moment coefficient $\left(\frac{\text{pitching moment}}{qS\bar{c}}\right)$

C_{m_R} ram-jet pitching-moment coefficient $\left(\frac{\text{ram-jet pitching moment}}{qS_R l_R}\right)$

C_{m_T} tip-tank pitching-moment coefficient $\left(\frac{\text{tip-tank pitching moment}}{qS_R l_T}\right)$

C_n yawing-moment coefficient $\left(\frac{\text{yawing moment}}{qSb}\right)$

M free-stream Mach number

S wing area, square feet

S_R ram-jet frontal area, square feet

S_T tip-tank frontal area, square feet

S_t exposed horizontal-tail area, square feet

V free-stream velocity, feet per second

b wing span, feet

b_t horizontal-tail span, feet

c wing chord, feet

$\bar{c}$ mean aerodynamic chord of the wing $\left(\frac{\int_0^{0.5b} c^2\,dy}{\int_0^{0.5b} c\,dy}\right)$, feet

c_t tail chord, feet

$\bar{c}_t$ mean aerodynamic chord of the exposed horizontal tail $\left(\frac{\int_{0.045b_t}^{0.5b_t} c_t^2\,dy}{\int_{0.045b_t}^{0.5b_t} c_t\,dy}\right)$, feet

i_t horizontal-tail incidence with respect to the fuselage reference line, positive with the trailing edge downward, degrees

l_R ram-jet length, feet

l_T tip-tank length, feet

n load factor $\left(\frac{\text{lift}}{\text{weight}}\right)$

q free-stream dynamic pressure $\left(\frac{1}{2}\rho V^2\right)$, pounds per square foot

y lateral distance from the model plane of symmetry, feet

α angle of attack of the fuselage reference line with respect to the wind axis, degrees

δ_a aileron deflection, positive downward, degrees

δ_{ab} airbrake deflection, positive downward, degrees

δ_{lf} leading-edge-flap deflection, positive downward, degrees

δ_r rudder deflection, positive to the left, degrees

δ_{tf} trailing-edge-flap deflection, positive downward, degrees

ρ mass density of the free stream, slugs per cubic foot

ψ angle of yaw of the fuselage reference line with respect to the wing axis, degrees

MODEL AND APPARATUS

The X-3 airplane model shown in figures 1(a) and 2 was the model used during the tests described in reference 1. The model scale was 0.16 and the model wing had an aspect ratio of 3.01 and a taper ratio of 0.4 with the 75-percent-chord line perpendicular to the plane of symmetry. The wing had a symmetrical hexagonal section 4.5 percent thick with rounded corners at 30 and 70 percent of the chord and sharp leading and trailing edges. Figure 2 shows a typical section through the wing. The horizontal tail was all-movable and had sharp leading and trailing edges with the 50-percent-chord line swept back 23°.

Plain full-span leading-edge flaps of constant chord (13.45 percent of the mean aerodynamic chord measured parallel to the model plane of symmetry) were used on the wing. Partial-span, split, trailing-edge flaps with a chord equal to 25 percent of the wing chord extended from the wing-fuselage juncture to the aileron. Thus, the length of each flap was 46.6 percent of the wing semispan.

A plain aileron with a chord equal to 25 percent of the wing chord was used on the left wing only; it extended in from the wing tip for 30 percent of the wing semispan. Additional information on the model is given in table I and in reference 1. The complete model configuration was identical with that of reference 1 except that the nose fins were omitted. Thus the complete model consisted of the following components: the fuselage, the tail boom, the canopy, the wing and empennage, and the external brackets for the wing control surfaces.

Figure 1(b) shows a typical airbrake installation. The plan forms of the various airbrakes and the fuselage stations at which they were mounted are shown in figure 3. The profile of the double brake was flat, but that of the single brakes conformed to the lower surface of the fuselage.

The model in the landing configuration with the elongated single brake is shown in figure 1(c). The landing-gear doors shown on the model were those developed from low-speed wind-tunnel tests in one of the Ames 7- by 10-foot wind tunnels and are not those used in the tests reported in reference 1.

The model equipped with wing-tip fuel tanks is shown in figure 1(e) and a detailed sketch of the tanks is presented in figure 4(a). The tanks were made with an NACA 111 fuselage form and a fineness ratio of 8.33. Normal force and pitching moment of the left tank that were imposed on the wing tip were measured with resistance-type electric strain gages mounted on a cantilever beam. (See fig. 4(a).) The model underwing tanks, shown in figures 1(d) and 4(b), were identical to the tip tanks except that no provision was made for measuring normal force or pitching moment.

The model wing-tip ram jets shown in figures 1(f) and 5 employed the same principle for measuring the normal force and pitching moment imposed on the wing tip as that used for the wing-tip fuel tank. The ram jets were symmetrical bodies of revolution with a fineness ratio of 8.22. Air flowed through the ram jets, but no attempt was made to measure the rate of flow.

The tests were made in the Ames 16-foot high-speed wind tunnel. The model was mounted on the sting support with the strain-gage balance enclosed within the model. For these tests, the angle of attack was measured by an inclinometer mounted in the model.

TESTS

The basic-pitch data of reference 1 (model without the nose fins) have been extended to obtain force and moment data for various combinations of leading-edge flap and horizontal-tail incidences. The model was tested with and without dummy air scoops (no air flow into the scoops) to see if the power-off flight configuration had satisfactory stability characteristics. Tests were made of airbrakes to find a design and a location that would satisfy the space limitations of the fuselage and have suitable aerodynamic characteristics.

Wing-tip ram jets and external stores were tested with the model pitched and yawed to investigate the static-stability and -control characteristics and to measure the normal force and pitching moment imposed on the wing tips of the model by these items. The aileron effectiveness was measured for the model with and without tip tanks or ram jets.

The tests were made at Mach numbers of 0.40 to 0.925 corresponding to a Reynolds number range of about 3.2×10^6 to 4.9×10^6 under the test conditions. An index to the figures giving the pertinent control-surface settings and the model configurations is presented in table II.

PRECISION AND CORRECTIONS

The estimated precision of the data is given in reference 1. Because of refinements in instrumentation, the angles of attack and of yaw presented in this report are believed to be accurate within $\pm 0.1^{\circ}$.

Corrections for the effect of the tunnel walls and of the interference of the sting support have been applied to the data as described in reference 1. Constriction corrections to account for the blocking effect of the model in the tunnel test section were applied according to the method of reference 2.

Pressures were measured at five points on the flat base of the fuselage (the area occupied by the tail-pipe outlets of the airplane) and the drag data were corrected to correspond to free-stream static pressure over this area.

Yawing-moment, rolling-moment, and side-force coefficients produced by yawing the model represent increments over the values obtained at 0° yaw.

RESULTS AND DISCUSSION

Aerodynamic Characteristics in Pitch

Basic aerodynamic characteristics.- The lift, pitching-moment, and tail hinge-moment characteristics of the model are presented in figure 6 for three leading-edge-flap deflections and three horizontal-tail incidences. Also included are the lift and pitching-moment characteristics with the tail off. The drag characteristics of the model with the tail on are shown in figure 7 and with the tail off in figure 8. These data are an extension and partial repetition of the data presented in reference 1.

A discussion of the lift, static-longitudinal-stability and -control, and drag characteristics of the model was presented in reference 1 and is generally applicable to the results of this test. Hence these items will not be discussed in detail except to show the over-all effects of Mach number.

The variations of lift, pitching-moment, and drag coefficient with Mach number are shown in figure 9. For angles of attack less than about 10°, there was a general increase of lift coefficient with increasing Mach number for Mach numbers between 0.40 and 0.925. At lift coefficients above 0.2, the pitching-moment coefficient decreased markedly (nosing-down tendency) for all test Mach numbers above about 0.86.

A slight increase in drag is shown in figure 9 for a Mach number of 0.925. However, the Mach number for drag divergence, as indicated by a marked increase in drag, was apparently not reached at any Mach number up to 0.925.

The lift-curve slope $(\partial C_L/\partial \alpha)_M$, static longitudinal stability $(-\partial C_m/\partial C_L)_M$, and tail effectiveness $(\partial C_m/\partial i_t)_M$ are presented in figure 10 for leading-edge-flap angles of 0°, 10°, and 20° and a lift coefficient of 0.3. Except for a slight decrease at a Mach number of about 0.90 with the flaps deflected, the lift-curve slope increased with Mach number throughout the Mach number range of the test. For a lift coefficient of 0.3, deflecting the leading-edge flaps increased the longitudinal stability at practically all Mach numbers of the test. However, at the higher lift coefficients, deflecting the leading-edge flaps 20° reduced the stability to such an extent that the model became unstable at a lift coefficient of about 0.8 at 0.40 Mach number. (See fig. 6.) The longitudinal stability increased markedly at a Mach number of about 0.925 (fig. 10) with the flaps deflected or undeflected. The tail effectiveness $(\partial C_m/\partial i_t)_M$ was independent of the leading-edge-flap setting, but increased gradually with Mach number for Mach numbers between 0.40 and 0.925. (See fig. 10).

Tail incidence required for pull-ups.- The tail incidence required during pull-ups of the airplane were calculated for a wing loading of 120 pounds per square foot. (See fig. 11.) Corrections were made to the tail incidence to account for the effect of curvature of the flight path. For load factors of one or greater and for altitudes of 20,000 feet or less, the data for the leading-edge flaps undeflected indicate a stable variation of tail angle with Mach number for Mach numbers less than about 0.85. At 40,000 feet, the stable region is not defined by the data, but an unstable variation of tail incidence with Mach number is apparent for Mach numbers above 0.86. Deflecting the leading-edge flaps, in general, reduced the Mach number range for stick-fixed stability and required a more negative tail incidence to balance the airplane. The change of tail incidence was caused primarily by a decrease of the lift coefficient for balance when the leading-edge flaps were deflected. (See fig. 6.)

Lift-drag ratio.- Lift-drag ratio as a function of lift coefficient is presented in figure 12. Deflecting the flaps 10° increased the lift-drag ratio for lift coefficients greater than about 0.2 and Mach numbers less than about 0.85. Increasing the flap deflection from 10° to 20°, while increasing the lift-drag ratio slightly at 0.40 Mach number, reduced the lift-drag ratio for most lift coefficients at all higher Mach numbers. For Mach numbers greater than about 0.85, deflecting the leading-edge flaps appeared to be of little value for improving the lift-drag ratio.

Maximum lift–drag ratios are plotted against Mach number in figure 13. Deflecting the leading–edge flaps 10° increased the maximum lift–drag ratio approximately 20 percent between Mach numbers of 0.40 and 0.75. However, for Mach numbers above about 0.85 deflecting the flaps 10° reduced the maximum lift–drag ratio.

Model with scoops.– The model was equipped with dummy air scoops in an attempt to duplicate the power–off flight conditions with no air flow through the ducts. In order to install the air scoops, it was necessary to remove the canopy. Thus, lift, pitching moment, and drag were measured with the canopy removed (fig. 14), and with the canopy removed but with the scoops added (fig. 15).

The data indicate an over–all decrease in static longitudinal stability and an increase in lift coefficient for balance when the scoops were added. The minimum drag coefficient was increased approximately 50 percent at all Mach numbers of the tests.

Airbrakes.– A brake was desired that would approximately triple the minimum drag coefficient of the model without causing excessive changes of the pitching–moment characteristics. No attempt was made to vary either the plan form of the brake or its location systematically since the construction of the airplane fuselage permitted only limited combinations. The plan forms and locations that were considered most adaptable to the fuselage are shown in figure 3.

The effects of the various brake installations on the lift, drag, and pitching moment of the model are shown in figure 16 for a Mach number of 0.40. Figure 16(a) shows that the double brake beneath the wing at fuselage station 65.55 or 71.32 inches increased the pitching moment, while forward of the wing at station 50.40 or 55.80 inches they decreased the pitching moment. In all cases, the stability was increased slightly for lift coefficients less than about 0.6, but the model became neutrally stable for lift coefficients near the stall with the brakes forward of the wing at fuselage stations 50.40 and 55.80 inches.

The effects of changes in the brake plan form are shown in figures 16(b), (c), and (d) for stations 41.00 and 52.60 inches. Although all the brakes reduced the lift coefficient for balance at these stations, their effect on the stability of the model appeared generally satisfactory with the exception that the double brake at station 52.60 inches made the model unstable for lift coefficients near the stall. The single brakes produced smaller increments of drag primarily because their frontal area was less than for the double brake. (See figs. 16(b), (c), and (d).) Checks of the stability characteristics of the model in the landing configuration were made with the elongated single brake at station 41.00 inches, with the revised single brake at station 52.60 inches, and with the double brake at station 52.60 inches. The landing configuration for these tests included the modified landing–gear doors developed from tests in one of the Ames 7– by 10–foot wind

tunnels as shown in figure 1(c). In all cases the model appeared to have satisfactory longitudinal-stability characteristics.

The lift, pitching-moment, and drag characteristics of the model for several deflections of the single brake at station 41.00 inches are shown in figure 17. The increments of drag and pitching-moment coefficient from deflecting the brake are shown in figure 18. For this particular installation, the effect on the pitching-moment coefficient was small except for brake angles greater than about 50°. The increment of drag coefficient was approximately proportional to the projected frontal area of the brake. Thus the data indicate that brake deflections greater than about 70° would give little increase in increment of drag, but would decrease the lift coefficient for balance.

External stores.- Fuel tanks were added separately beneath the wing and to the wing tips of the model. (See figs. 1(d), (e), 4(a), and (b).) Lift, pitching-moment, and drag characteristics of the model with the underwing tanks are presented in figure 19 for 0° leading-edge-flap setting, while similar data are presented for the model with the tip tanks in figure 20 for leading-edge-flap settings of 0°, 10°, and 20°. Tail-off data with the tip tanks are shown in figure 21. Both installations appeared feasible inasmuch as the aerodynamic effects on the lift or pitching-moment characteristics were not excessive.

Adding the underwing tanks increased the angle of attack for zero lift about 0.5° and slightly reduced the lift-curve slope and the stalling lift coefficient. The principal effect on the pitching-moment characteristics was to reduce the longitudinal stability for lift coefficients in the vicinity of 0.2 and Mach numbers less than about 0.85 as shown by comparing figures 6 and 19. An increase in drag coefficient for zero lift of approximately 0.003 occurred for Mach numbers of 0.85 or less. The data also indicate that the Mach number for drag divergence was slightly reduced.

With the tanks on the wing tips, the lift data show a noticeable increase in lift-curve slope and insignificant changes in the angle of attack for zero lift or in the stalling lift coefficient. (Compare figs. 6 and 20(a).) Although adding the tip tanks reduced the lift coefficient for balance, some improvement is noted in the static-longitudinal-stability characteristics in that the variation of pitching moment with lift was more nearly linear, both with the tail on and with the tail off. At 0.3 lift coefficient with the leading-edge flaps undeflected, adding the tip tanks increased the static-longitudinal-stability parameter $(-\partial C_m/\partial C_L)_M$ from 0.067 to 0.090 at 0.40 Mach number and from 0.065 to 0.117 at 0.85 Mach number. The tip tanks increased the drag coefficient for zero lift about 0.003 for Mach numbers of 0.85 or less. Although the end-plate effect of the tip tanks was not sufficient to reduce significantly the drag of the clean model (see figs. 7(b) and 20(a)), less drag was generally indicated with the tip tanks than with the underwing tanks for

lift coefficients greater than about 0.2 and Mach numbers less than 0.85 (see figs. 19 and 20(a)).

Tip-tank normal force and pitching moment.- The normal force and pitching moment transmitted to the wing tips by the tip tanks are presented in figure 22 for various aileron and leading-edge-flap settings. The normal force increased almost linearly with angle of attack up to the wing stall (about 12° at 0.40 Mach number) and then increased at a reduced rate.

There was a stable variation of tip-tank pitching moment about the model center of gravity for normal-force coefficients below the wing stall. In terms of longitudinal stability of the model, however, this stabilizing effect is practically negligible and would not account for the gain in stability from adding the tip tanks. A comparison of the tail-off pitching-moment data of figures 6 and 21 indicates that the gain in stability was probably caused by a rearward shift in the aerodynamic center of the wing-fuselage combination when the tanks were added.

Wing-tip ram jets.- The lift, pitching-moment, and drag characteristics of the model with the wing-tip ram jets are presented in figures 23(a), (b), and (c) for leading-edge flap angles of 0°, 10°, and 20°, respectively. Tail-off data are presented in figure 24 for a leading-edge-flap angle of 0°. Adding the ram jets increased the lift-curve slope and reduced the lift coefficient for balance, but did not significantly change the over-all static longitudinal stability of the model. (See figs. 6 and 23(a).) The variation of pitching-moment coefficient with lift coefficient was more nearly linear both with the tail on and with the tail off. There was an increase in minimum drag of 0.011 at 0.40 Mach number and 0.018 at 0.90 Mach number as shown from a comparison of figures 7(b) and 23.

Ram-jet normal force and pitching moment.- The ram-jet normal force and pitching moment imposed on the wing tips are presented in figure 25 for several aileron and leading-edge-flap settings. For angles of attack below the wing stall, there was an approximately linear variation of normal force with angle of attack and of pitching moment with normal force.

Aileron rolling moment.- The variation of the rolling-moment coefficient produced by the left aileron with angle of attack is presented in figures 26, 27, and 28 for the clean model, for the model with wing-tip tanks, and for the model with wing-tip ram jets, respectively. A comparison of the aileron effectiveness for these three configurations is made in figure 29. At 0.40 Mach number, the clean model had an aileron effectiveness of 0.00094 and 0.00104 at 0° and 6° angle of attack, respectively. The aileron maintained approximately 50-percent effectiveness for several degrees above the wing stall.

Although there was a decrease in effectiveness for Mach numbers greater than 0.85 at 6° angle of attack, the aileron retained approximately 80 percent of its low-speed effectiveness at 0.925 Mach number. For an angle of attack of 12°, the aileron effectiveness increased continuously as the Mach number was increased from 0.40 to 0.90. Adding the wing-tip fuel tanks or the ram jets increased the aileron effectiveness at 0° angle of attack except at the highest Mach numbers, but reduced it at 6° and 12°. At 0° angle of attack, adding the tip tanks or the ram jets reduced the Mach number at which there was a loss of effectiveness.

Aerodynamic Characteristics in Yaw

Model with external stores.- Yawing moment, rolling moment, and side force are presented in figures 30 and 31 for the model with the underwing tanks and with the wing-tip tanks, respectively. The directional-stability parameter $(-\partial C_n/\partial\psi)_\alpha$, the lateral-stability parameter $(\partial C_l/\partial\psi)_\alpha$, and the side force due to yaw $(\partial C_C/\partial\psi)_\alpha$, averaged for angles of yaw between 0° and 6°, are shown in figure 32 for the clean model and for the model with external stores. The values of the parameters for the clean model were computed from data presented in reference 1.

Although some increase is noted in the value of the parameter $(\partial C_C/\partial\psi)$ when the external stores were added, their effect on the directional- or lateral-stability characteristics appeared insignificant. Adding the underwing tanks might be expected to reduce the value of $(\partial C_l/\partial\psi)_\alpha$ because increasing the vertical area below the center of gravity generally produces a destabilizing effect. Since no significant decrease of $(\partial C_l/\partial\psi)_\alpha$ was measured, it is believed that the interference of the tank installations caused a change in the lift distribution of the wing sufficient to offset the expected decrease.

Model with ram jets.- Yawing moment, rolling moment, and side force are presented in figures 33, 34, and 35 for the model with both ram jets, with the right ram jet, and with the left ram jet, respectively. The parameters $(-\partial C_n/\partial\psi)_\alpha$, $(\partial C_l/\partial\psi)_\alpha$, and $(\partial C_C/\partial\psi)_\alpha$ for the clean model are compared in figure 36 with those for the model with the lift, right, and both ram jets. The values shown represent averages for angles of yaw between 0° and 6°. Some increase was noted in the value of $(\partial C_C/\partial\psi)_\alpha$ when ram jets were added to either or both wing tips, but the over-all effects on the parameters $(-\partial C_n/\partial\psi)_\alpha$ and $(\partial C_L/\partial\psi)_\alpha$ were of secondary importance.

A comparison of figures 33 and 34 or of figures 33 and 35 shows that a ram jet on one wing tip would cause an unbalanced yawing and rolling moment at 0° angle of yaw. Although these unbalanced moments might be

greater at higher angles of attack, values of rudder effectiveness (from unpublished low-speed wind-tunnel data ($\partial C_n/\partial \delta_r$) was about -0.004) and aileron effectiveness (fig. 29) indicate that deflecting the rudder about 1.5° and deflecting both ailerons about 3.5° would balance the model at 0° yaw.

CONCLUDING REMARKS

Wind-tunnel tests of the 0.16-scale model of the X-3 airplane at low and high subsonic Mach numbers indicated a stable variation of tail incidence with Mach number for Mach numbers less than about 0.85. Deflecting the leading-edge flaps, in general, reduced the Mach number range for this stick-fixed static-longitudinal stability and increased the negative tail incidence required to trim the airplane in level flight.

For certain leading-edge-flap deflections, the maximum lift-drag ratio was increased and the drag was reduced at lift coefficients greater than about 0.2 and Mach numbers less than about 0.85.

Tests of the model equipped with airbrakes indicated generally satisfactory longitudinal-stability characteristics with either a single or a double brake forward of the wing at fuselage station 41.00 inches.

Adding fuel tanks or ram jets to the wing tips or fuel tanks beneath the wing appeared to be aerodynamically feasible inasmuch as the static lateral or longitudinal stability and control were not excessively affected. Although the wing-tip tanks reduced the lift coefficient for balance, they increased the lift-curve slope and the static longitudinal stability. The underwing tanks reduced the longitudinal stability in the region of 0.2 lift coefficient. Both tank installations increased the drag coefficient at zero lift about 0.003 at the lower Mach numbers, but the tip tanks produced less drag than the underwing tanks at lift coefficients above about 0.2 and Mach numbers less than 0.85. The principal effect of the wing-tip ram jets was to increase the lift-curve slope and to reduce the lift coefficient for balance.

The normal force imposed on the wing tips by the tip tanks or by the ram jets increased approximately linearly with angle of attack up to the wing stall.

At an angle of attack of 6° and a Mach number of 0.925, the aileron retained approximately 80 percent of its low-speed effectiveness.

Ames Aeronautical Laboratory,
National Advisory Committee for Aeronautics,
Moffett Field, Calif.

REFERENCES

1. Hamilton, William T., and Cleary, Joseph W.: Wind-Tunnel Tests of a 0.16-Scale Model of the X-3 Airplane at High Subsonic Speeds. - Stability and Control Characteristics. NACA RM A50A03, 1950.

2. Herriot, John G.: Blockage Corrections for Three-Dimensional-Flow Closed-Throat Wind Tunnels, with Consideration of the Effect of Compressibility. NACA RM A7B28, 1947.

TABLE I.- MODEL DIMENSIONS

Wing	
Area, square feet	4.094
Aspect ratio	3.01
Taper ratio	0.4
Span, feet	3.51
Root section (at plane of symmetry) chord, feet	1.666
Thickness, percent of chord	4.5
Dihedral (wing reference plane), degree	0
Incidence, degree	0
Mean aerodynamic chord, feet	1.238
Sweepback (75-percent-chord line), degree	0
Aileron	
Span, feet	0.526
Wing station at inner end, feet	1.227
Wing station at outer end, feet	1.753
Chord at inner end, feet	0.241
Chord at outer end, feet	0.167
Horizontal tail	
Area, square feet	0.794
Area, exposed, square feet	0.701
Aspect ratio	3.01
Taper ratio	0.4
Span, feet	1.547
Tail length (center of gravity to one-quarter mean aerodynamic chord of horizontal tail), feet	3.393
Section at spanwise station 0.377 inch (fuselage juncture),	
Chord, feet	0.752
Thickness, percent of chord	7.5
Section at spanwise station, 3.095 inch	
Chord, feet	0.587
Thickness, percent of chord	4.5
Tip section	
Chord, feet	0.294
Thickness, percent of chord	4.5
Dihedral, degree	0
Incidence	variable
Mean aerodynamic chord, feet	0.545
Mean aerodynamic chord, exposed, feet	0.521
Sweepback (50-percent-chord line), degree	23

TABLE I.- CONCLUDED

Vertical tail	
Area, square feet	0.678
Aspect ratio	1.32
Taper ratio	0.25
Span, feet	0.947
Tail length (center of gravity to one-quarter mean aerodynamic chord of vertical tail), feet	3.410
Root section	
Chord, feet	1.147
Thickness, percent of chord	4.5
Tip section	
Chord, feet	0.287
Thickness, percent of chord	4.5
Mean aerodynamic chord, feet	0.802
Sweepback (90-percent-chord line), degree	0
Rudder	
Span, feet	0.705
Height of lower end above fuselage reference plane, feet	0.690
Height of upper end above fuselage reference plane, feet	1.395
Chord at inboard end, feet	0.227
Chord at outboard end, feet	0.162
Tip and underwing tanks	
Length, feet	2.015
Frontal area, square feet	0.0460
Volume (each tank) cubic feet	0.0545
Fineness ratio	8.333
Incidence, degree	0
Wing-tip ram jets	
Length, feet	2.600
Frontal area, square feet	0.0788
Fineness ratio	8.220
Incidence, degree	-2

TABLE II.- FIGURE INDEX

Photographs and sketches	Fig. No.
Three-quarter-front views of several configurations	1
The 0.16-scale model of the X-3 airplane	2
Airbrake plan forms and locations	3
Wing-tip tanks	4(a)
Underwing tanks	4(b)
Wing-tip ram jets	5

Basic aerodynamic data

Wing, fuselage, and tail boom									Type of data and figure number											
Scoops	Tail	Canopy	Wing-tip tanks	Underwing tanks	Wing-tip ram jets	i_t	δ_{lf}	δ_a	δ_{ab}	C_L vs α	C_m vs C_L	C_D vs C_L	C_{h_t} vs C_L	C_l vs α	C_{N_T} vs α	C_{m_T} vs C_{N_T}	C_{N_R} vs α	C_{m_R} vs C_{N_R}	C_C vs ψ	C_n vs ψ	C_l vs ψ
off	on	on	off	off	off	0°,-2°,-4°	0°,10°,20°	0°	0°	6(a to g)	6(a to g)	- - -	6(a to g)	- - -	- - -	- - -	- - -	- - -	- - -	- - -	- - -
off	off	on	off	off	off	- - -	0°,10°,20°	0°	0°	6(a to g)	6(a to g)	- - -	6(a to g)	- - -	- - -	- - -	- - -	- - -	- - -	- - -	- - -
off	on	on	off	off	off	0°,-2°,-4°	0°,10°,20°	0°	0°	- - -	- - -	7(a to c)	- - -	- - -	- - -	- - -	- - -	- - -	- - -	- - -	- - -
off	off	on	off	off	off	- - -	0°,10°,20°	0°	0°	- - -	- - -	8	- - -	- - -	- - -	- - -	- - -	- - -	- - -	- - -	- - -
off	on	off	off	off	off	-2°	0°	0°	0°	14	14	14	- - -	- - -	- - -	- - -	- - -	- - -	- - -	- - -	- - -
on	on	off	off	off	off	-2°	0°	0°	0°	15	15	15	- - -	- - -	- - -	- - -	- - -	- - -	- - -	- - -	- - -
off	on	on	off	off	off	-2°	0°	0°	30° to 90°	17	17	17	- - -	- - -	- - -	- - -	- - -	- - -	- - -	- - -	- - -
off	on	on	off	on	off	-2°	0°	0°	0°	19	19	19	- - -	- - -	- - -	- - -	- - -	- - -	- - -	- - -	- - -
off	on	on	on	off	off	-2°	0°,10°,20°	0°	0°	20(a to c)	20(a to c)	20(a to c)	- - -	- - -	- - -	- - -	- - -	- - -	- - -	- - -	- - -
off	off	on	on	off	off	- - -	0°	0°	0°	21	21	21	- - -	- - -	- - -	- - -	- - -	- - -	- - -	- - -	- - -
off	on	on	on	off	off	-2°	0°,10°,20°	-10° to 10°	0°	- - -	- - -	- - -	- - -	- - -	22(a to g)	22(a to g)	- - -	- - -	- - -	- - -	- - -
off	on	on	off	off	on	-2°	0°,10°,20°	0°	0°	23(a to c)	23(a to c)	23(a to c)	- - -	- - -	- - -	- - -	- - -	- - -	- - -	- - -	- - -
off	off	on	off	off	on	- - -	0°	0°	0°	24	24	24	- - -	- - -	- - -	- - -	- - -	- - -	- - -	- - -	- - -
off	on	on	off	off	on	-2°	0°,10°,20°	-10° to 10°	0°	- - -	- - -	- - -	- - -	- - -	- - -	- - -	25(a to g)	25(a to g)	- - -	- - -	- - -
off	on	on	off	off	off	-2°	0°	-10° to 10°	0°	- - -	- - -	- - -	- - -	26	- - -	- - -	- - -	- - -	- - -	- - -	- - -
off	on	on	on	off	off	-2°	0°	-10° to 10°	0°	- - -	- - -	- - -	- - -	27	- - -	- - -	- - -	- - -	- - -	- - -	- - -
off	on	on	off	off	on	-2°	0°	-10° to 10°	0°	- - -	- - -	- - -	- - -	28	- - -	- - -	- - -	- - -	- - -	- - -	- - -
off	on	on	off	on	off	-2°	0°	0°	0°	- - -	- - -	- - -	- - -	- - -	- - -	- - -	- - -	- - -	- - -	- - -	- - -
off	on	on	on	off	off	-2°	0°	0°	0°	- - -	- - -	- - -	- - -	- - -	- - -	- - -	- - -	- - -	30	30	30
off	on	on	off	off	on	-2°	0°	0°	0°	- - -	- - -	- - -	- - -	- - -	- - -	- - -	- - -	- - -	31	31	31
off	on	on	off	off	right only	-2°	0°	0°	0°	- - -	- - -	- - -	- - -	- - -	- - -	- - -	- - -	- - -	33	33	33
off	on	on	off	off	left only	-2°	0°	0°	0°	- - -	- - -	- - -	- - -	- - -	- - -	- - -	- - -	- - -	34	34	34
																			35	35	35

Miscellaneous aerodynamic data

Wing, fuselage, and boom									Type of data	Fig. No.
Scoops	Tail	Canopy	Wing-tip tanks	Underwing tanks	Wing-tip ram jets	i_t	δ_{lf}	δ_a	δ_{ab}	
off	on	on	off	off	off	-2°	0°	0°	0°	C_L vs M, C_m vs M, C_D vs M	9
off	on	on	off	off	off	-2°	0°	0°	0°	$(\partial C_L/\partial\alpha)_M$ vs M, $(-\partial C_m/\partial C_L)_M$ vs M, $(\partial C_m/\partial i_t)_M$ vs M	10
off	on	on	off	off	off	Variable	0°,10°,20°	0°	0°	i_t vs M	11
off	on	on	off	off	off	-2°	0°,10°,20°	0°	0°	L/D vs C_L	12
off	on	on	off	off	off	-2°	0°,10°,20°	0°	0°	$(L/D)_{max}$ vs M	13
off	on	on	off	off	off	-2°	0°	0°	variable	ΔC_D vs δ_{ab}, ΔC_m vs δ_{ab}	18

Comparative aerodynamic data

Results of data	Type of data	Fig. No.
Effects of various brakes and brake locations	C_D vs C_L, C_L vs α, $C_m$vs C_L	16
Aileron effectiveness	$(\partial C_l/\partial\delta_a)_\alpha$ vs M	29
Effect of external stores	$(-\partial C_n/\partial\psi)_\alpha$ vs M, $(\partial C_l/\partial\psi)_\alpha$ vs M, $(\partial C_l/\partial\psi)_\alpha$ vs M	32
Effect of ram jets	$(-\partial C_n/\partial\psi)_\alpha$ vs M, $(\partial C_l/\partial\psi)_\alpha$ vs M, $(\partial C_C/\partial\psi)_\alpha$ vs M	36

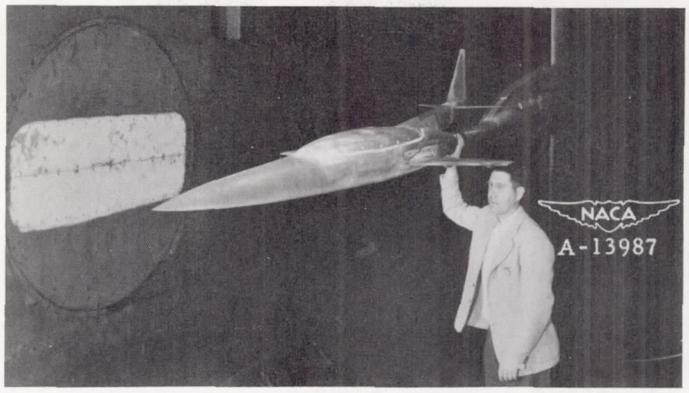

(a) Model.

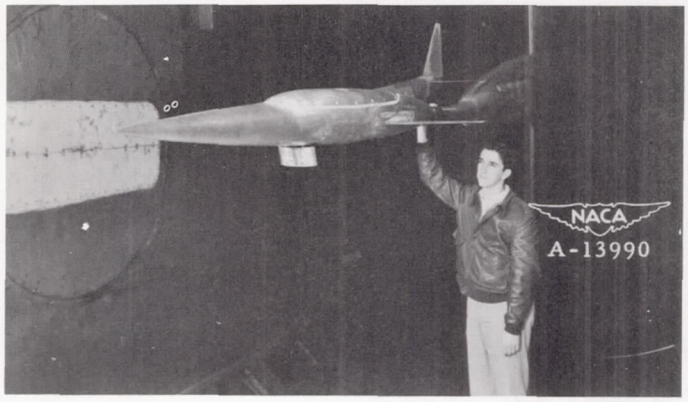

(b) Model with the single airbrake at fuselage station 41.00 inches.

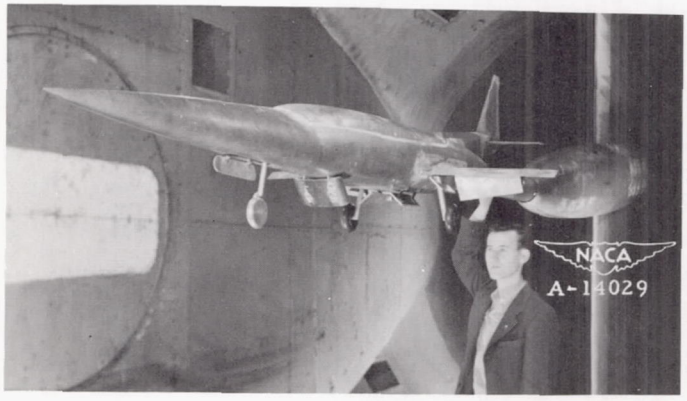

(c) Model with the elongated single airbrake at fuselage station 41.00 inches and with the landing gear extended.

Figure 1.- Three-quarter-front views of several configurations of the X-3 model.

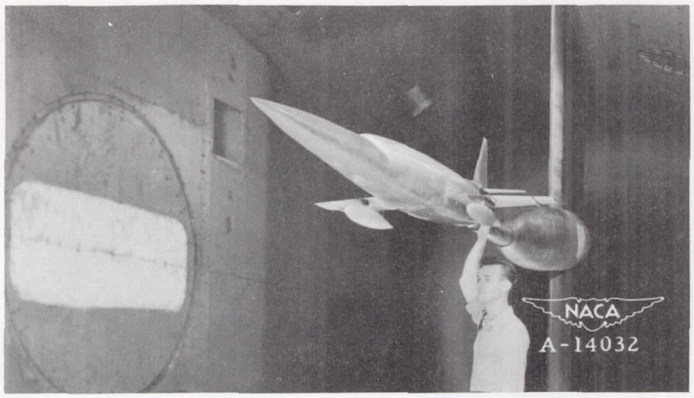

(d) Model with underwing tanks.

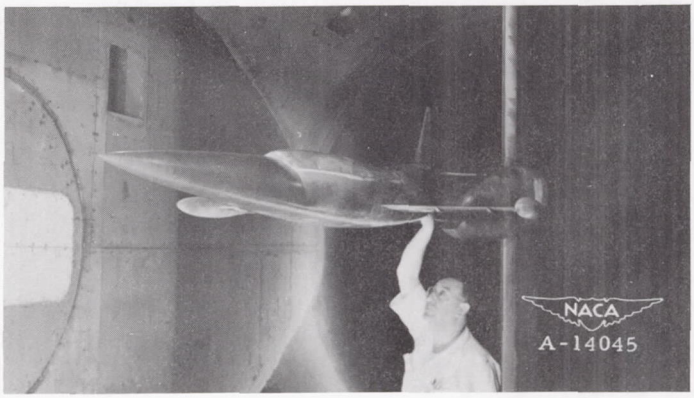

(e) Model with wing-tip tanks.

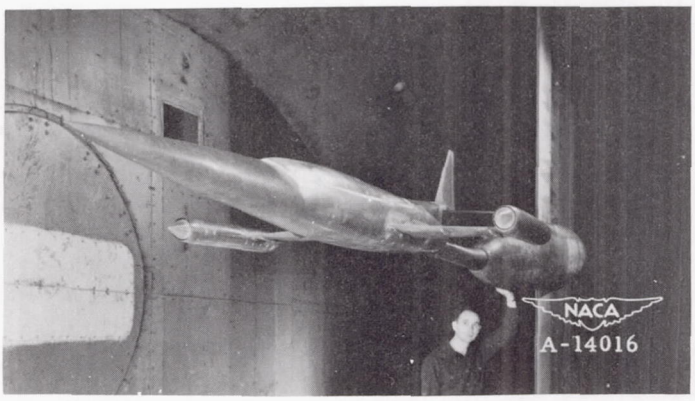

(f) Model with wing-tip ram jets.

Figure 1.- Concluded.

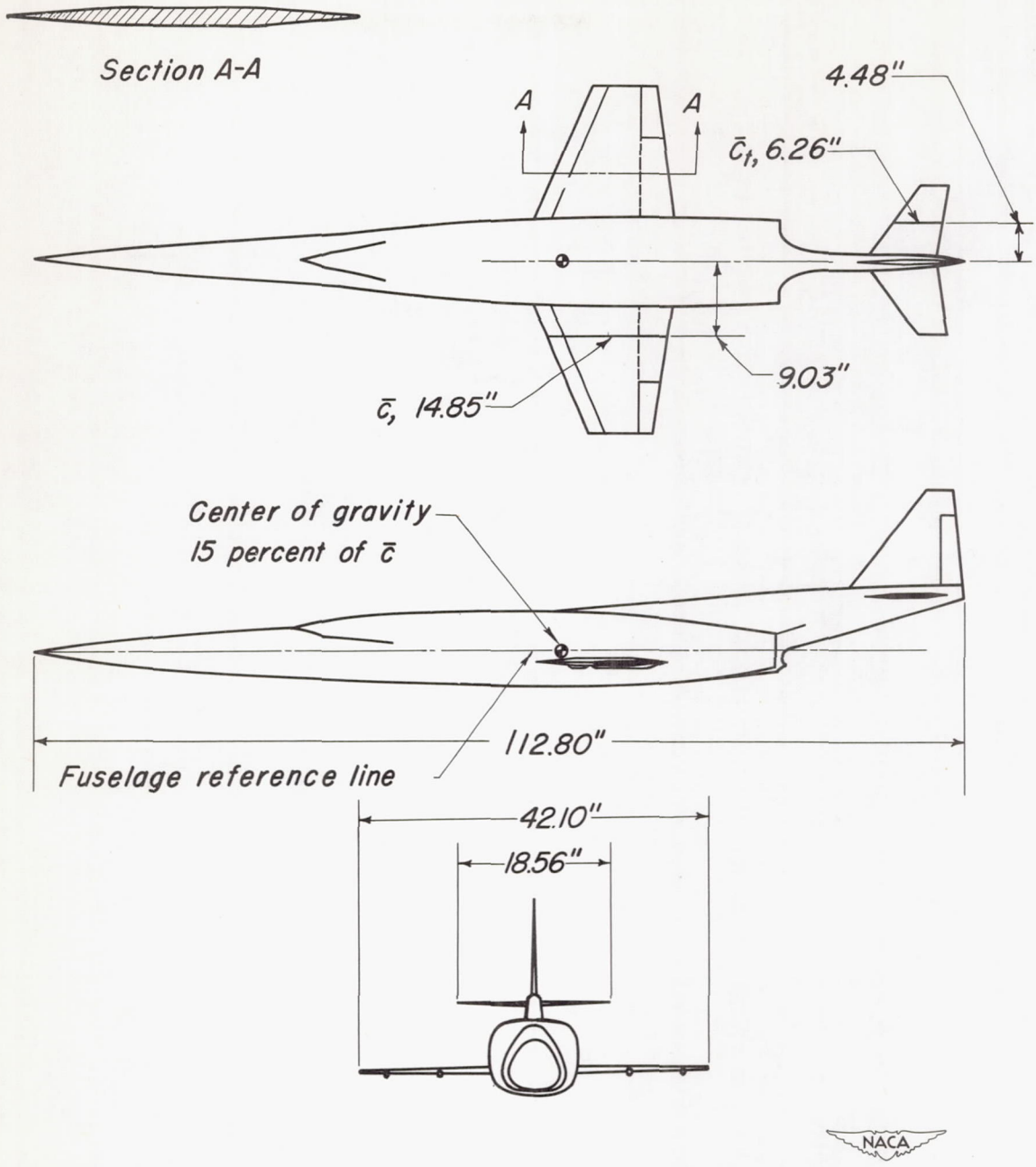

Figure 2.- The 0.16-scale model of the X-3 airplane.

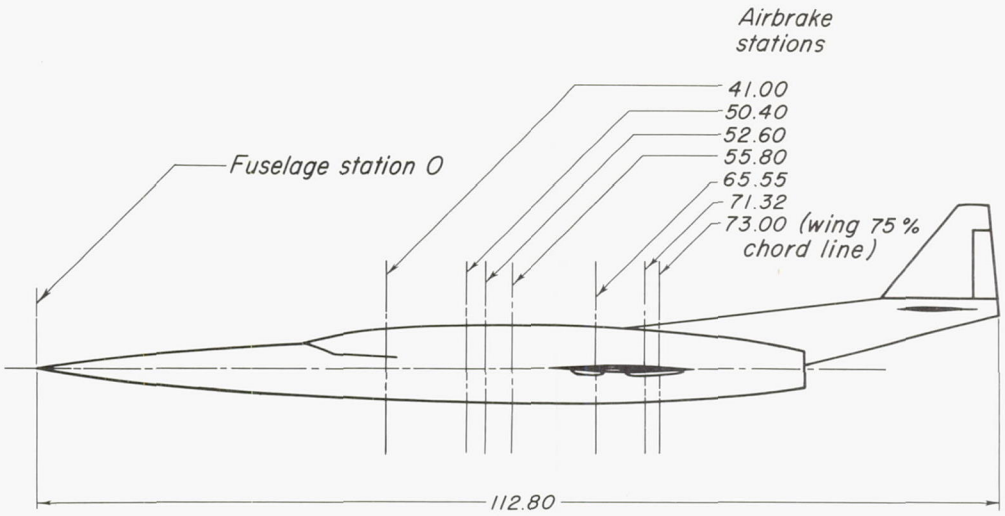

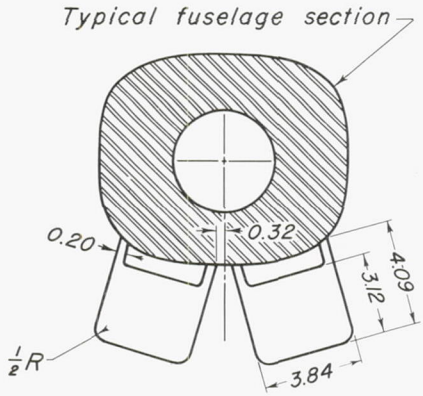

Double brake

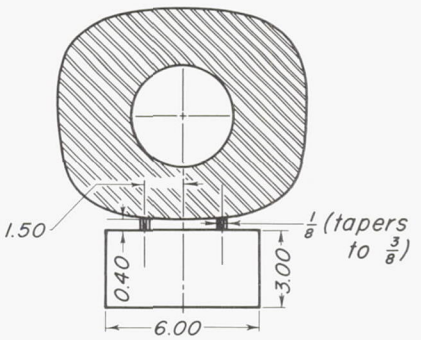

Single brake

Airbrake	Projected area	Contour
Double	24.40	Flat
Single	18.12	Curved-conforms to fuselage contour
Elongated single	21.88	
Revised single	25.25	

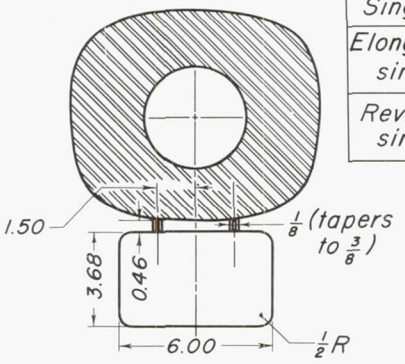

Elongated single brake

Note:-All dimensions are in inches and areas in square inches unless otherwise specified.

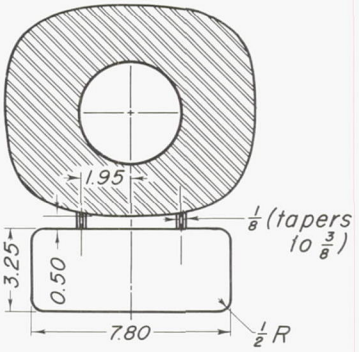

Revised single brake

NACA

Figure 3.–The plan form and location of the airbrakes on the X-3 model.

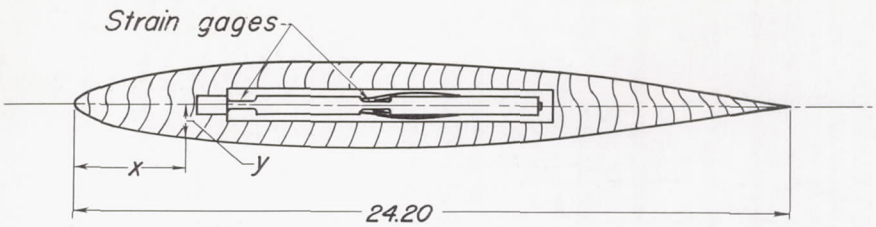

Section A – A

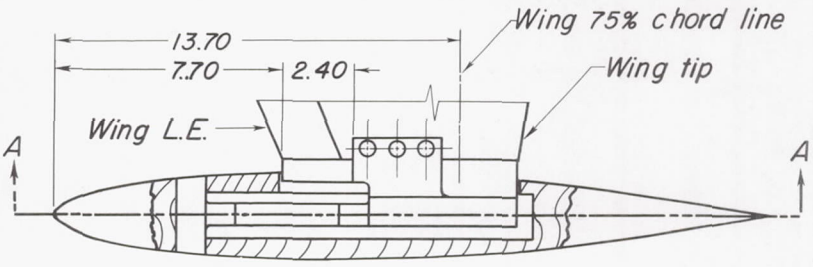

Top view

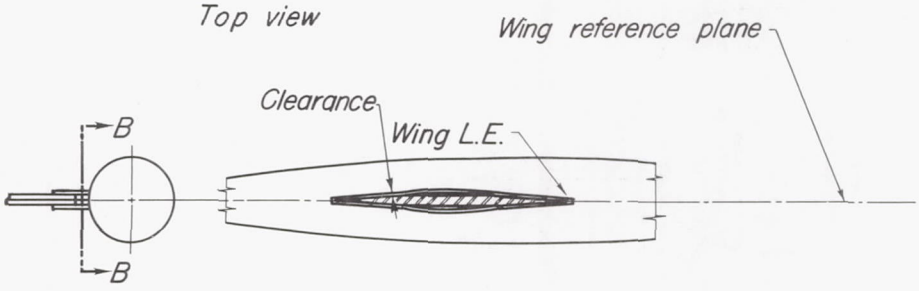

Front view Section B – B

Tip tank coordinates (NACA fuselage form III)			
x	y	x	y
0	—		
0.30	0.301	14.52	1.289
.60	.455	16.94	1.067
1.21	.682	19.36	.747
2.42	.976	20.57	.571
4.84	1.289	21.78	.386
7.26	1.423	22.99	.195
9.40	1.452	23.60	.098
12.10	1.408	24.20	0

Note: all dimensions are in inches unless otherwise specified.

(a) The wing-tip tanks.

Figure 4.– The external stores of the X-3 model.

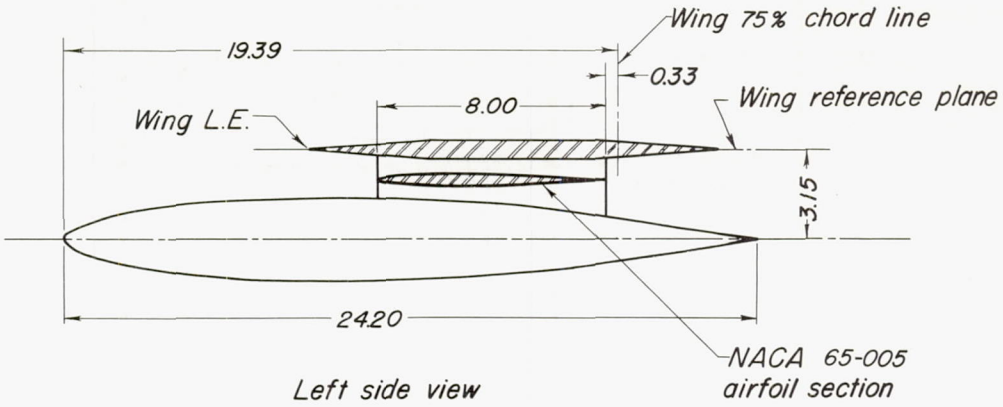

Left side view

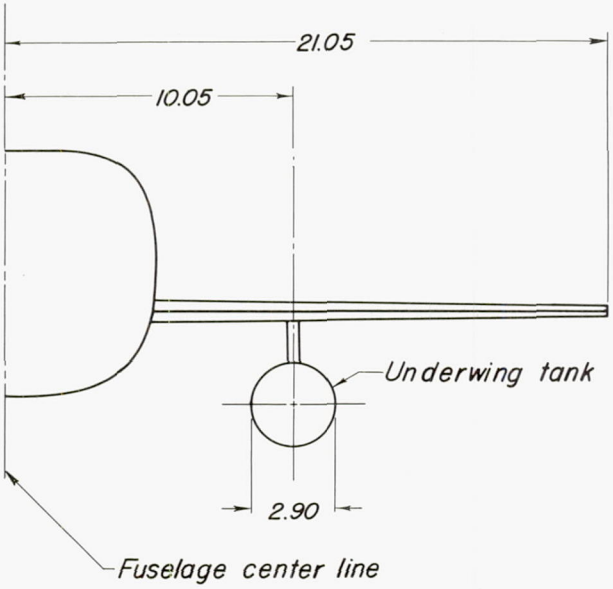

Front view

Notes: 1. All dimensions are in inches unless otherwise specified.

2. Underwing tank coordinates same as those of tip tanks.

(b) The underwing tanks.

Figure 4.– Concluded.

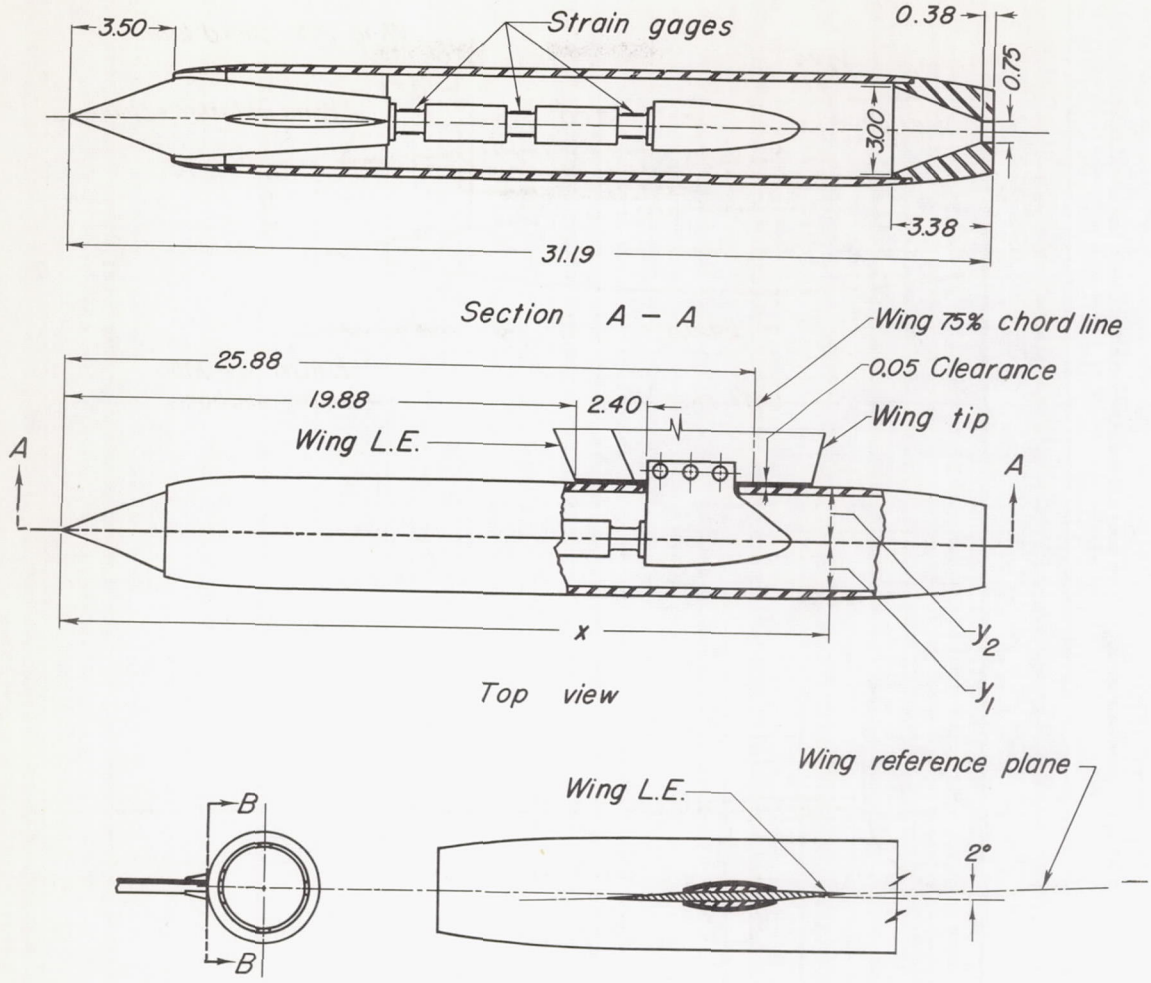

Ram jet coordinates					
x	y_1	y_2	x	y_1	y_2
3.50	1.50	1.50	12.00 to 25.00	1.60	1.90
3.75	1.55	1.60			
4.00	1.58	1.65	26.00	1.60	1.87
5.00	1.60	1.78	27.00	1.60	1.85
6.00	1.60	1.82	27.82	1.60	1.81
7.00	1.60	1.85	28.00	See sect	1.80
8.00	1.60	1.86	29.00	A-A for	1.72
9.00	1.60	1.87	30.00	dim. of	1.62
10.00	1.60	1.88	31.00		1.45
11.00	1.60	1.89	31.19	tail plug	1.40

Note: All dimensions are in inches unless otherwise specified.

Figure 5.– The wing-tip ram jets of the X-3 model.

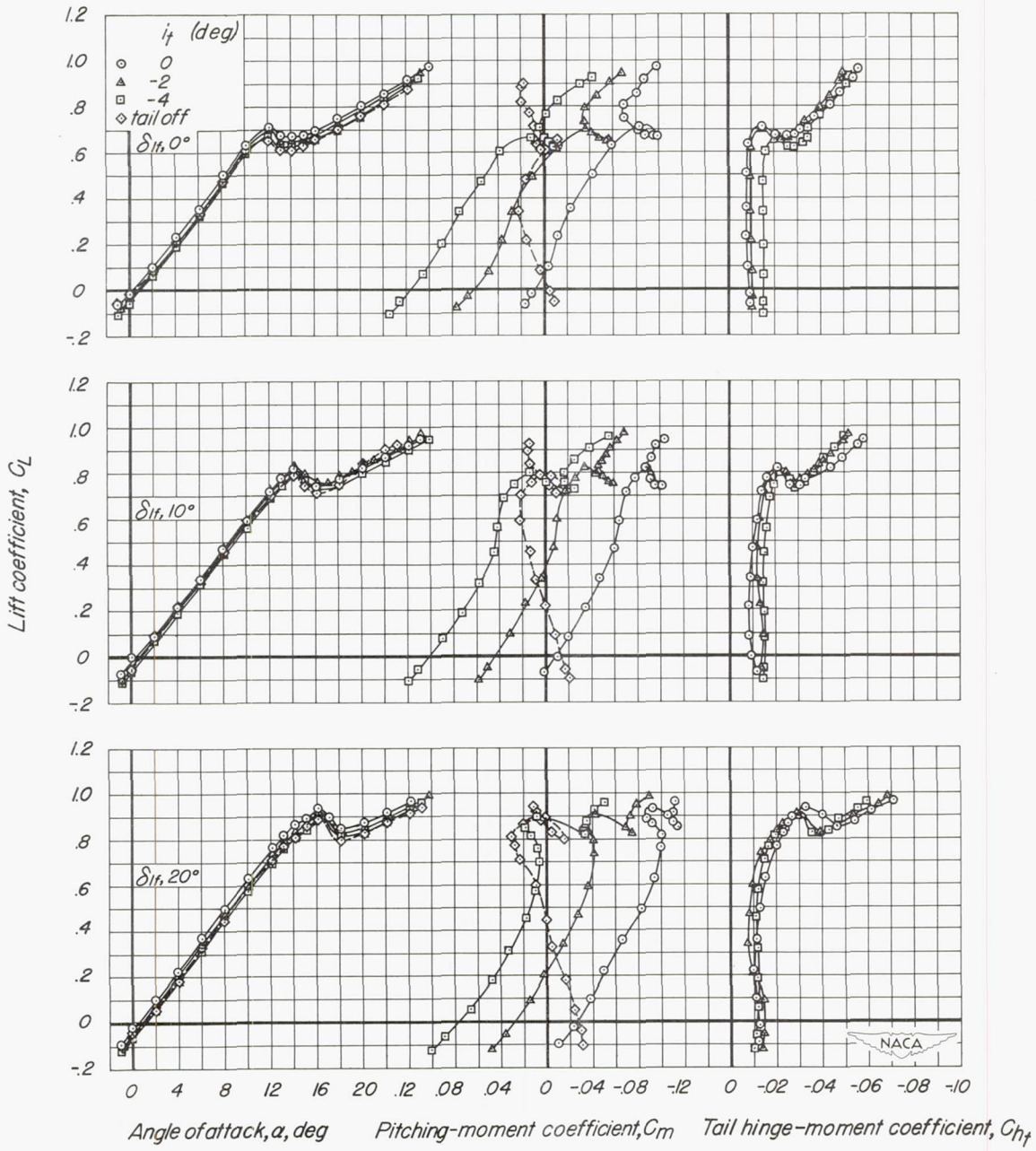

(a) Mach number, 0.40.

Figure 6.–The lift, pitching-moment, and tail hinge-moment characteristics of the X-3 model.

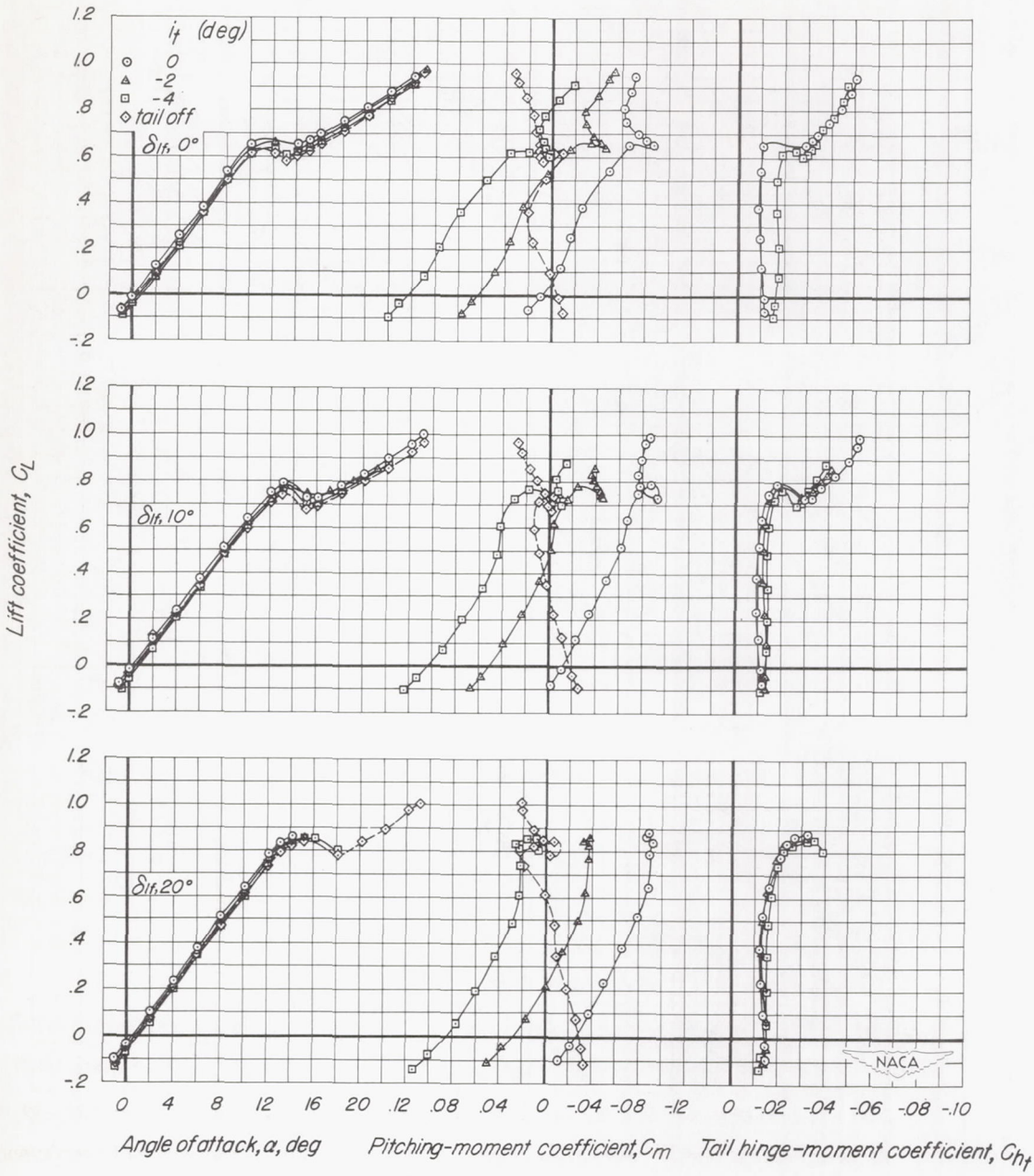

(b) Mach number, 0.60.

Figure 6.- Continued.

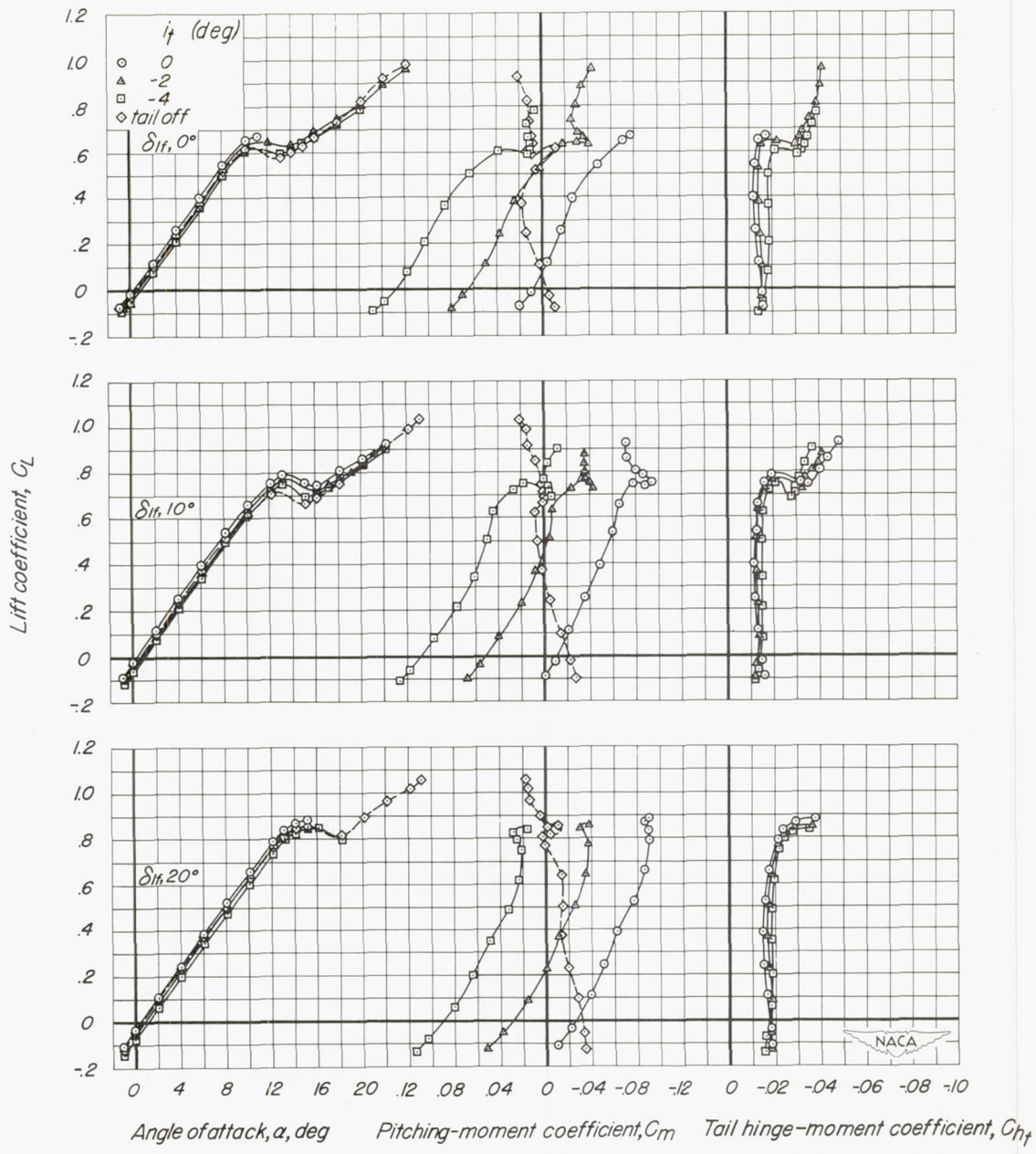

(c) Mach number, 0.70.

Figure 6.– Continued.

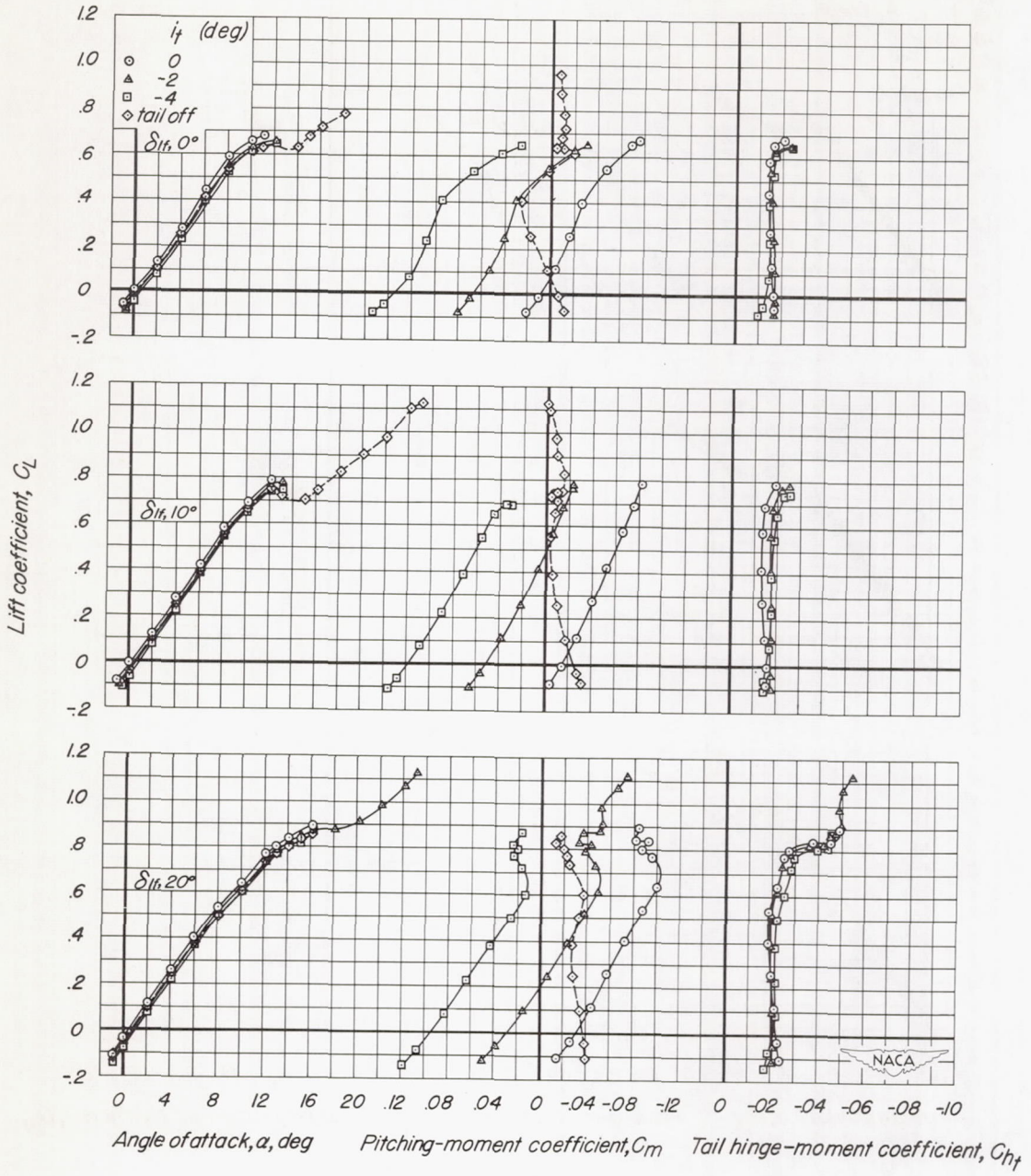

(d) Mach number, 0.80.

Figure 6.– Continued.

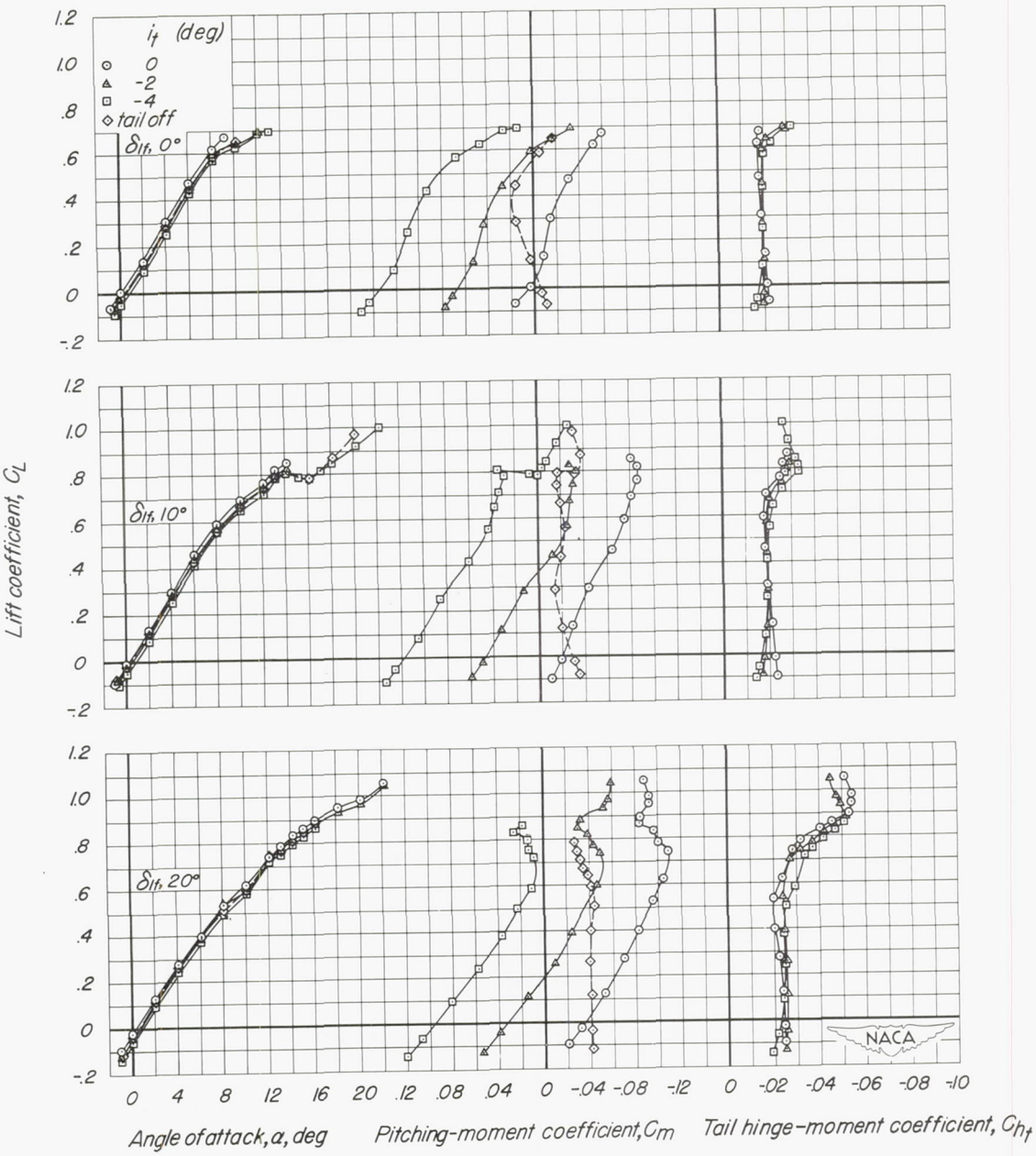

(e) Mach number, 0.85.

Figure 6.- Continued.

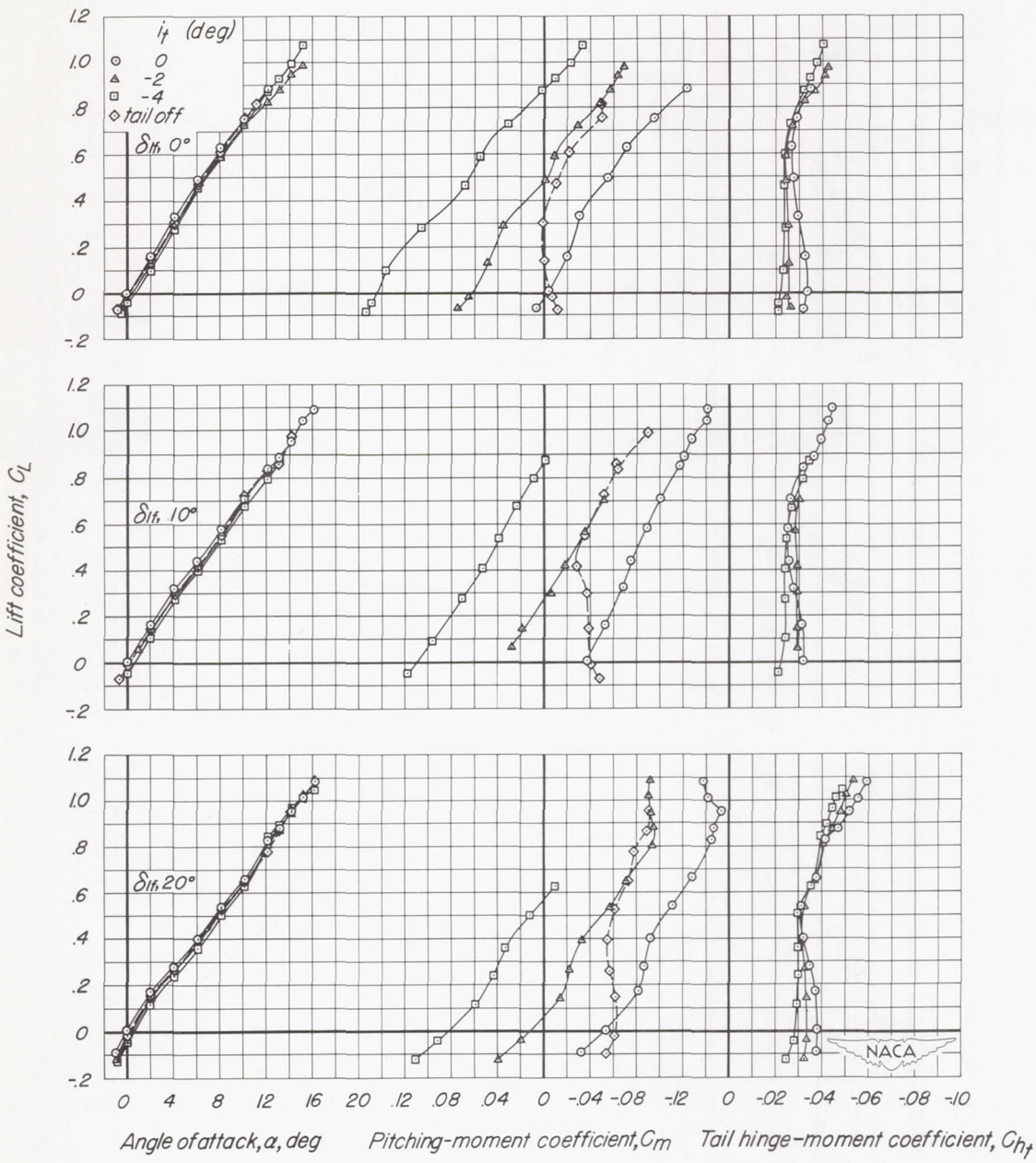

(f) Mach number, 0.90.

Figure 6.– Continued.

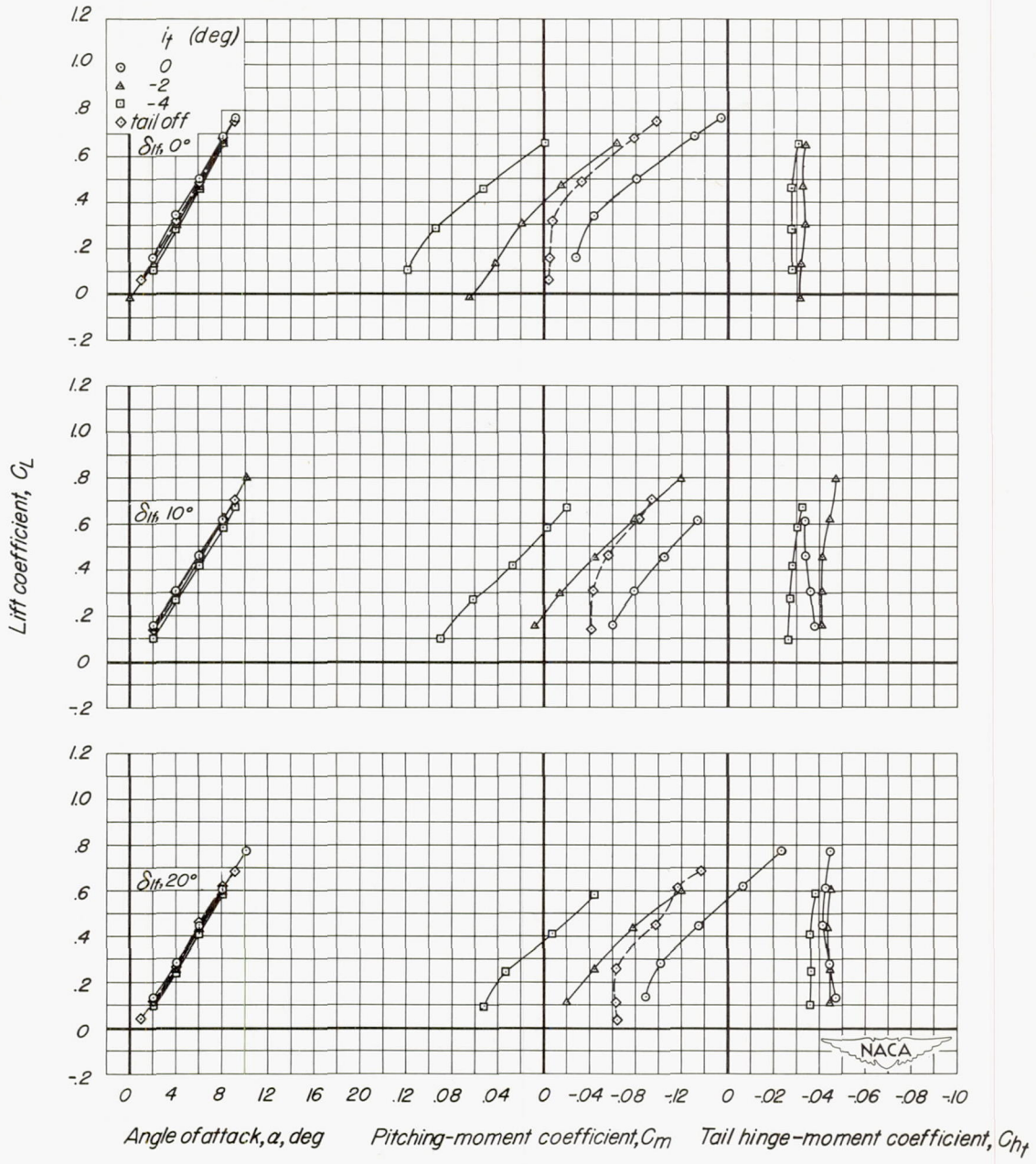

(g) Mach number, 0.925.

Figure 6.– Concluded.

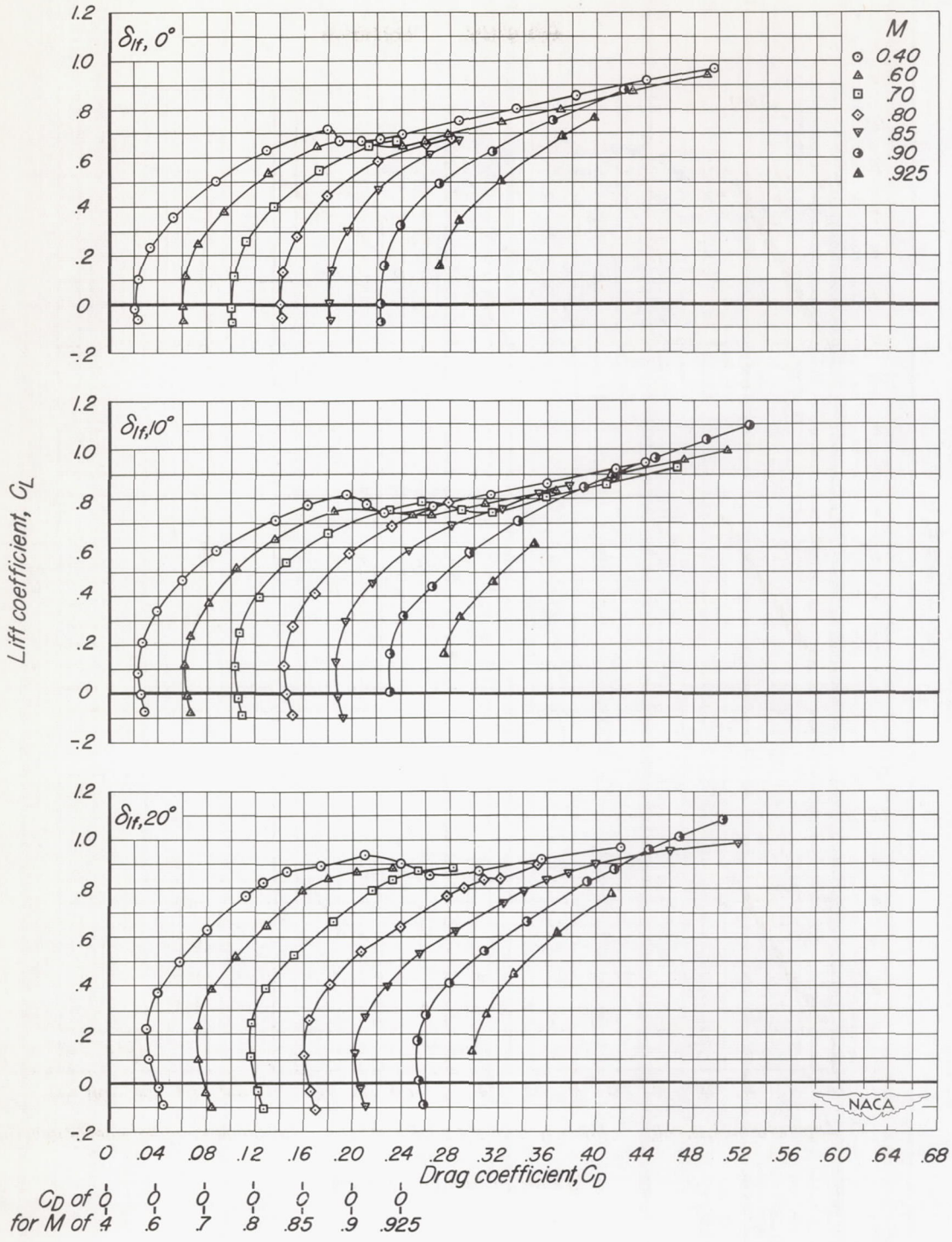

(a) Horizontal-tail incidence, 0°.

Figure 7.—The drag characteristics of the X-3 model.

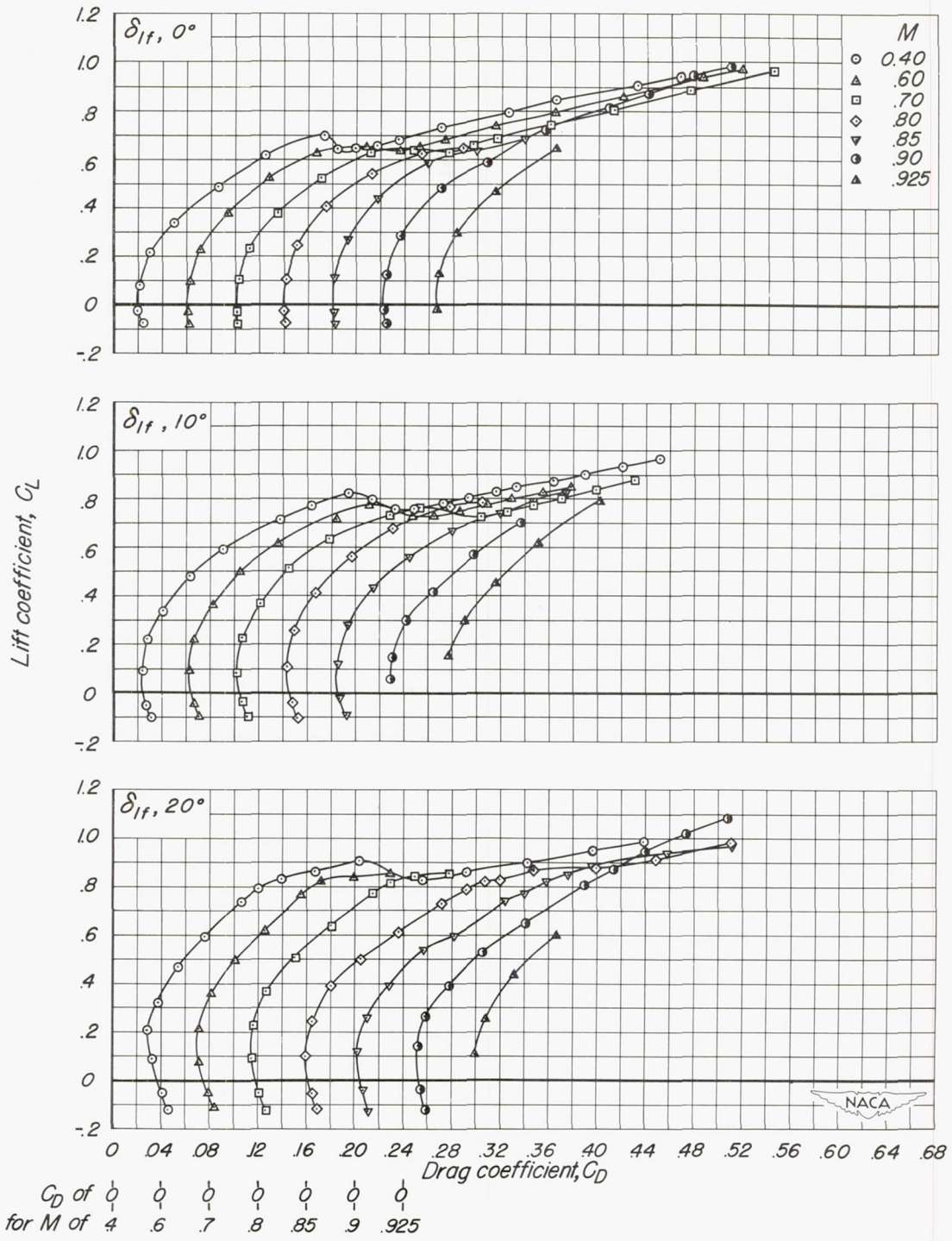

(b) Horizontal-tail incidence, -2°.

Figure 7.- Continued.

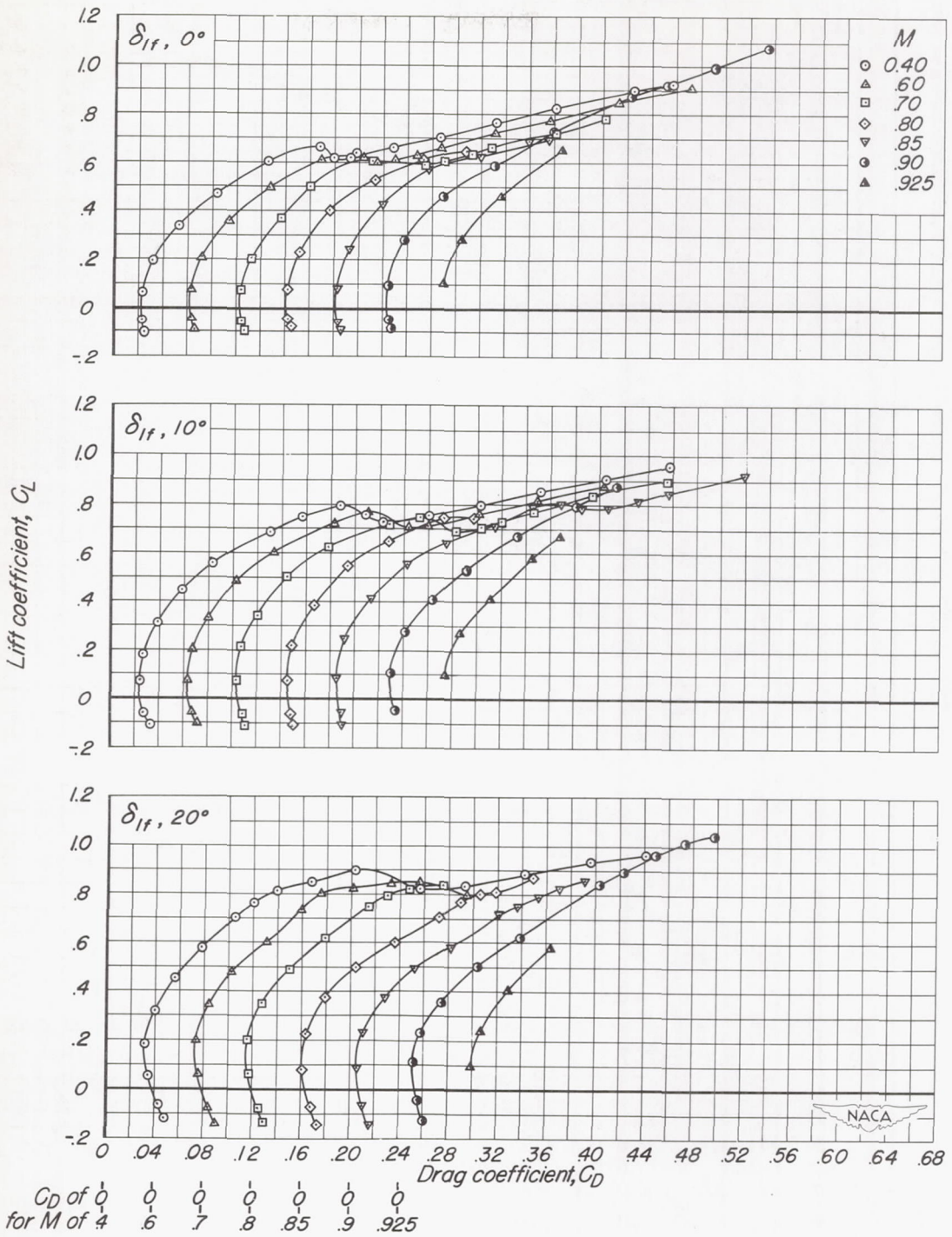

(c) Horizontal-tail incidence, -4°.

Figure 7.– Concluded.

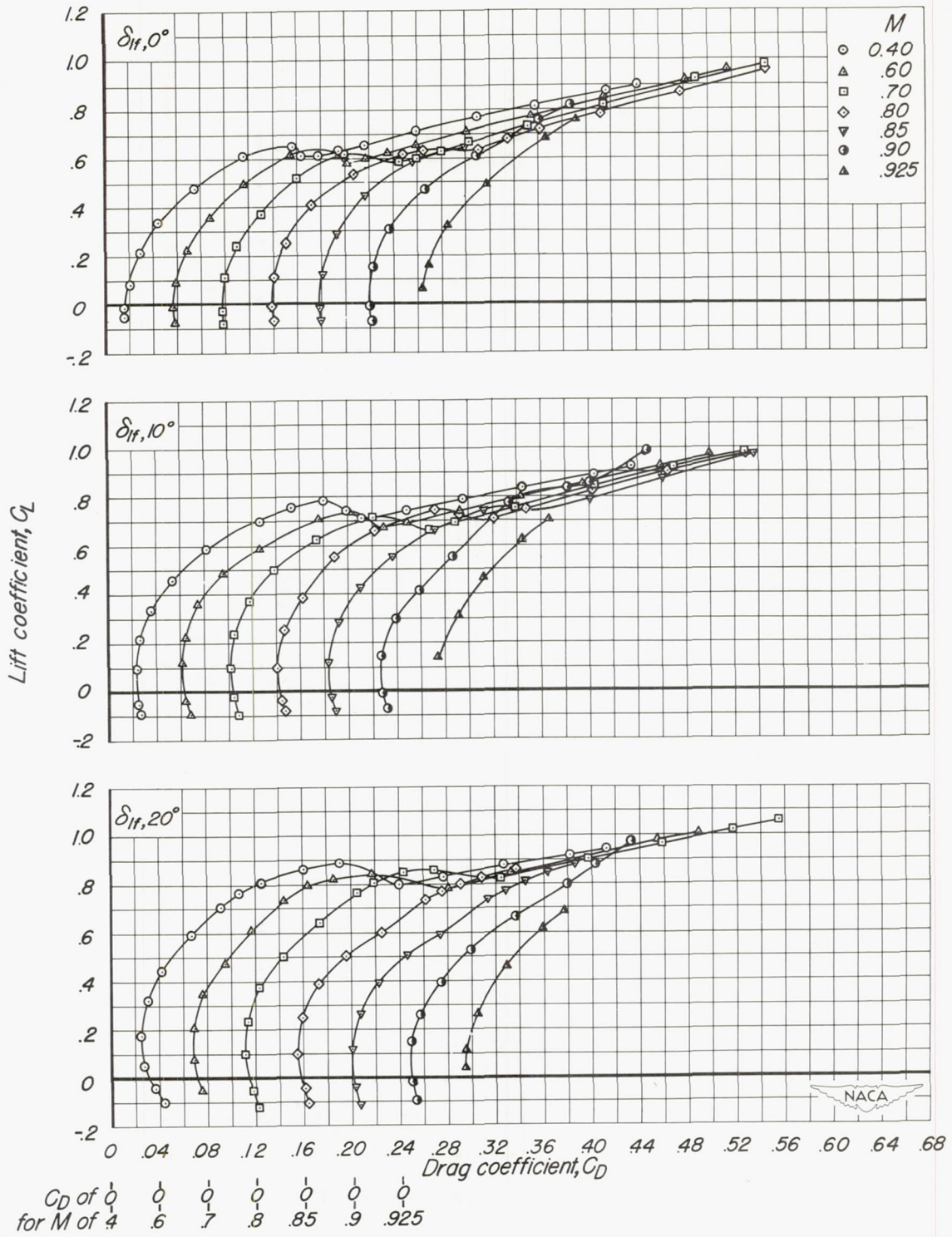

Figure 8.– The drag characteristics of the X-3 model less the empennage.

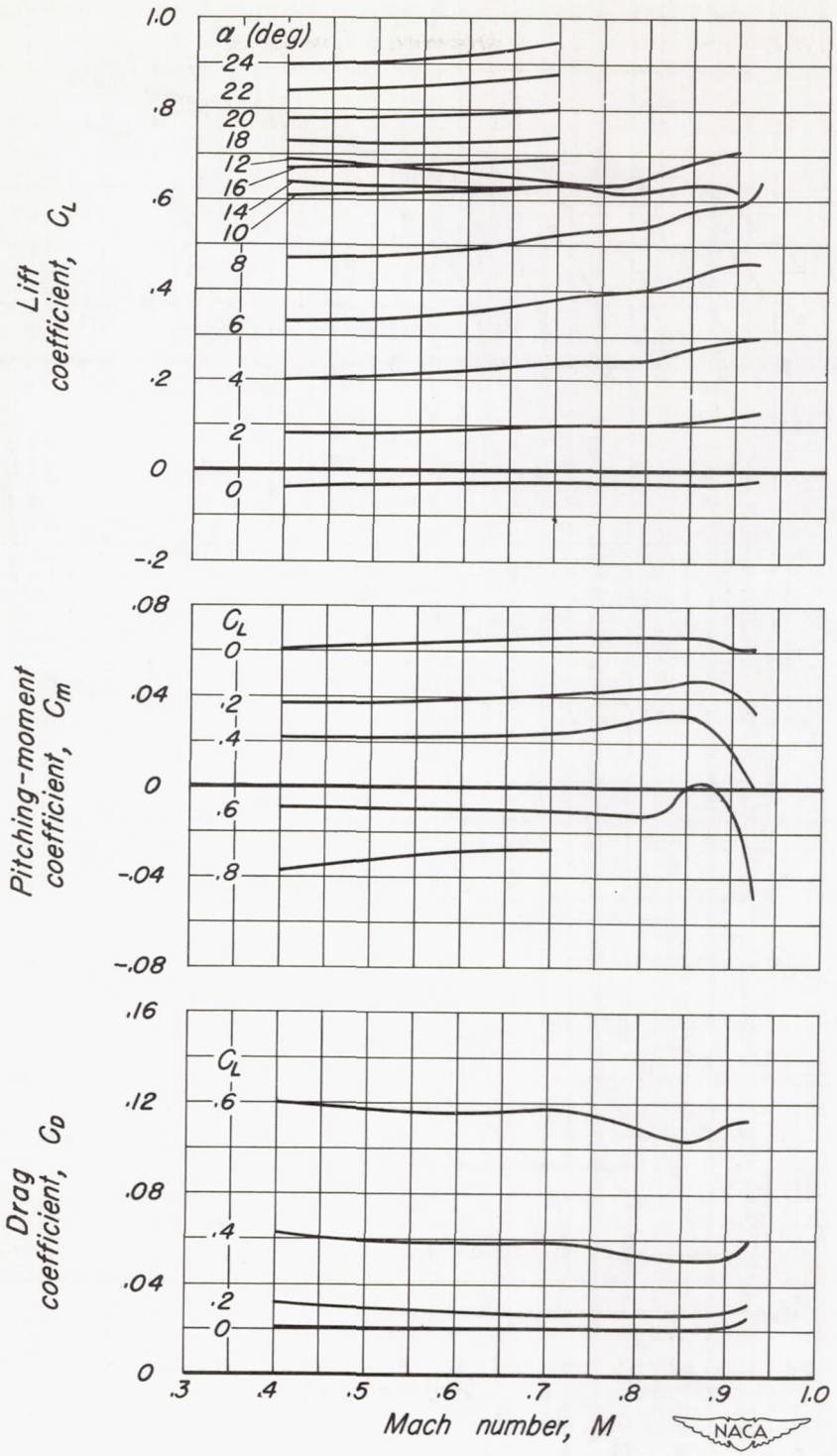

Figure 9.—The variation of lift, pitching-moment, and drag coefficient with Mach number for the X-3 model. δ_{lf}, 0°; i_t, -2°.

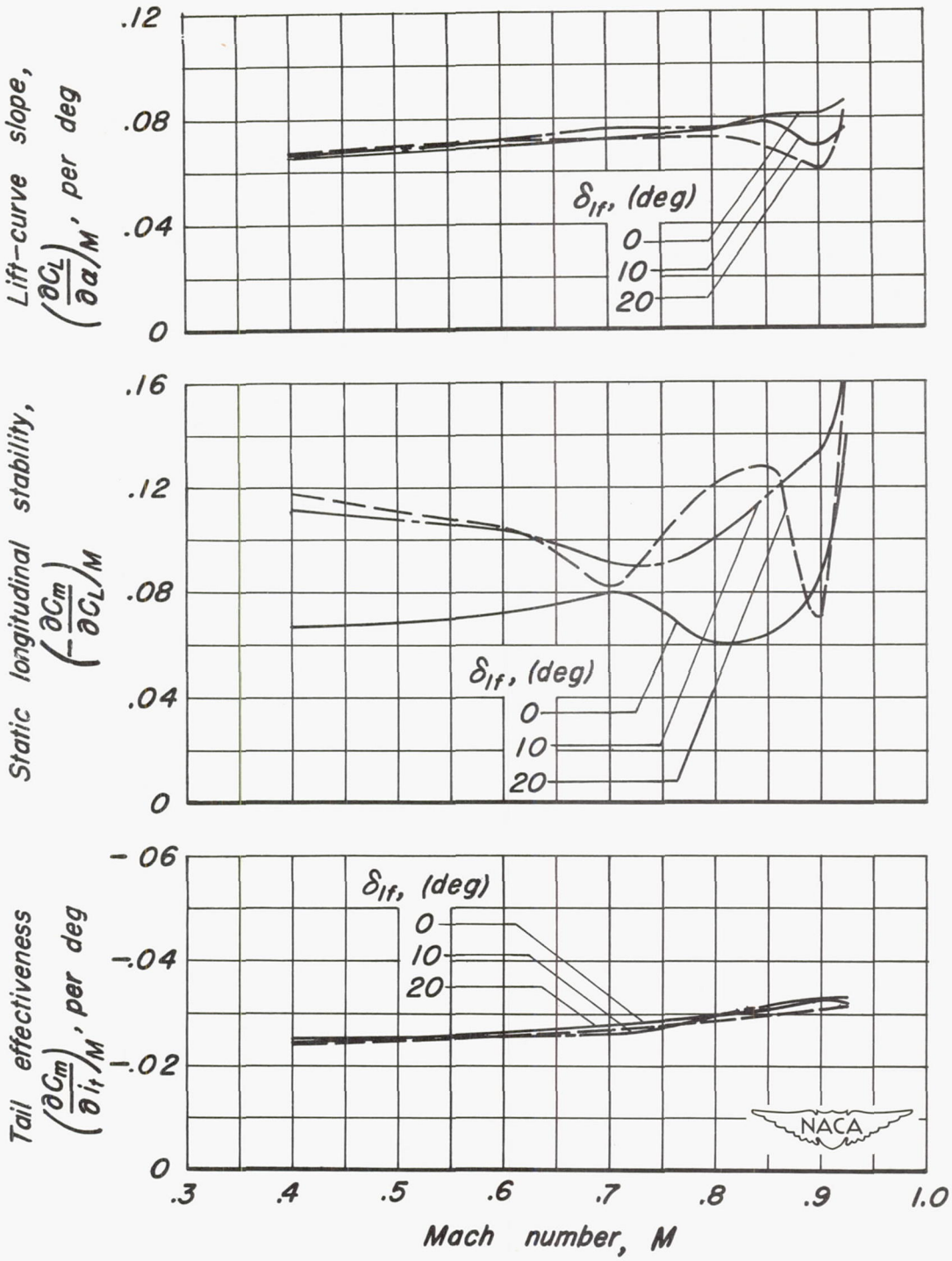

Figure 10.– The variation of lift-curve slope, static longitudinal stability, and tail effectiveness with Mach number for the X-3 model. i_t, -2°; C_L, 0.3.

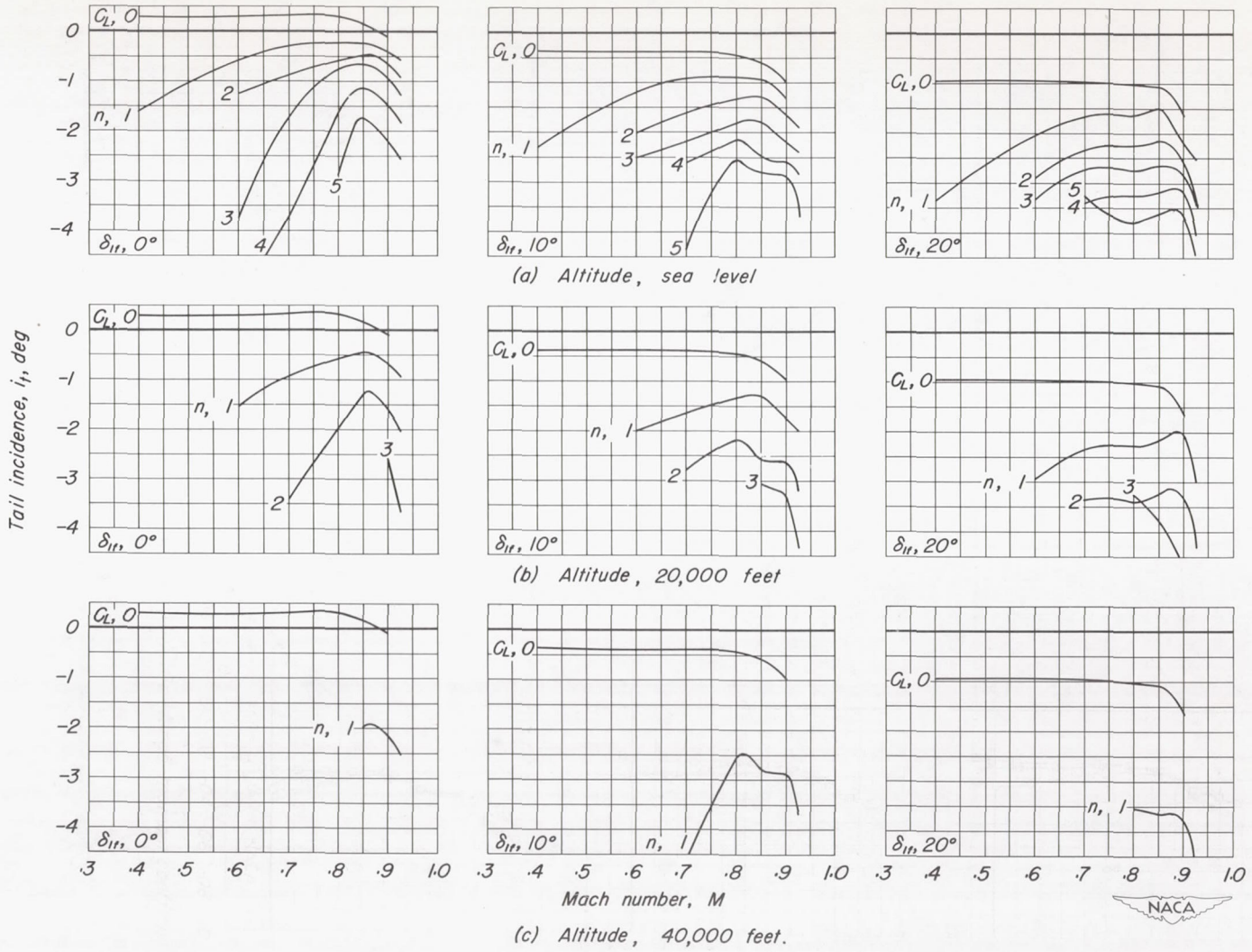

Figure 11.–The calculated tail incidence required by the X-3 airplane. Wing loading, 120 pounds per square foot.

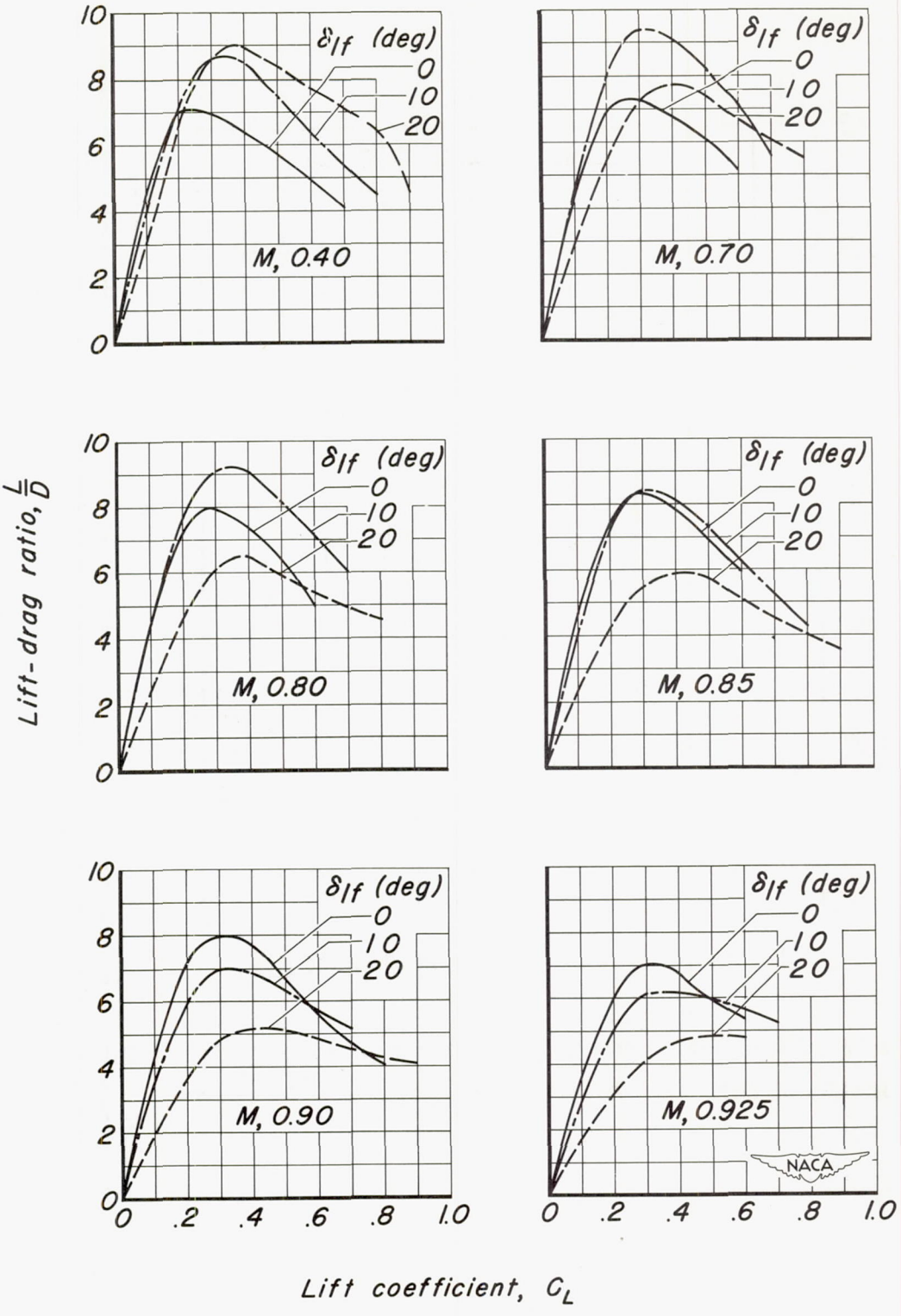

Figure 12.- The lift-drag ratios of the X-3 model. i_t, -2°.

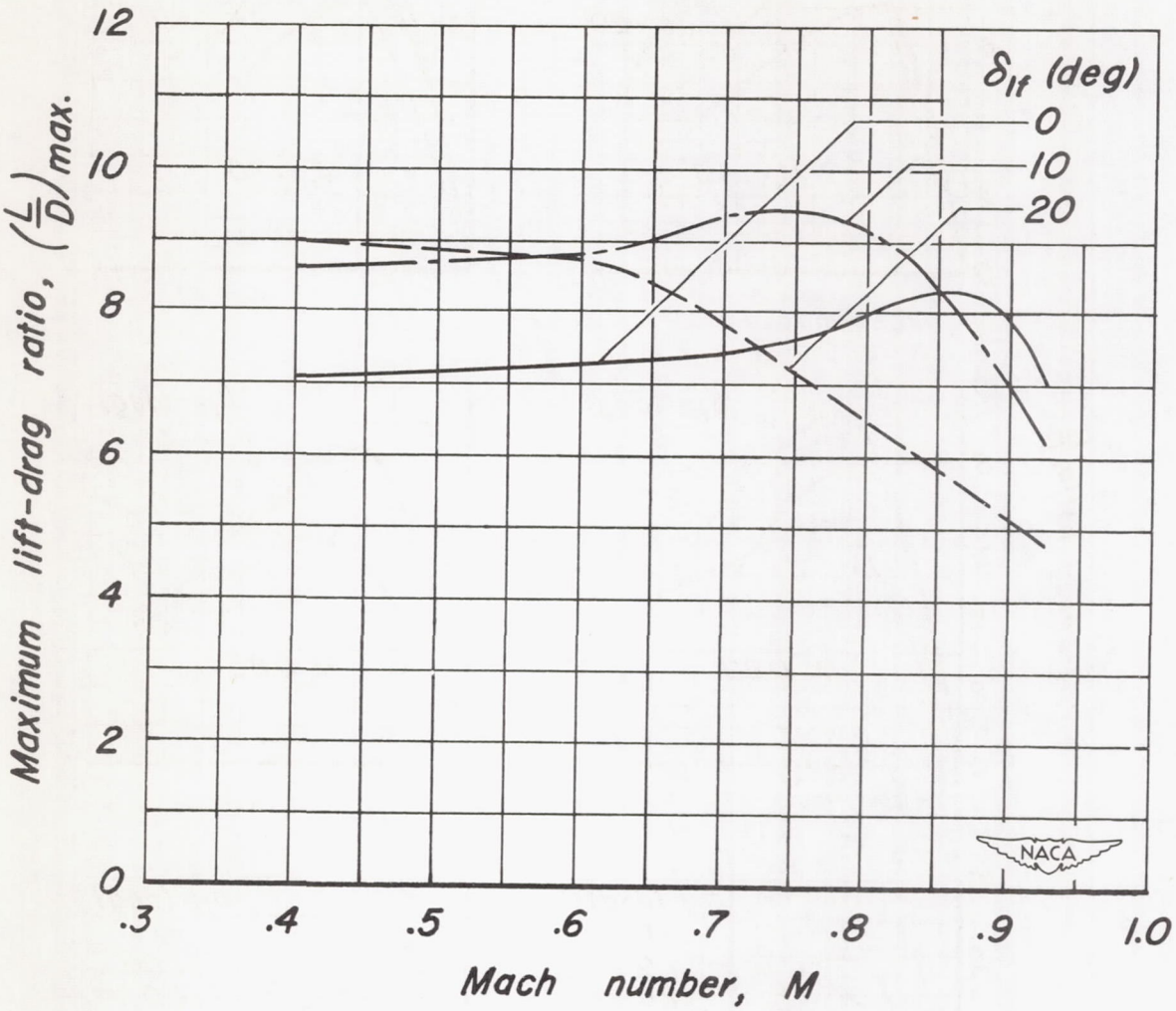

Figure 13.– The variation of maximum lift-drag ratio with Mach number for the X-3 model. i_f, -2°

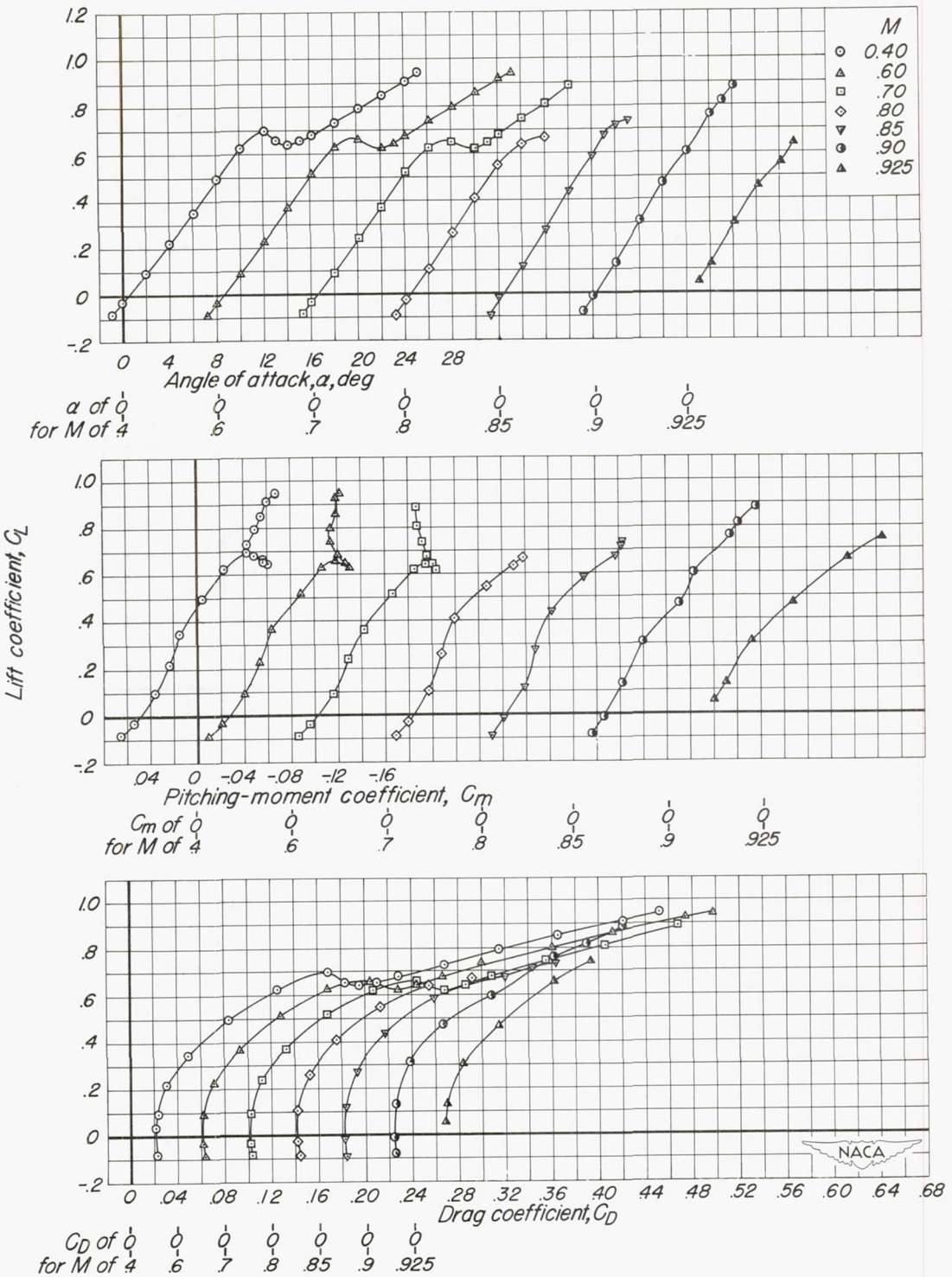

Figure 14.—The aerodynamic characteristics of the X-3 model without the canopy. δ_{lf}, 0°; i_t, -2°.

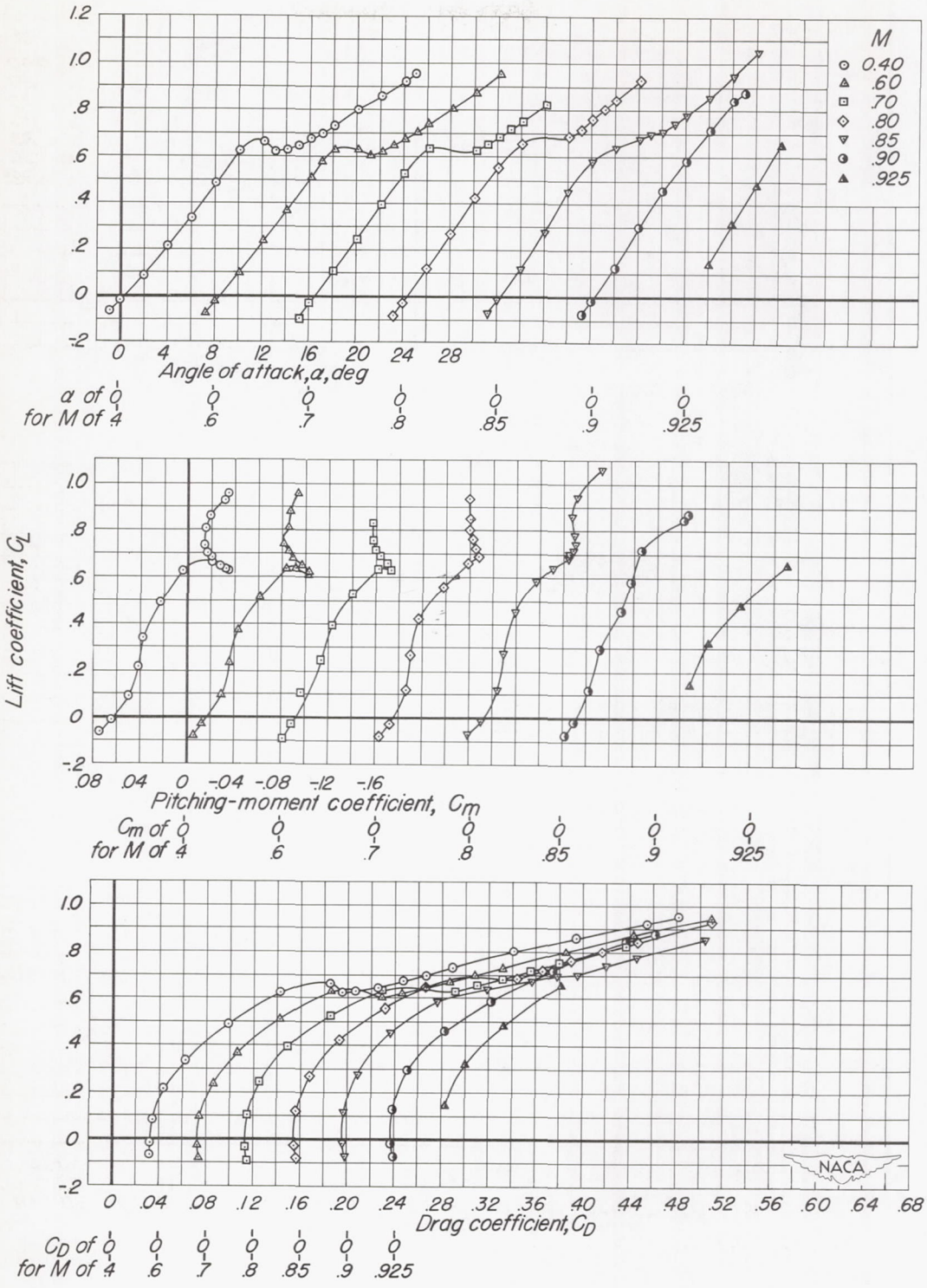

Figure 15.– The aerodynamic characteristics of the X-3 model with air scoops but without the canopy. δ_{lf}, 0°; i_t, -2°.

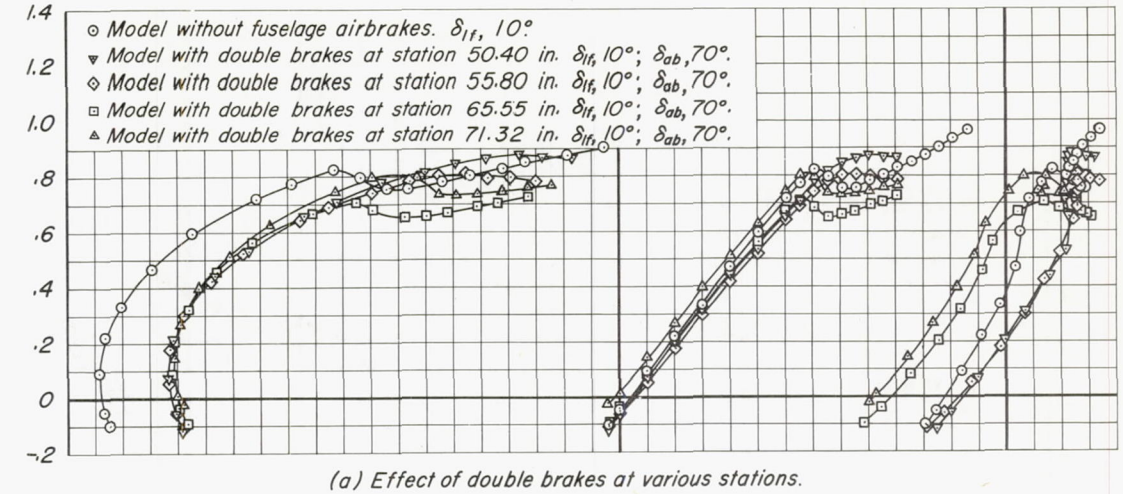

(a) Effect of double brakes at various stations.

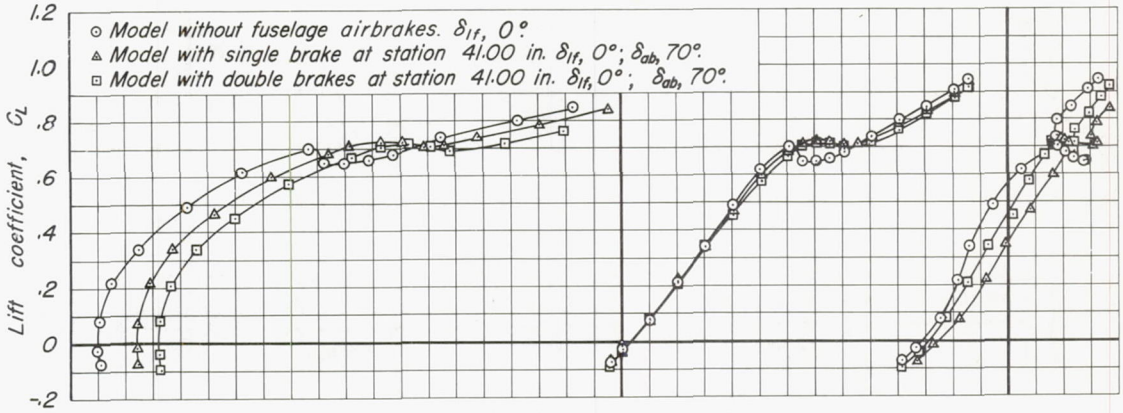

(b) Effect of brakes at station 41.00 in.

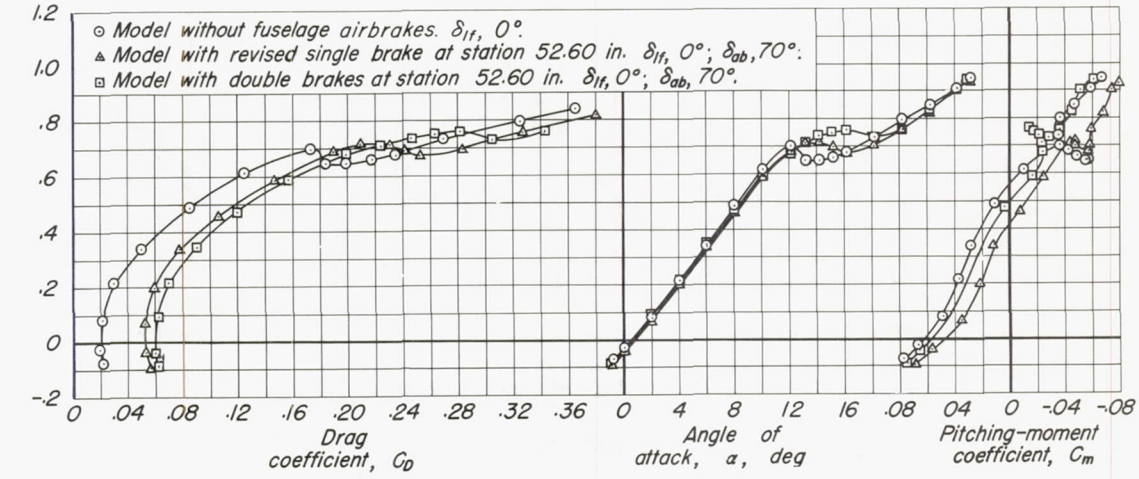

(c) Effect of brakes at station 52.60. in.

NACA

Figure 16.–The aerodynamic characteristics of the X-3 model equipped with airbrakes. Mach number, 0.40.

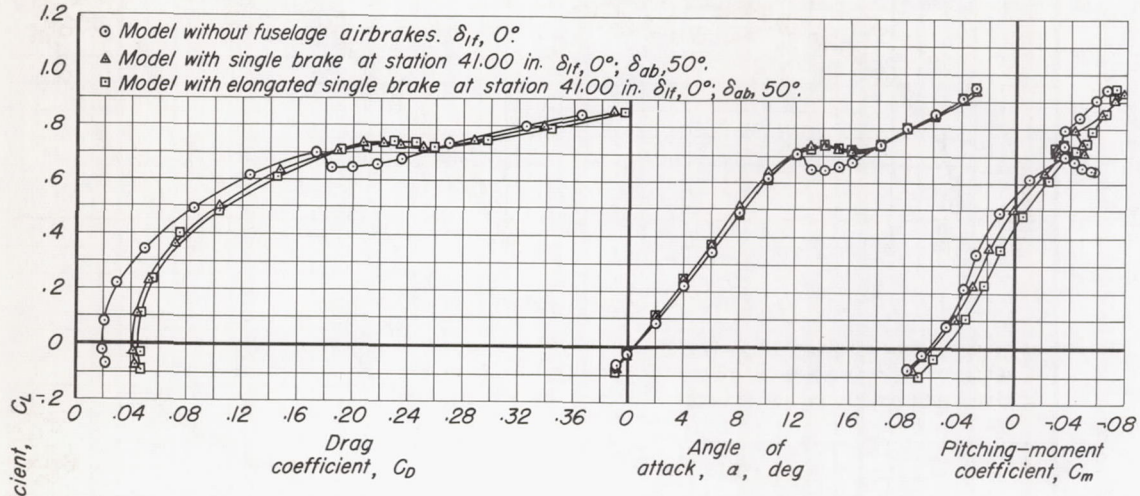

(d) Effect of elongating the chord of the single brake.

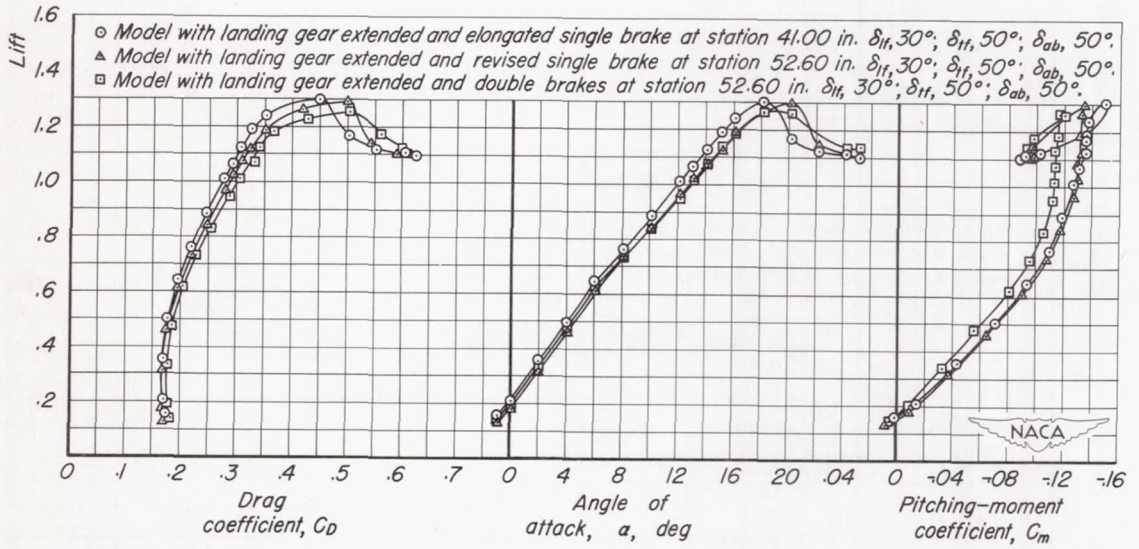

(e) Landing gear extended.

Figure 16.–Concluded.

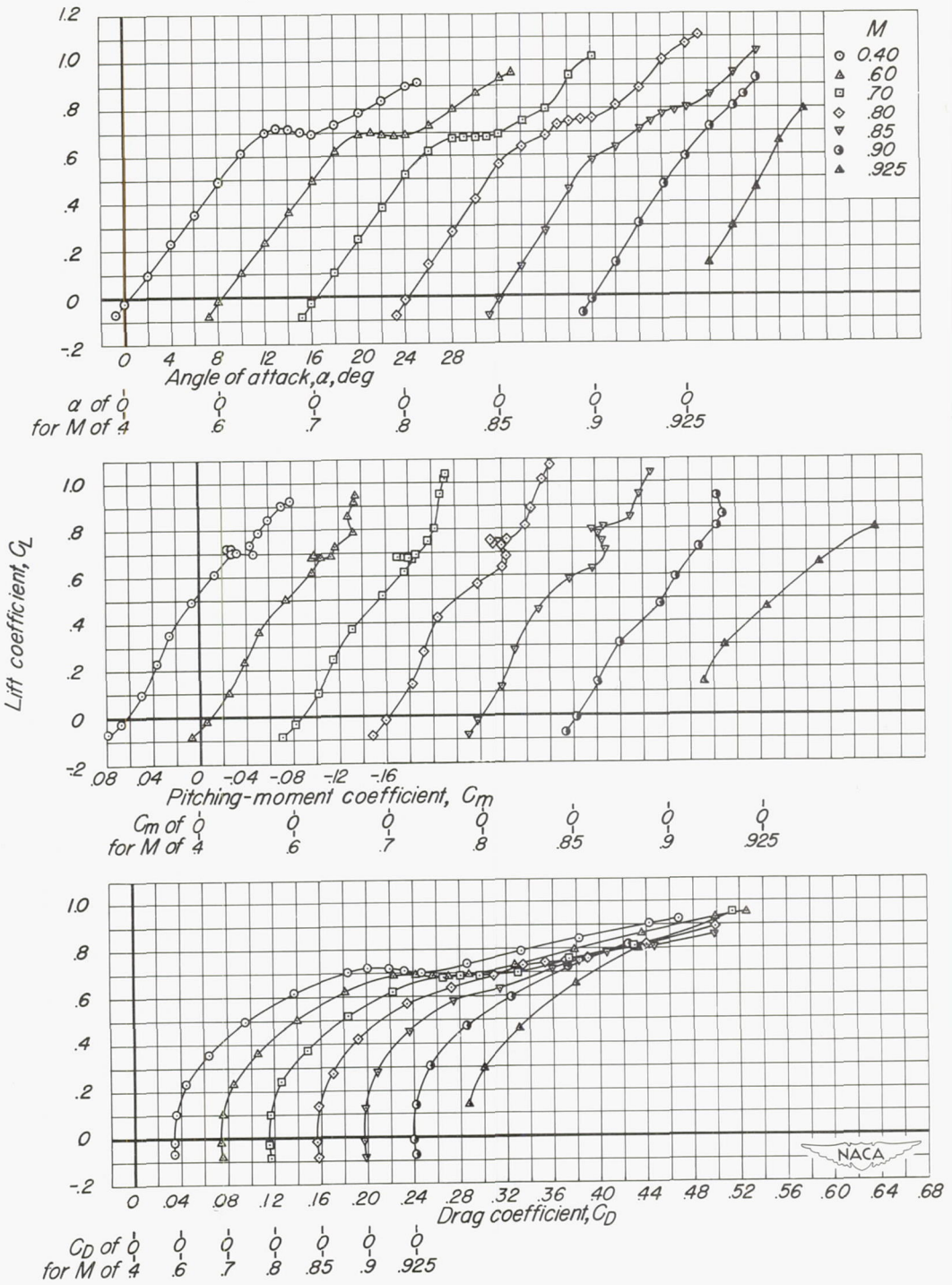

(a) Airbrake angle, 30°.

Figure 17.– The aerodynamic characteristics of the X-3 model with the single airbrake at station 41.00 in. δ_{1f}, 0°; i_f, -2°.

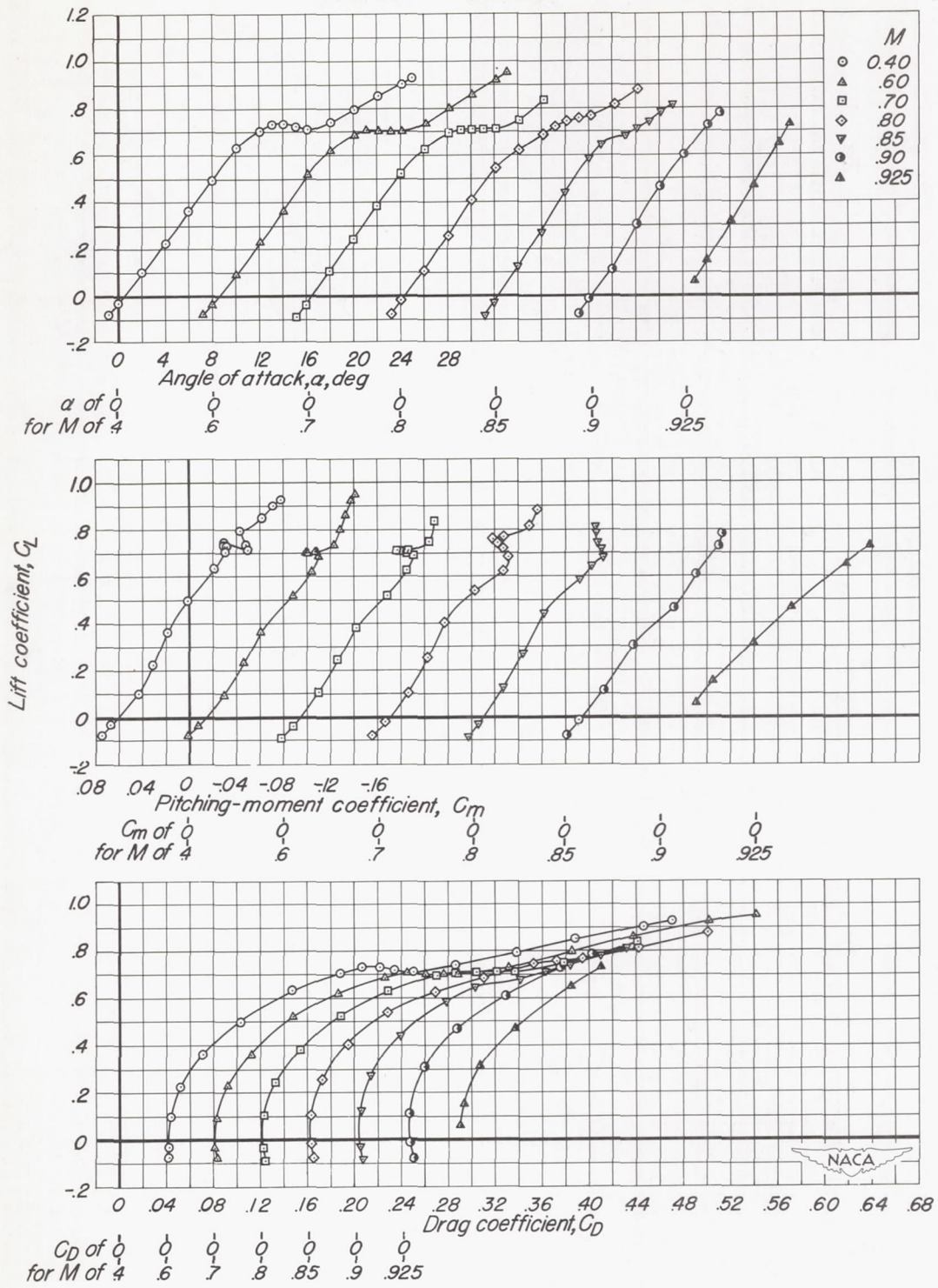

(b) Airbrake angle, 50°.

Figure 17.– Continued.

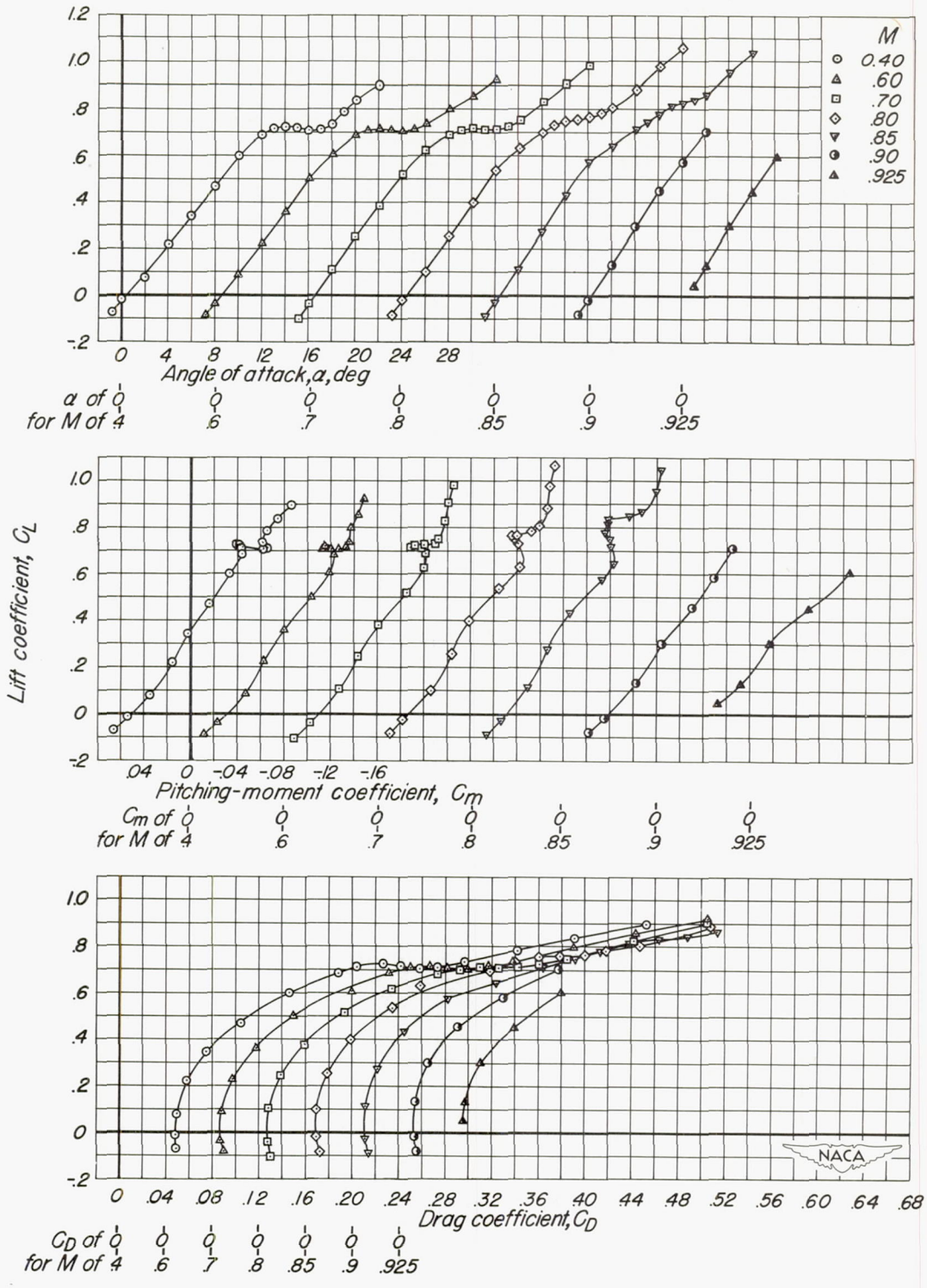

(c) Airbrake angle, 70°.

Figure 17.– Continued.

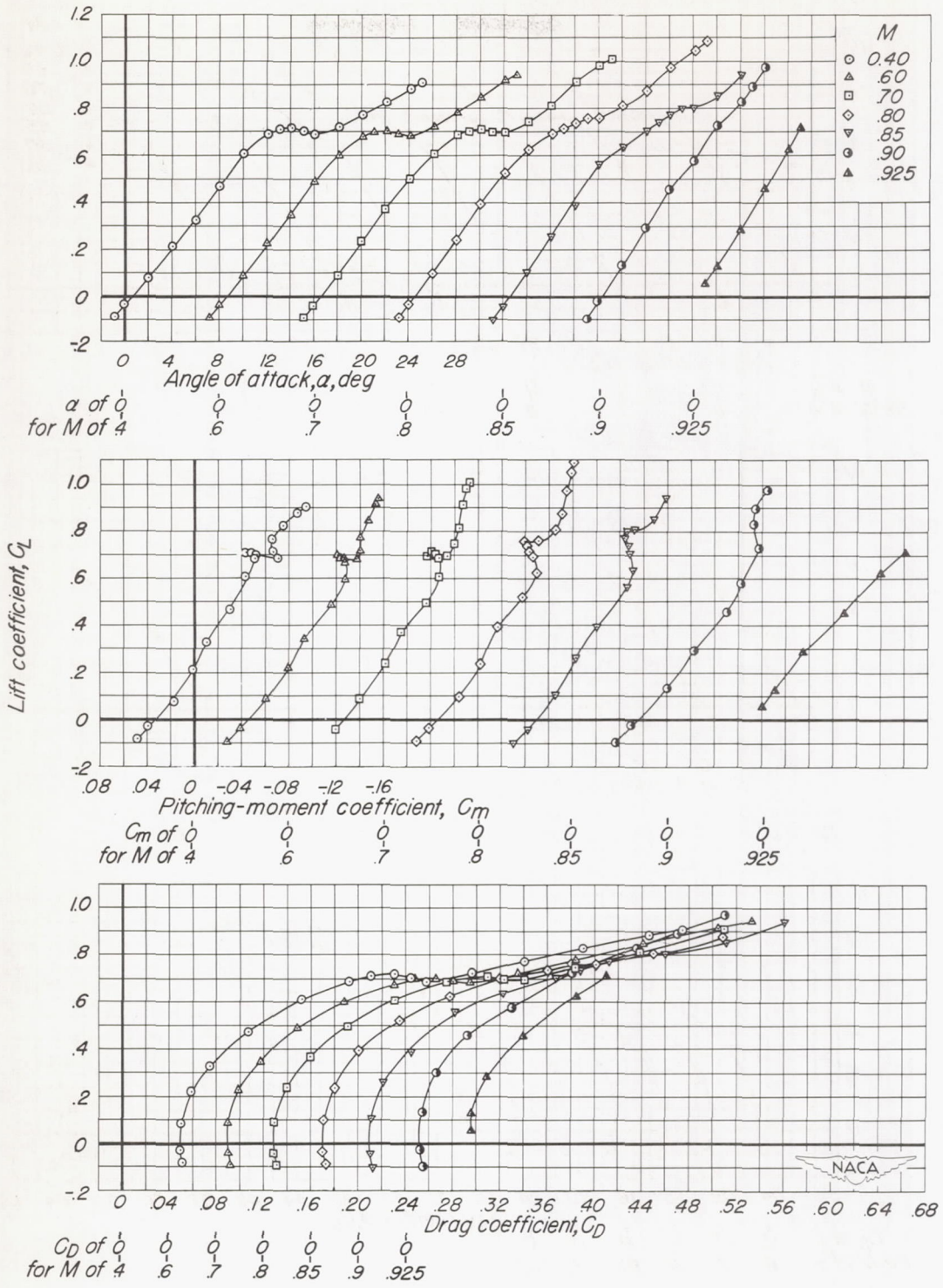

(d) Airbrake angle, 90°.

Figure 17.— Concluded.

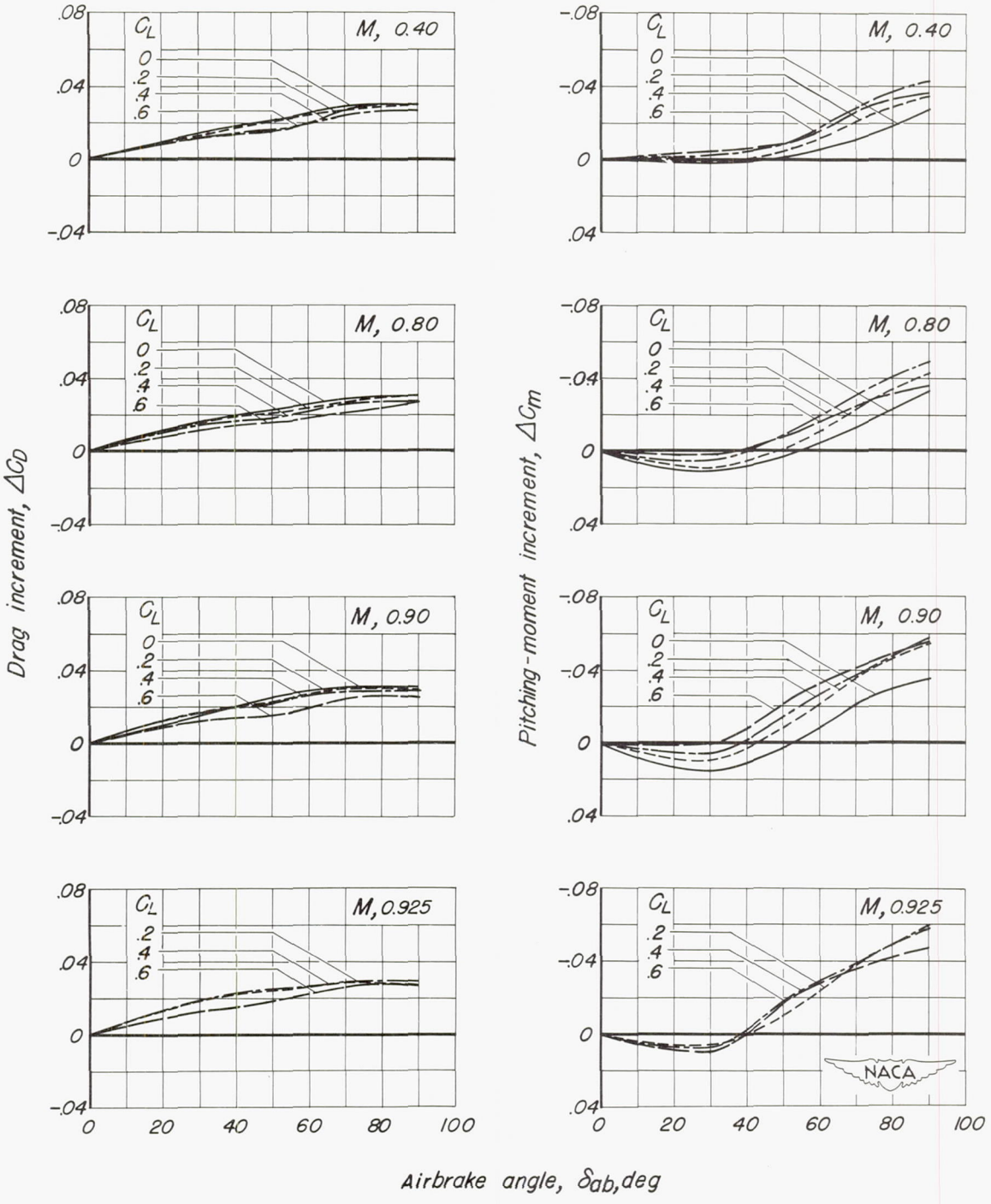

Figure 18.- The increment of drag and pitching-moment coefficient from deflecting the single brake at station 41.00 in. δ_{lf}, 0°; i_t, -2°.

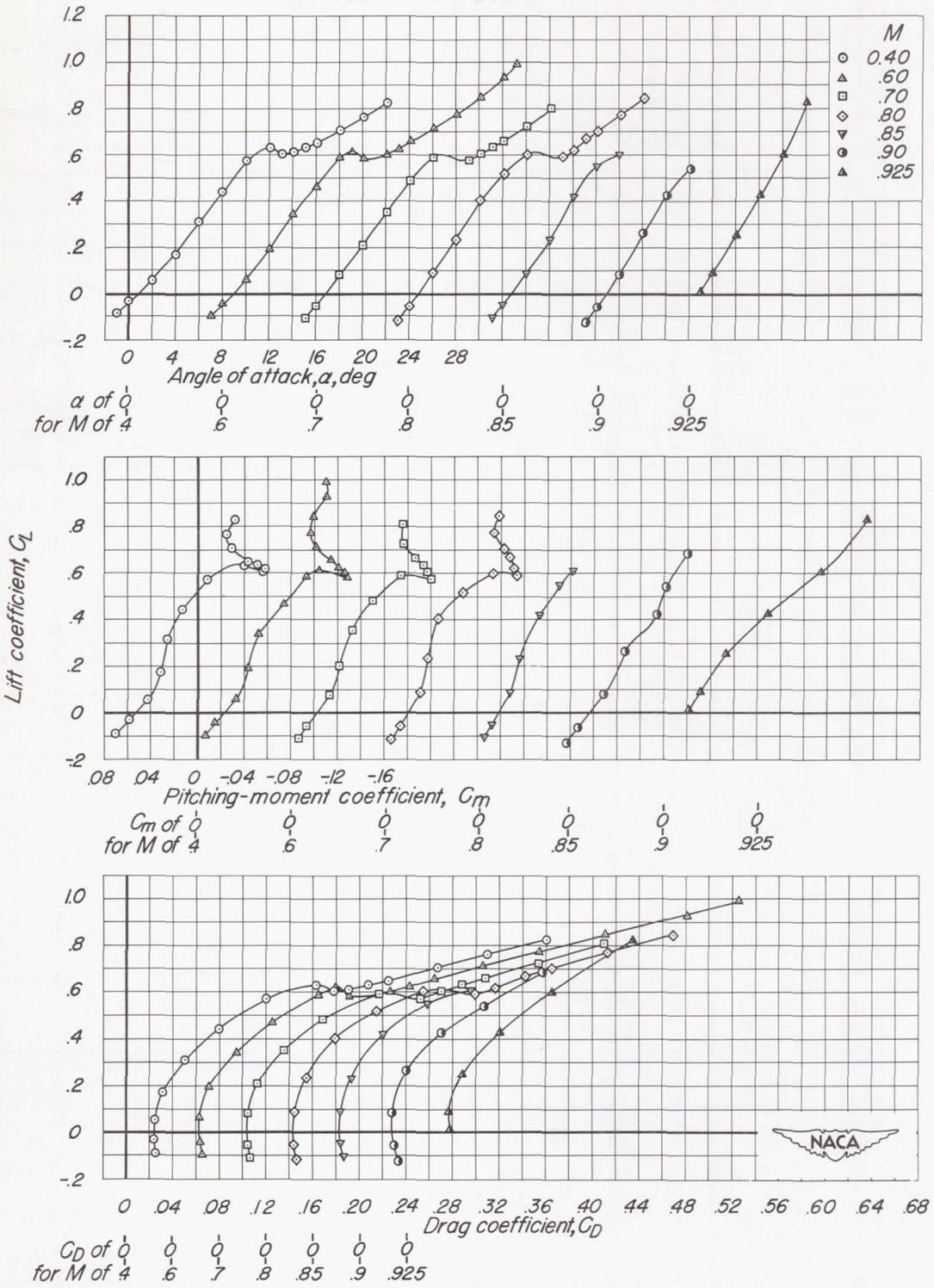

Figure 19.—The aerodynamic characteristics of the X-3 model with the underwing tanks. δ_{lf}, 0°; i_t, -2°.

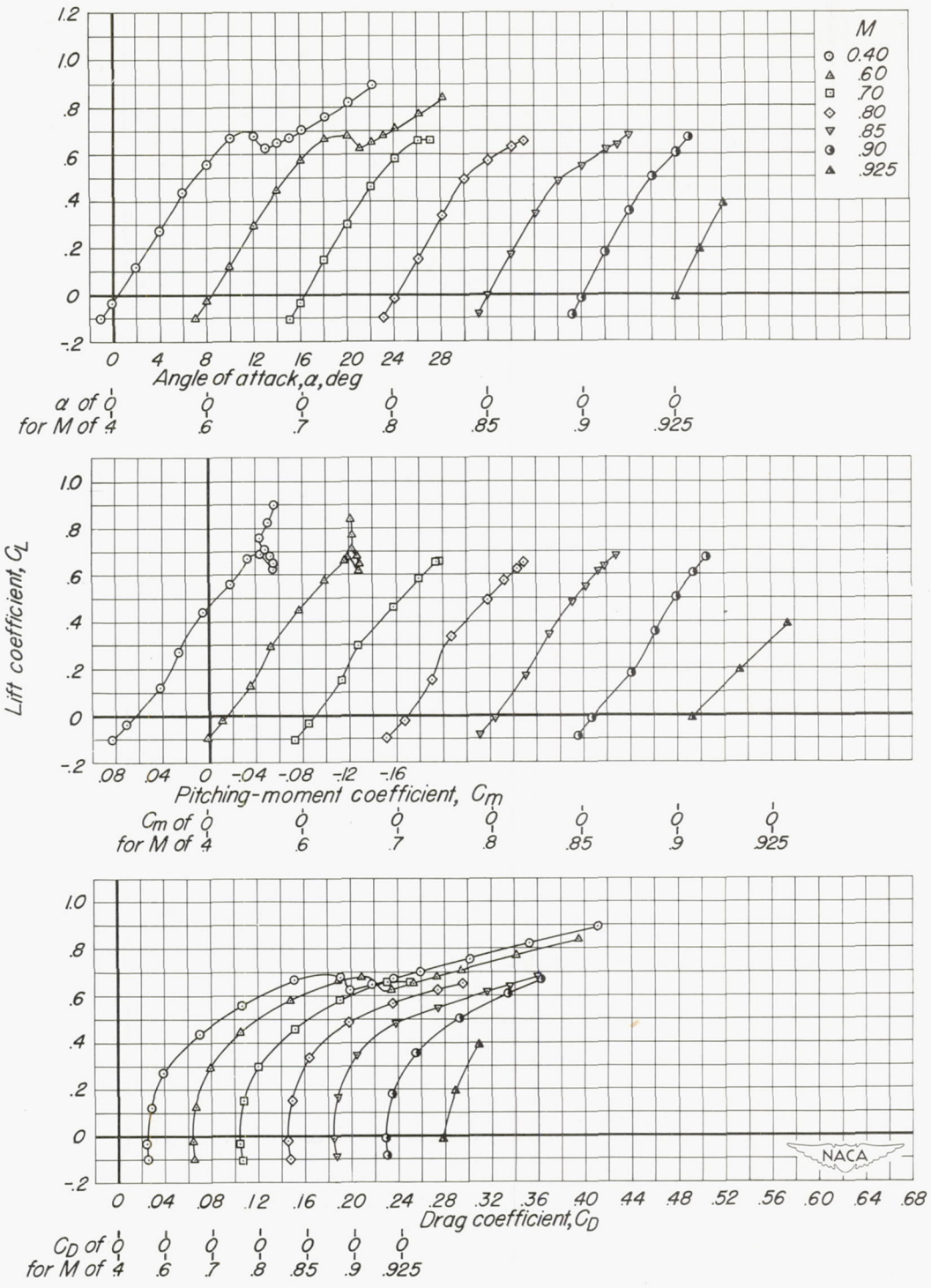

(a) Leading-edge-flap angle, 0.°

Figure 20.—The aerodynamic characteristics of the X-3 model with the wing-tip tanks. i_t, -2°.

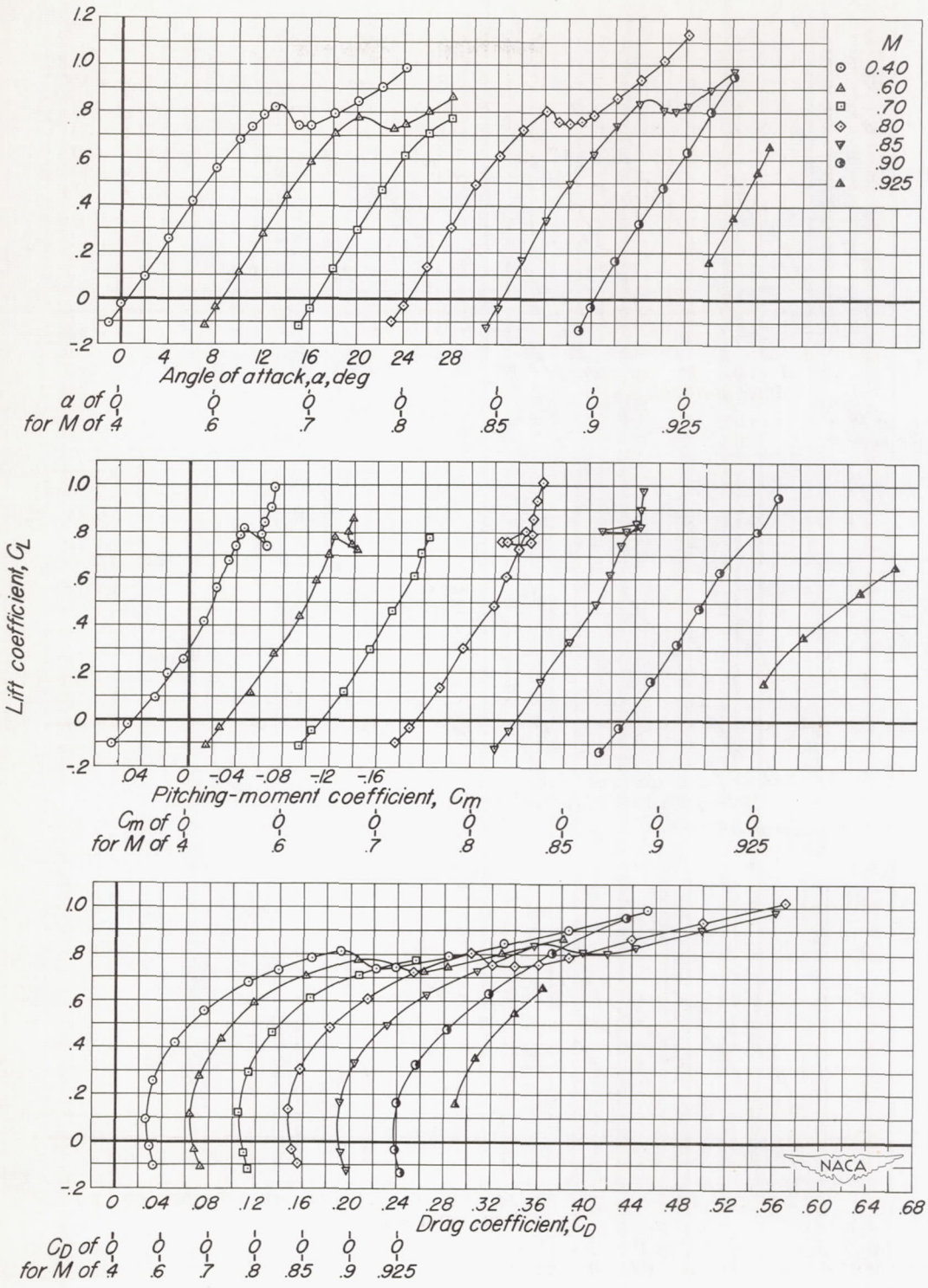

(b) Leading-edge-flap angle, 10°

Figure 20.- Continued.

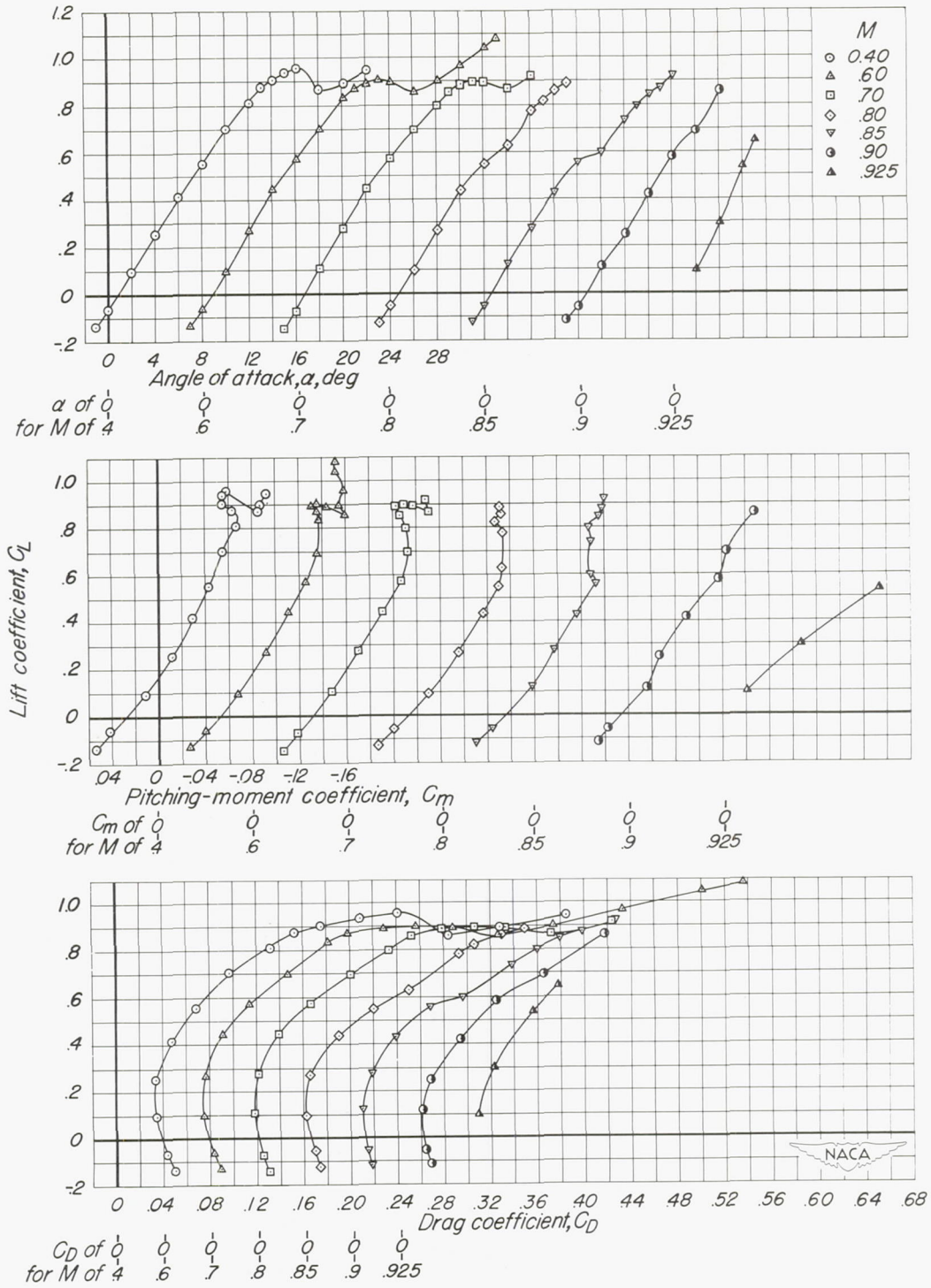

(c) Leading-edge-flap angle, 20°

Figure 20.– Concluded.

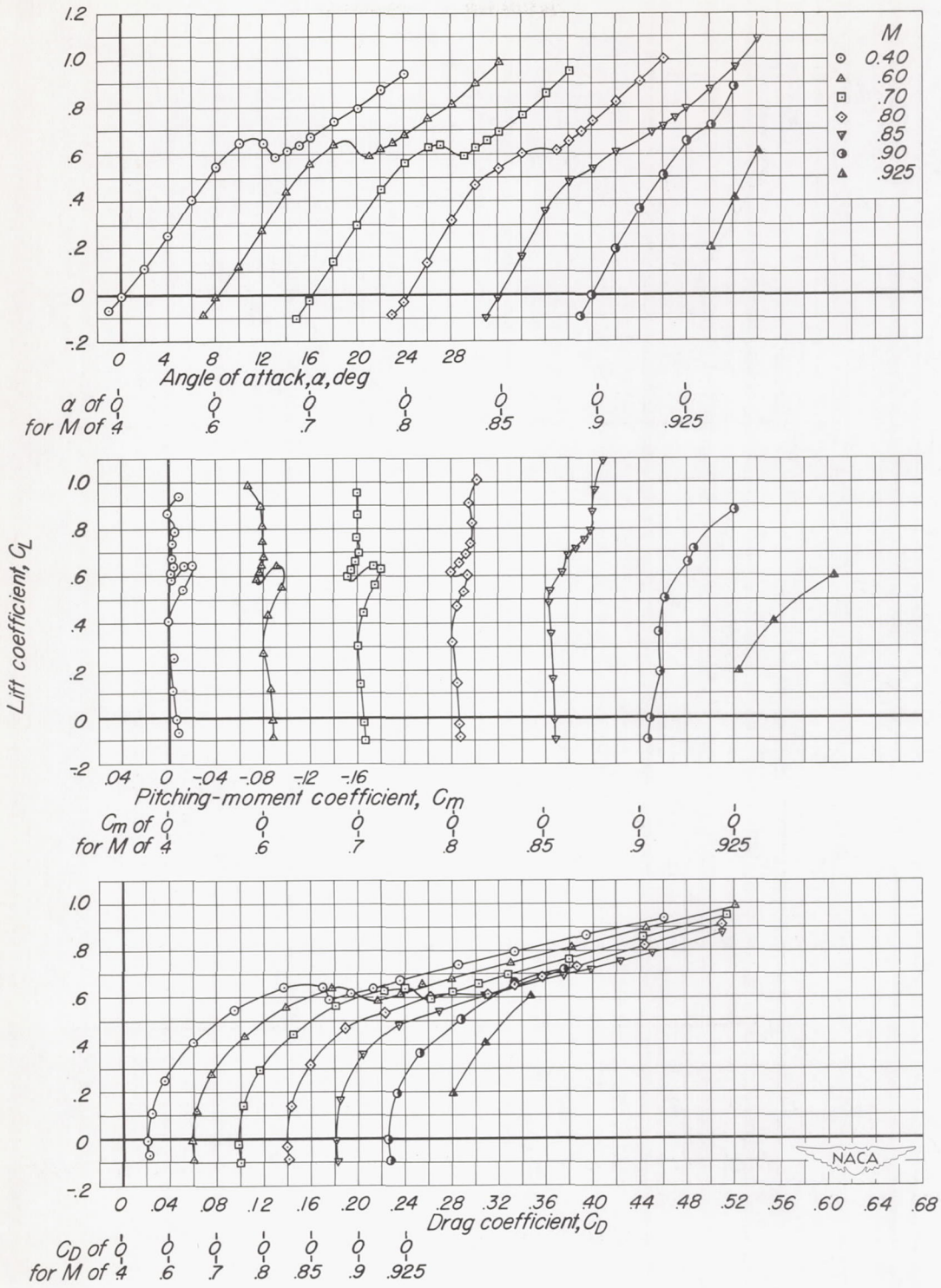

Figure 21.- The aerodynamic characteristics of the X-3 model with the wing-tip tanks but without the empennage. δ_{1f}, 0°

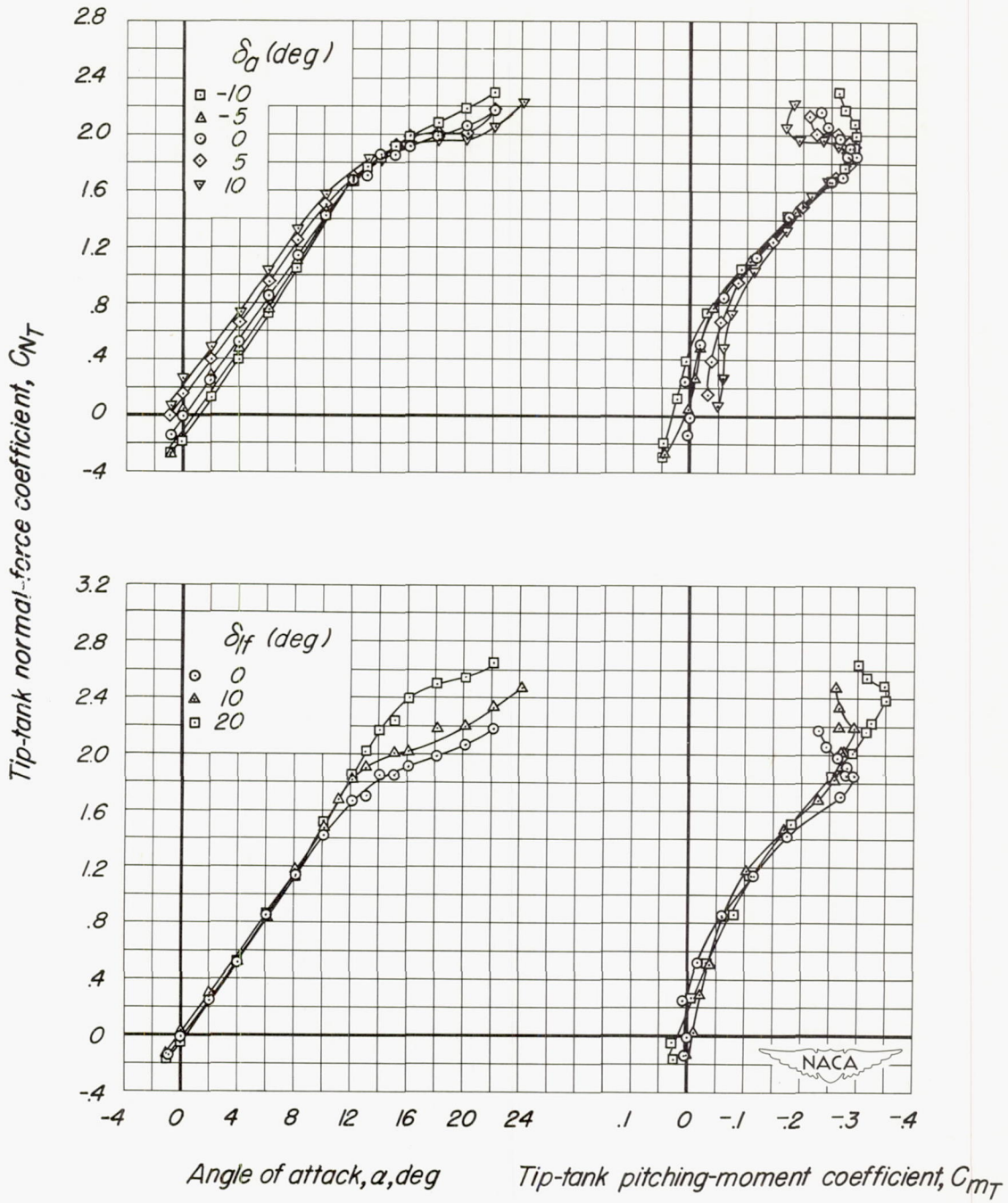

(a) Mach number, 0.40.

Figure 22.– The normal-force and pitching-moment characteristics of the wing-tip tanks on the X-3 model.

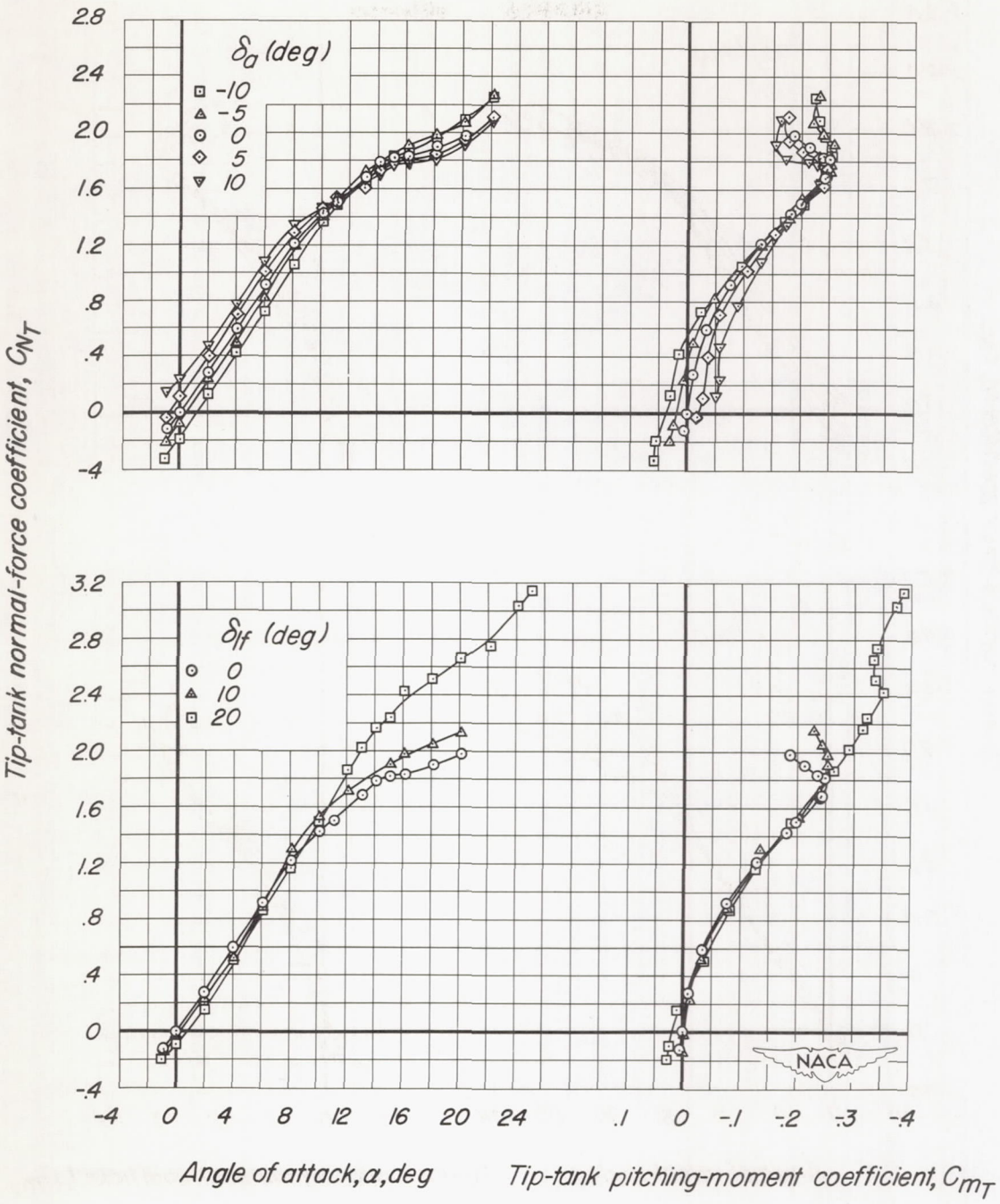

(b) Mach number, 0.60.

Figure 22.- Continued.

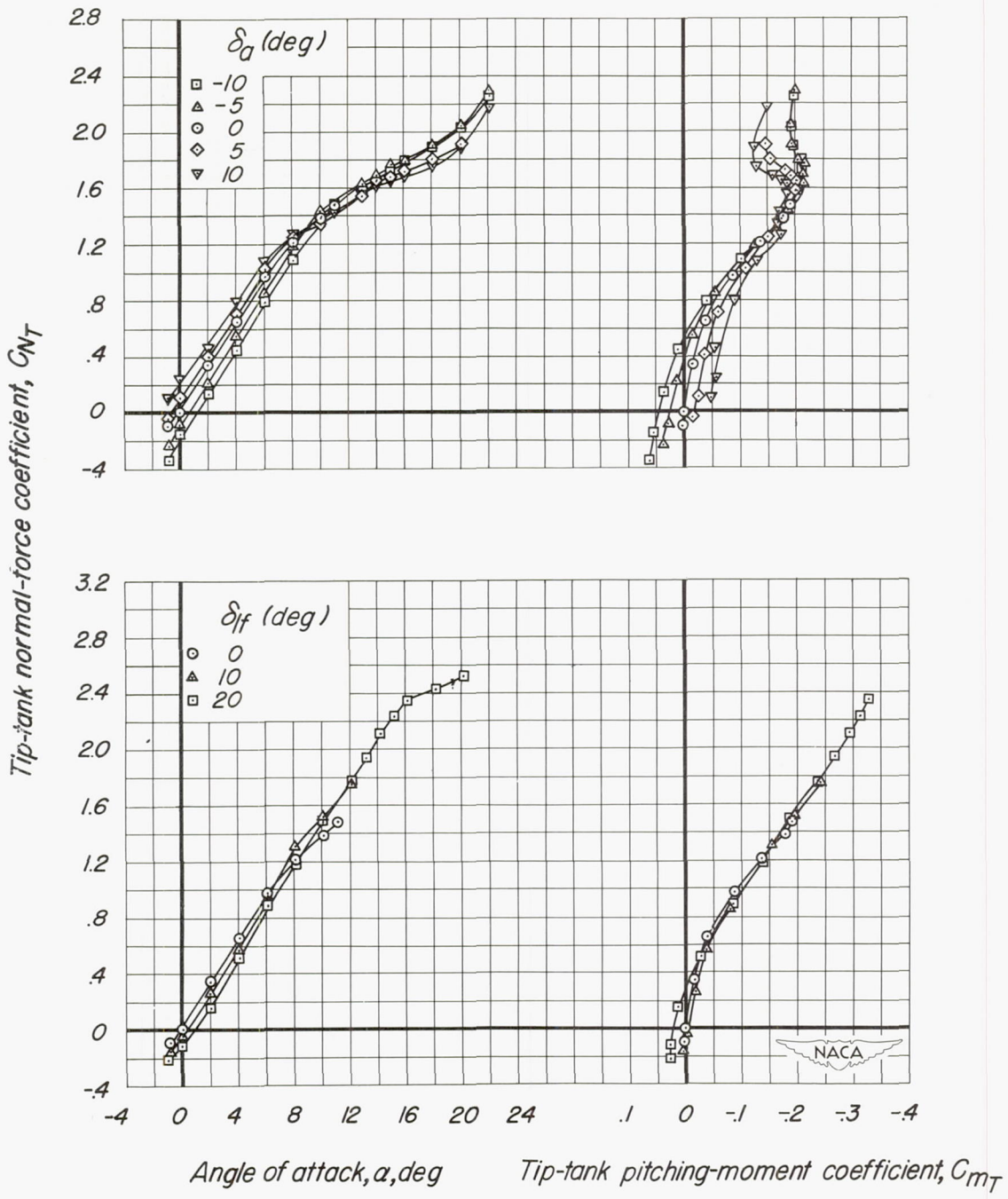

(c) Mach number, 0.70.

Figure 22.- Continued.

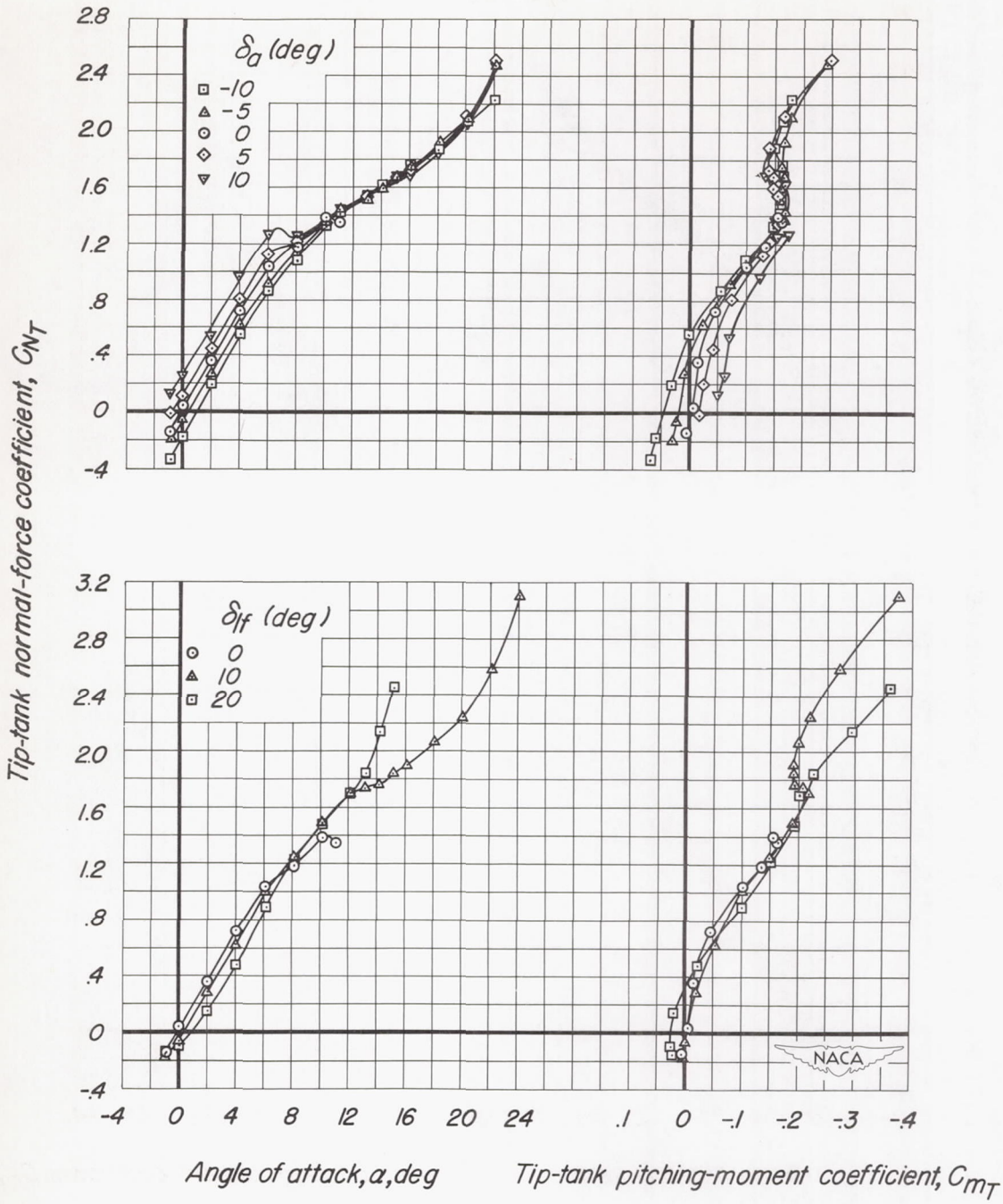

(d) Mach number, 0.80.

Figure 22.- Continued.

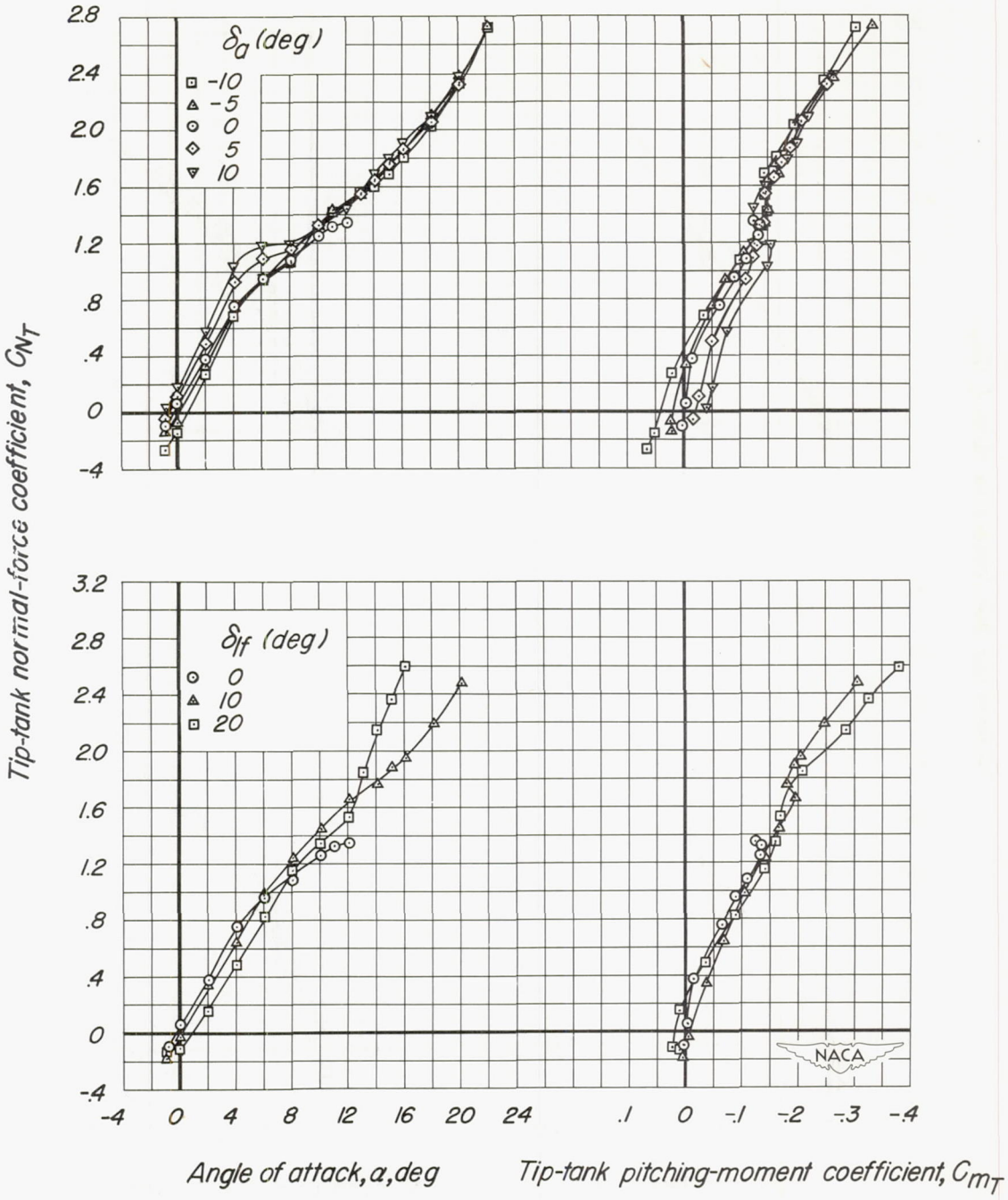

(e) Mach number, 0.85.

Figure 22.- Continued.

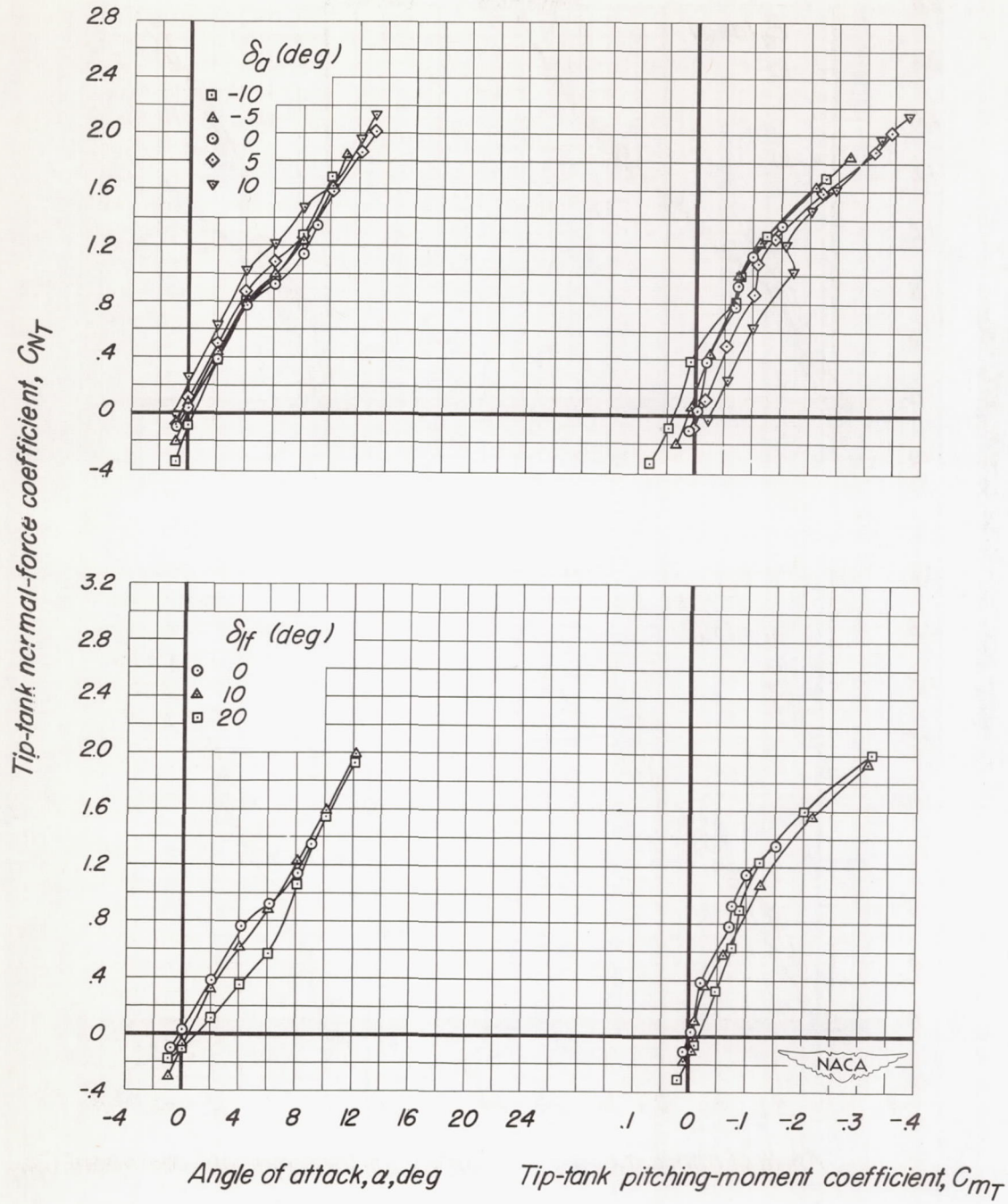

(f) Mach number, 0.90.

Figure 22.- Continued.

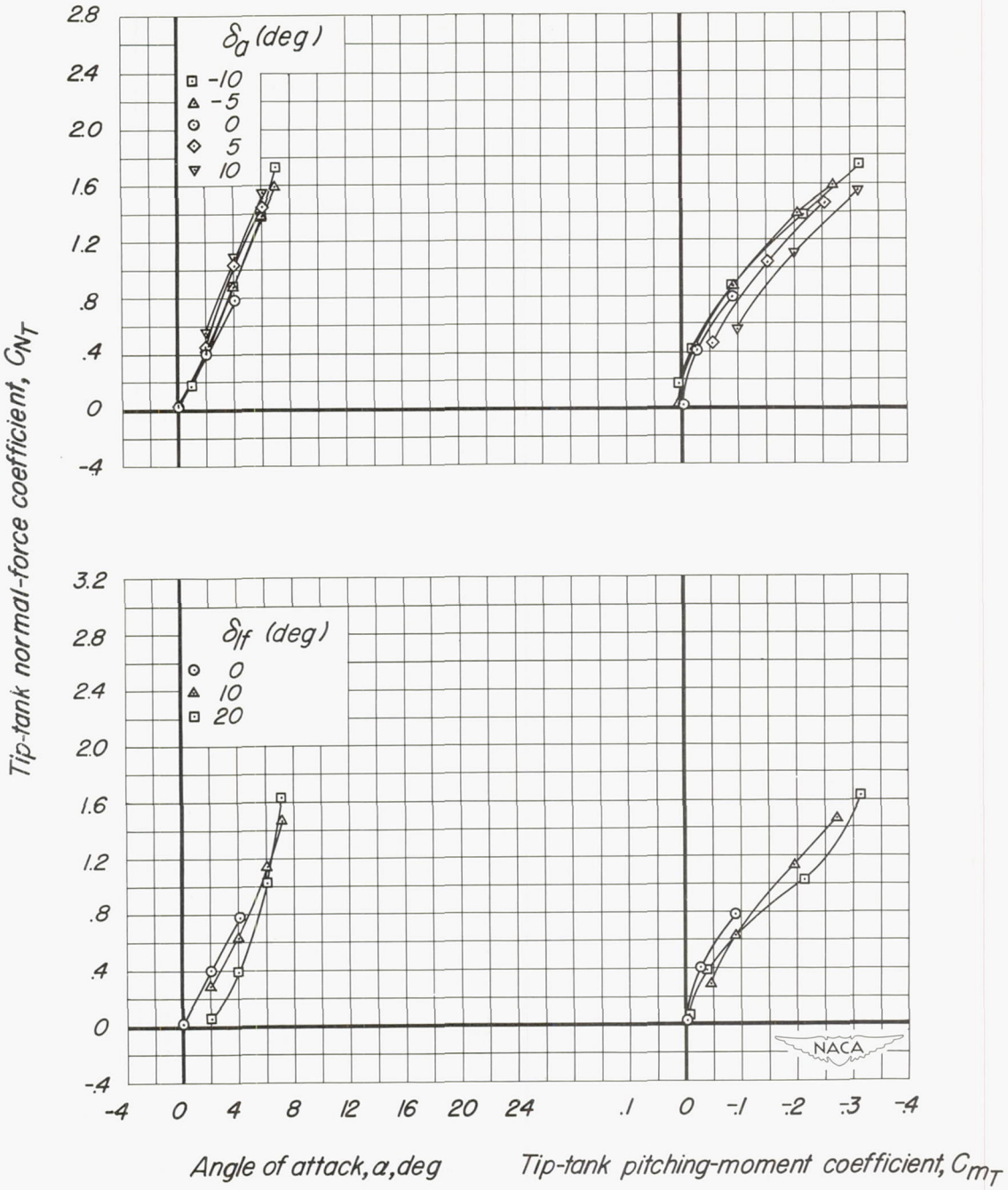

(g) Mach number, 0.925.

Figure 22.- Concluded.

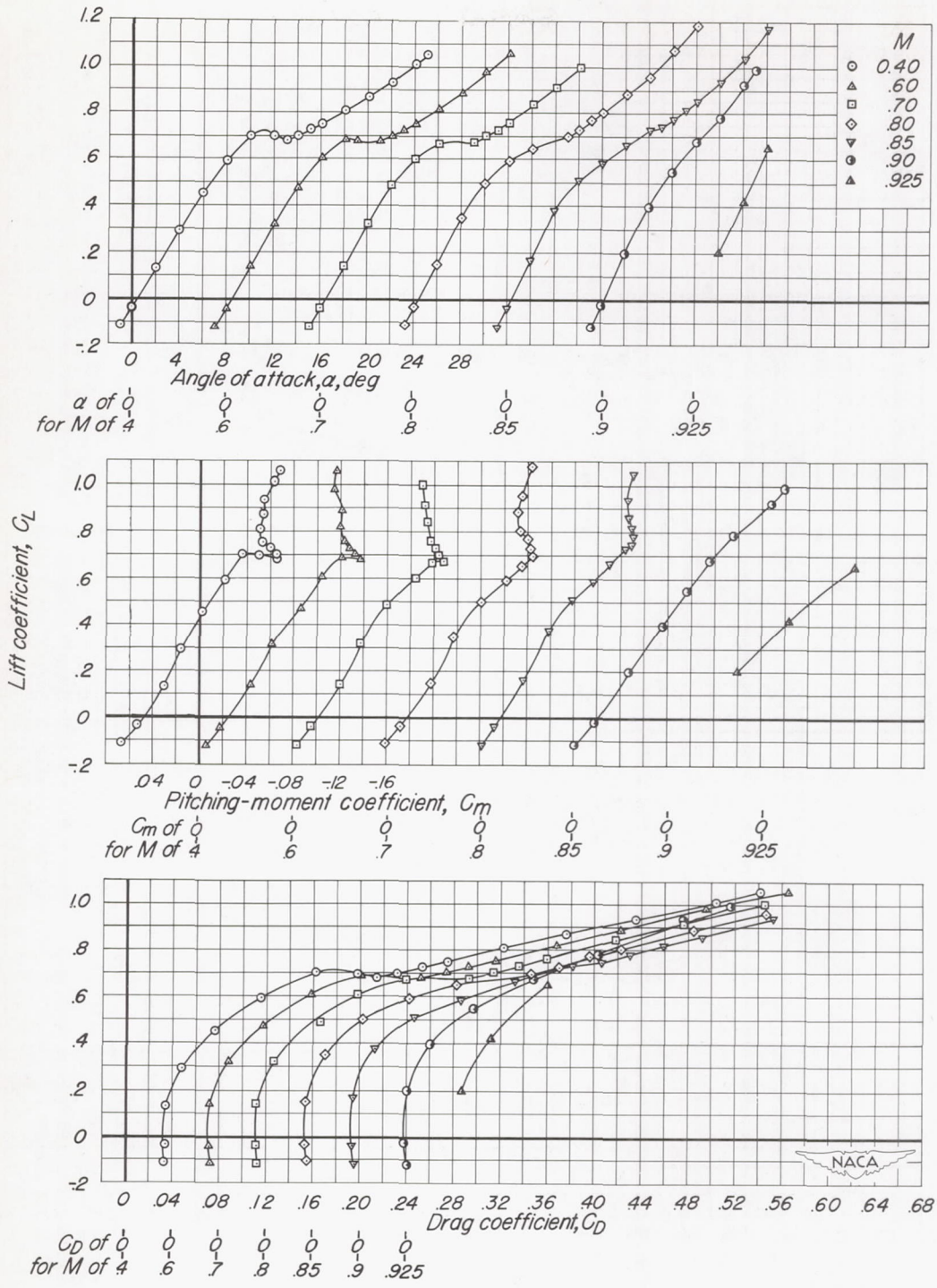

(a) Leading-edge-flap angle, 0.°

Figure 23.– The aerodynamic characteristics of the X-3 model with the wing-tip ram jets. i_t, -2°.

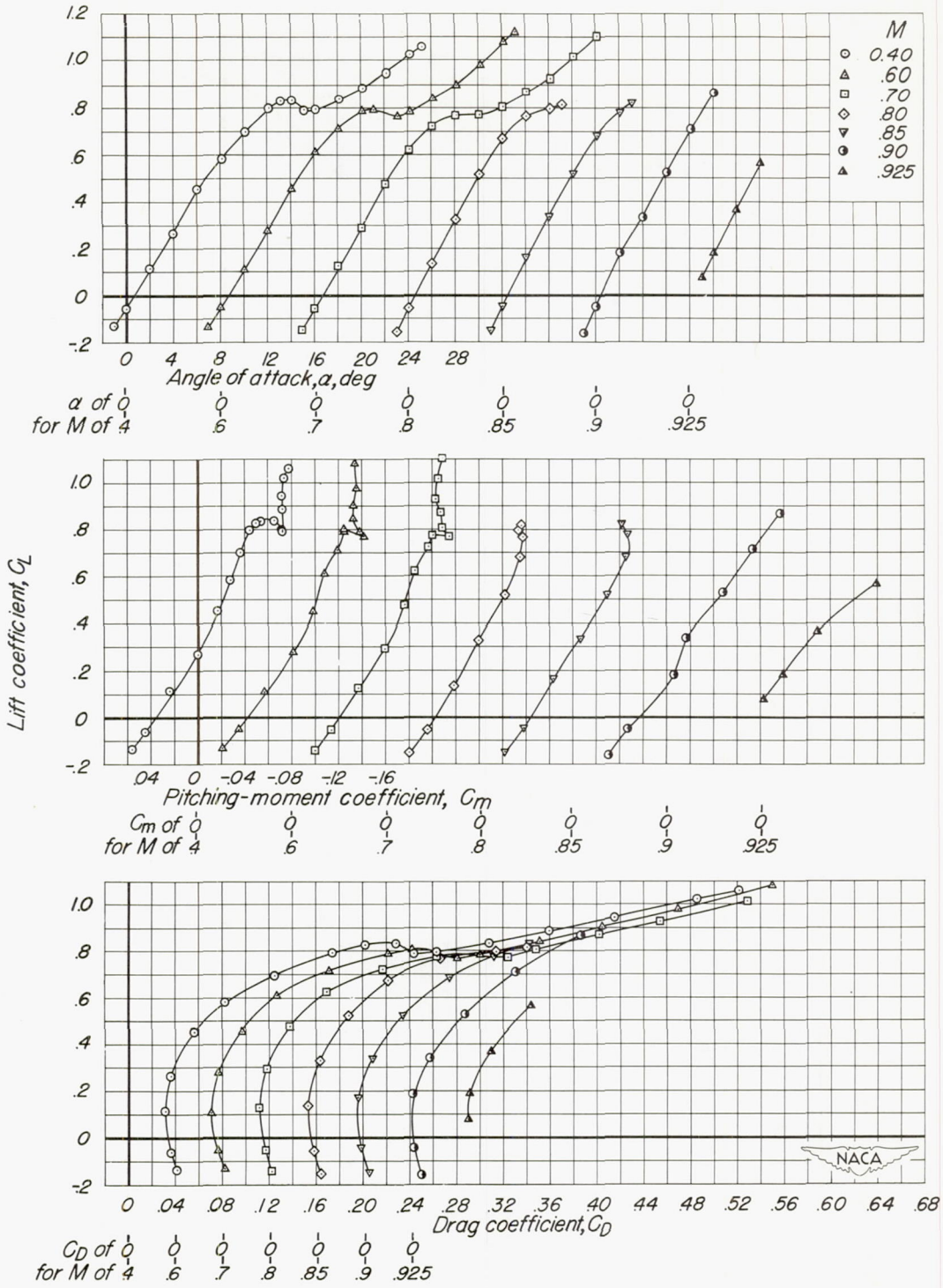

(b) Leading-edge-flap angle, 10°

Figure 23.- Continued.

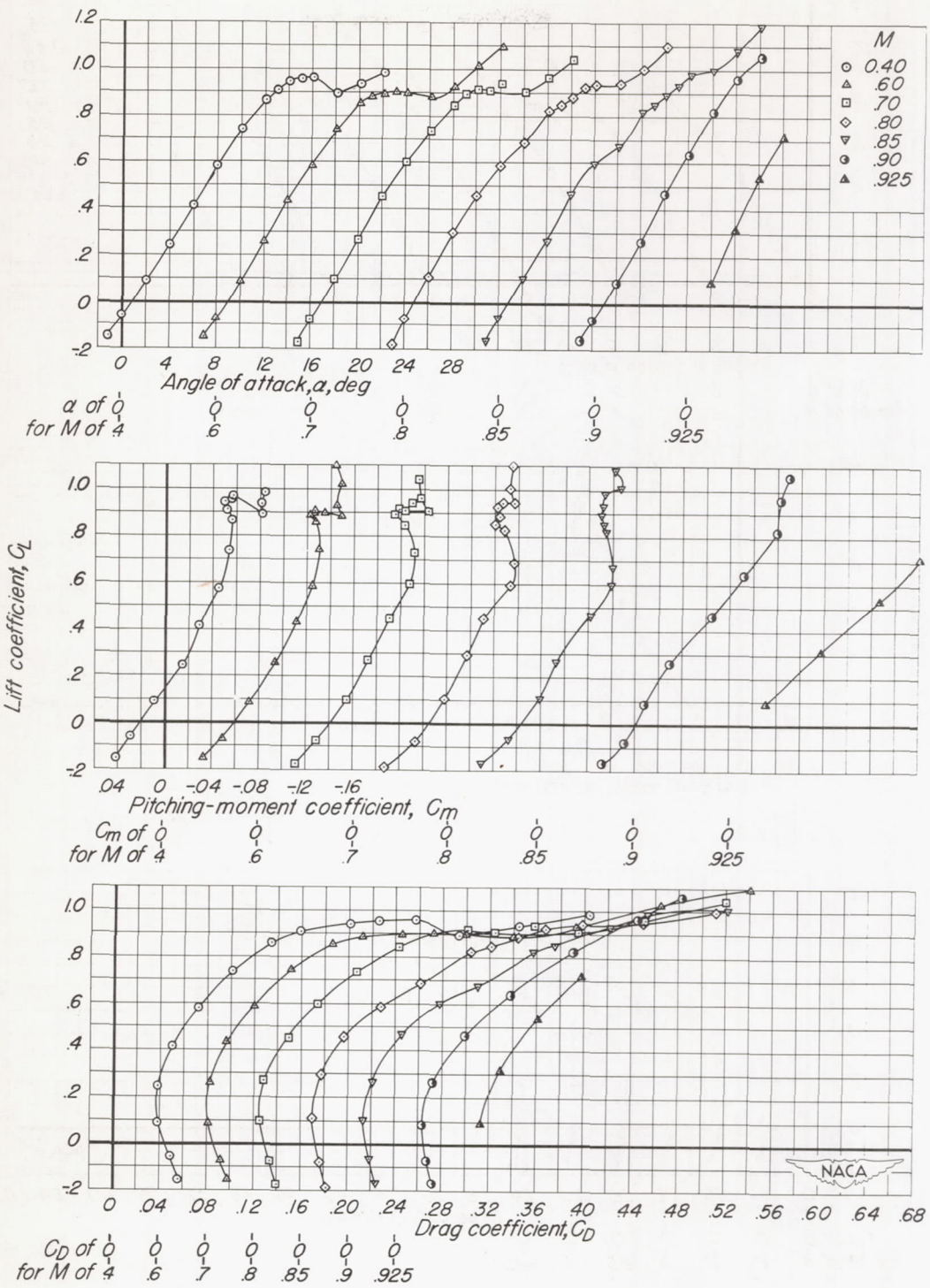

(c) Leading-edge-flap angle, 20°

Figure 23.– Concluded.

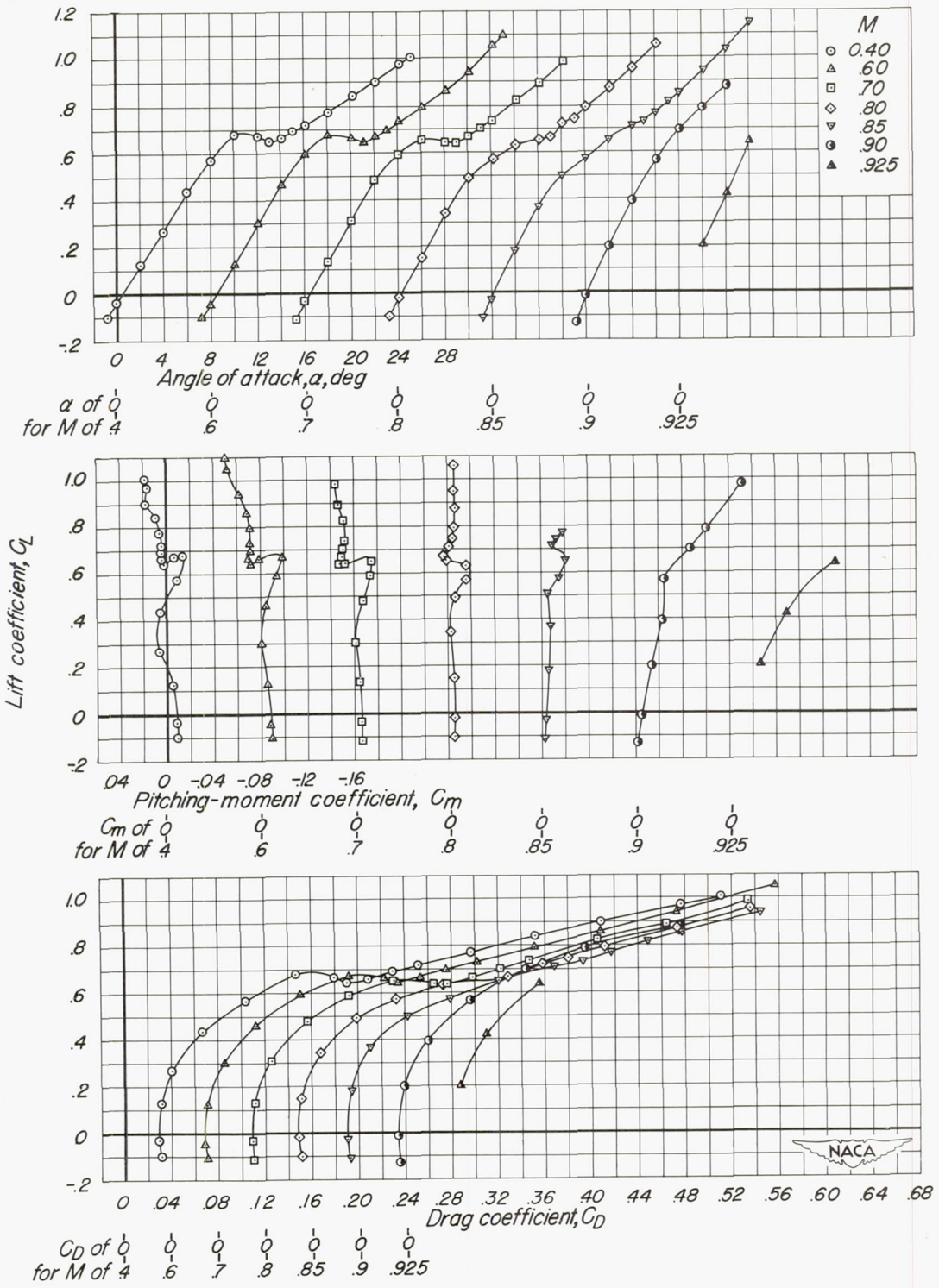

Figure 24.- The aerodynamic characteristics of the X-3 model with the wing-tip ram jets but without the empennage. δ_{lf}, 0°.

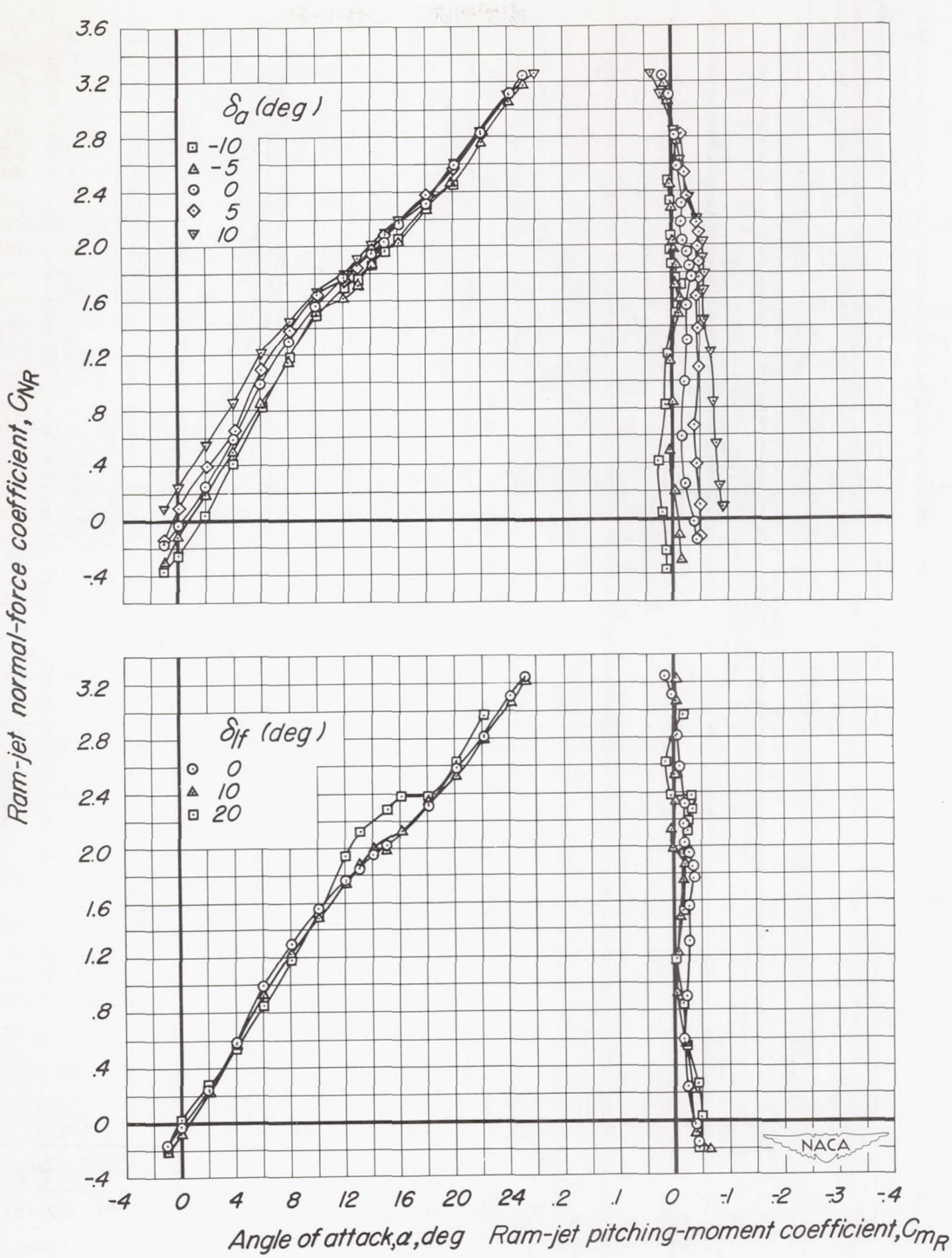

(a) Mach number, 0.40.

Figure 25.- The normal-force and pitching-moment characteristics of the wing-tip ram jet on the X-3 model.

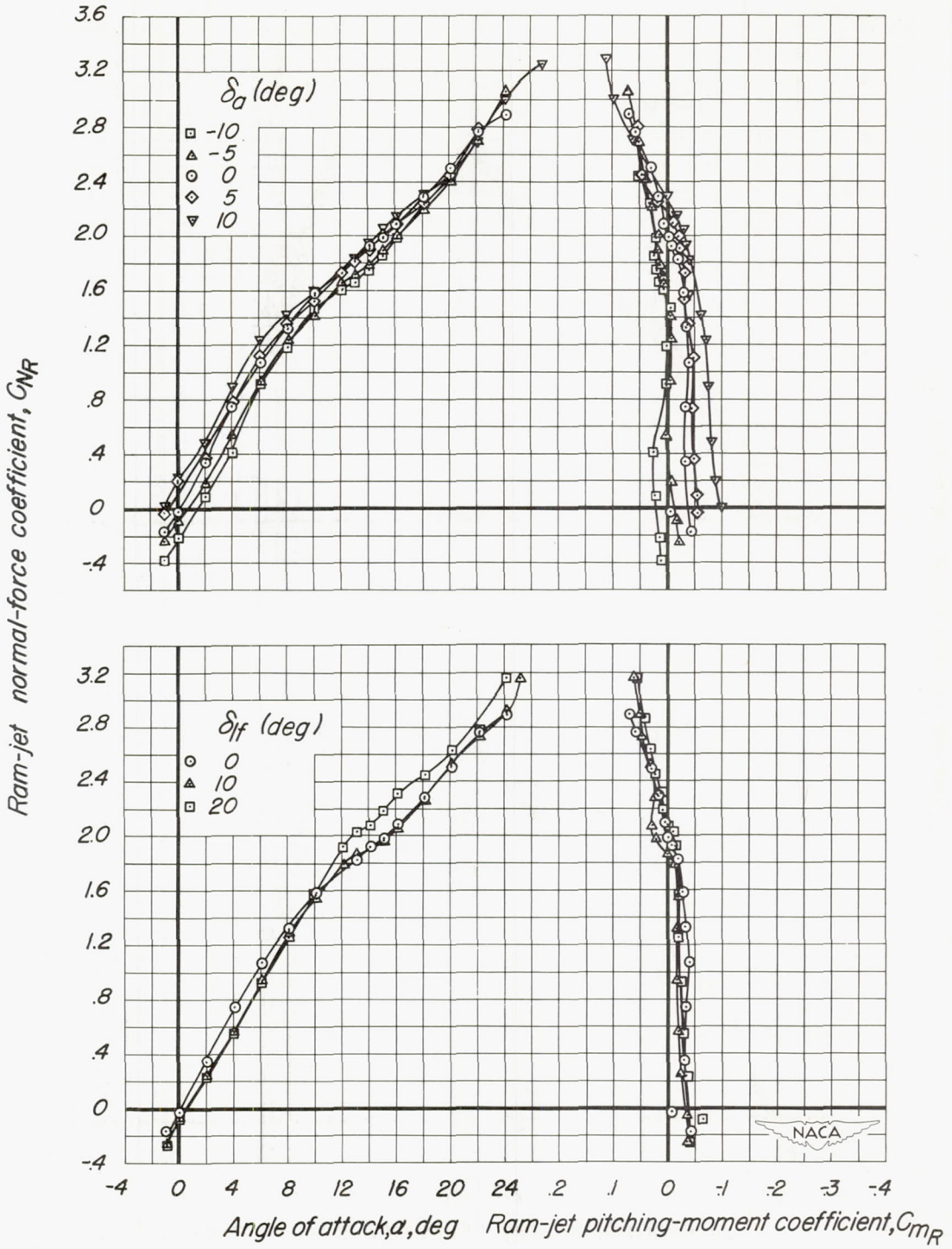

(b) Mach number, 0.60.

Figure 25.– Continued.

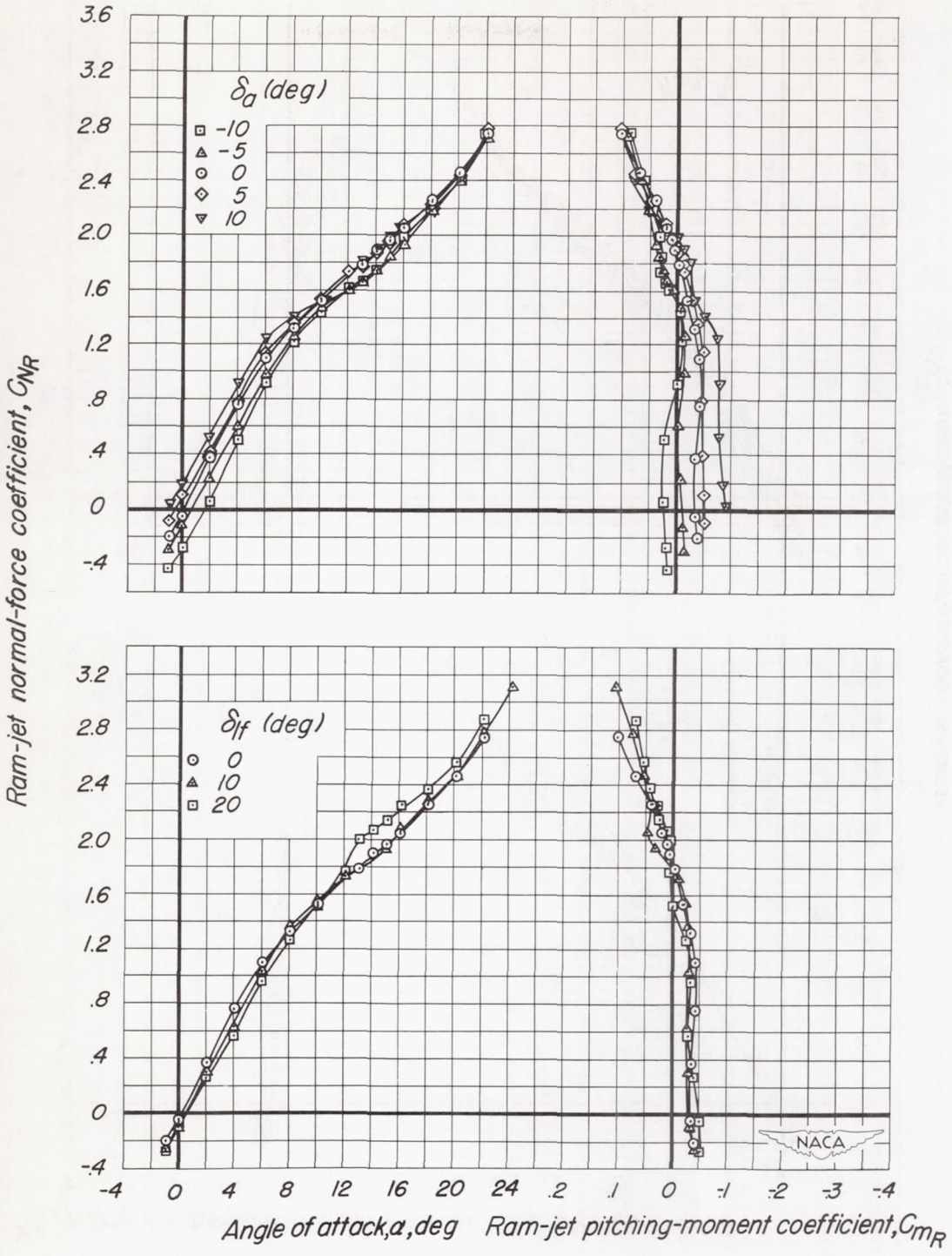

(c) Mach number, 0.70.

Figure 25.—Continued.

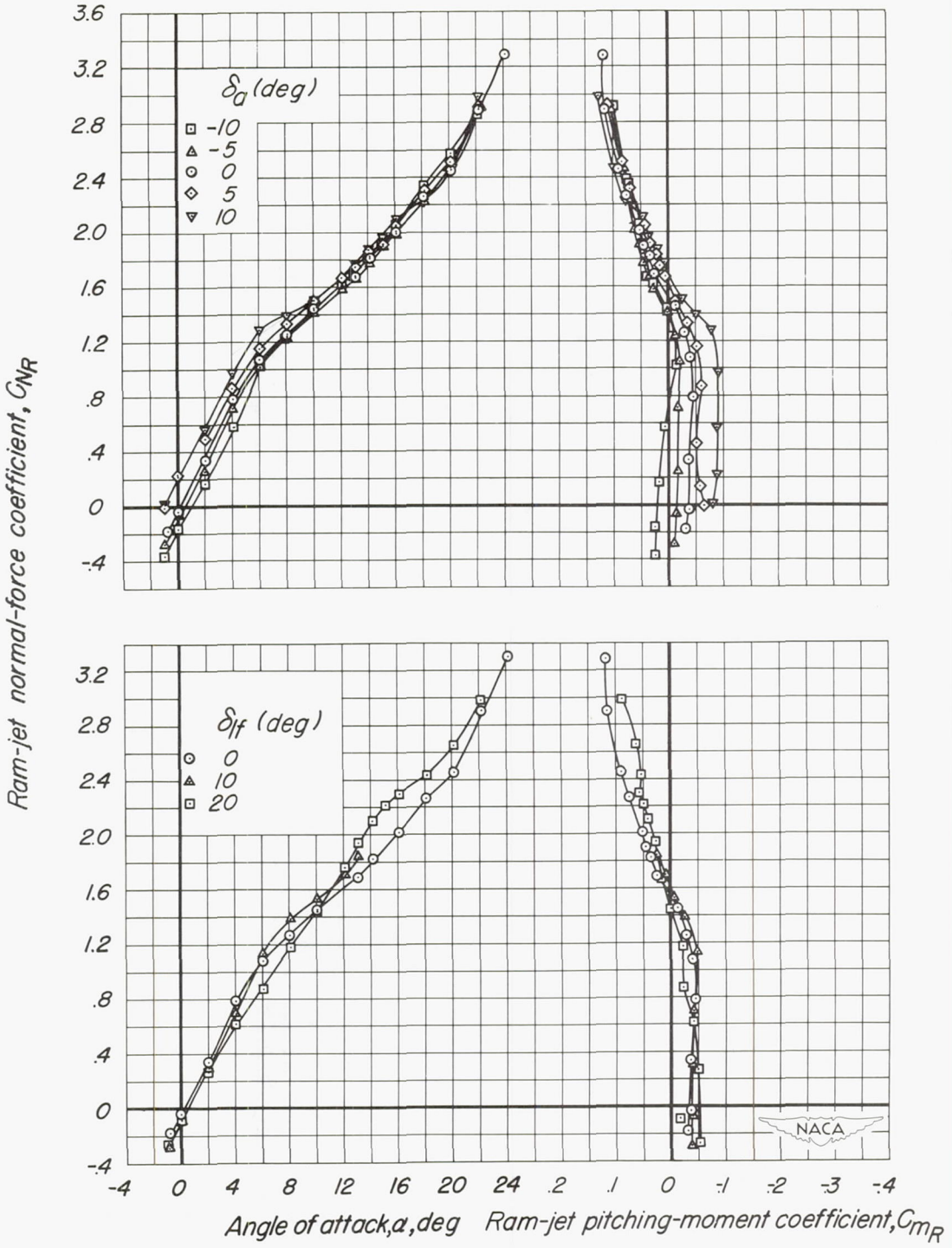

(d) Mach number, 0.80.

Figure 25.–Continued.

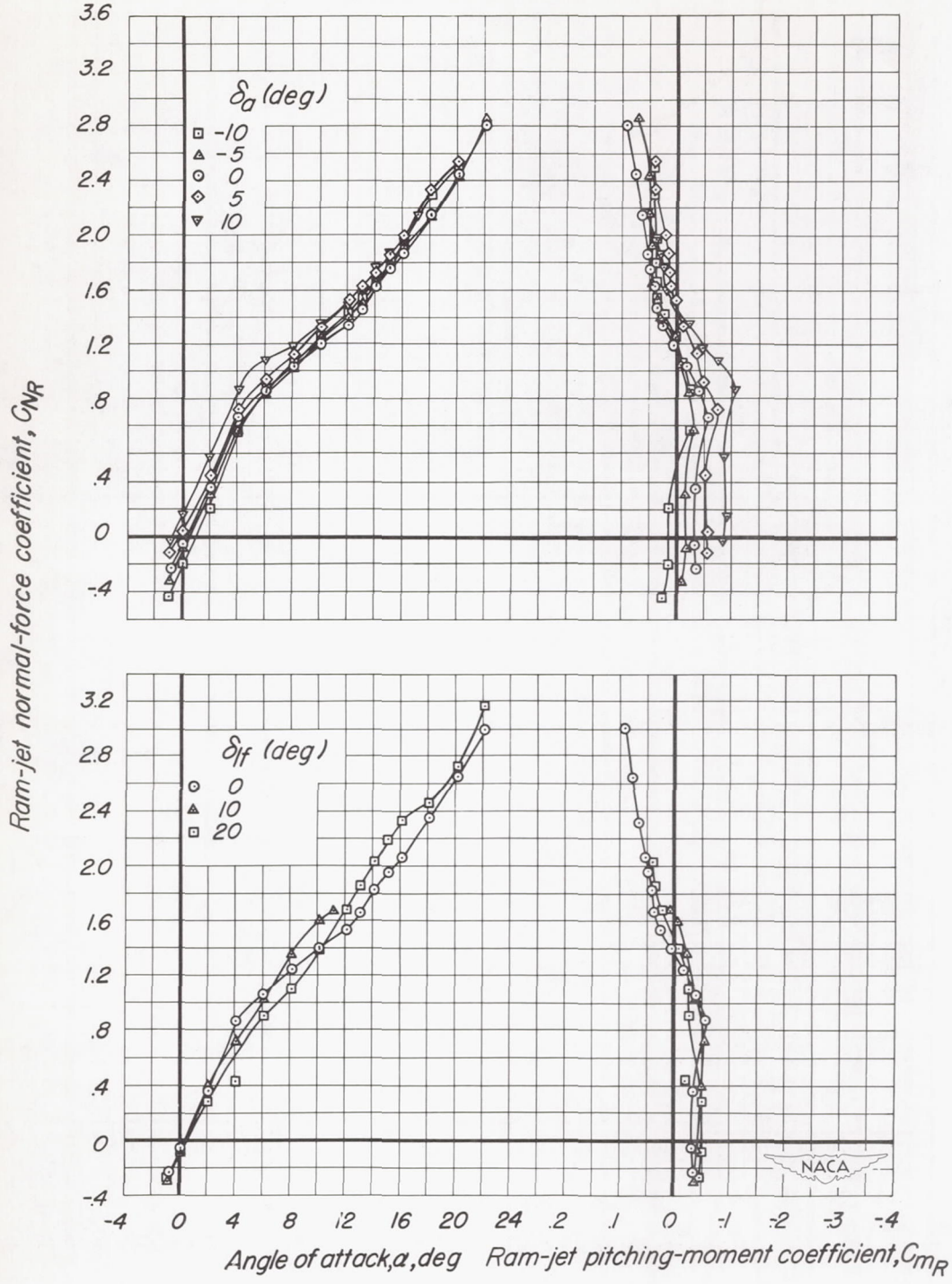

(e) Mach number, 0.85.

Figure 25.- Continued.

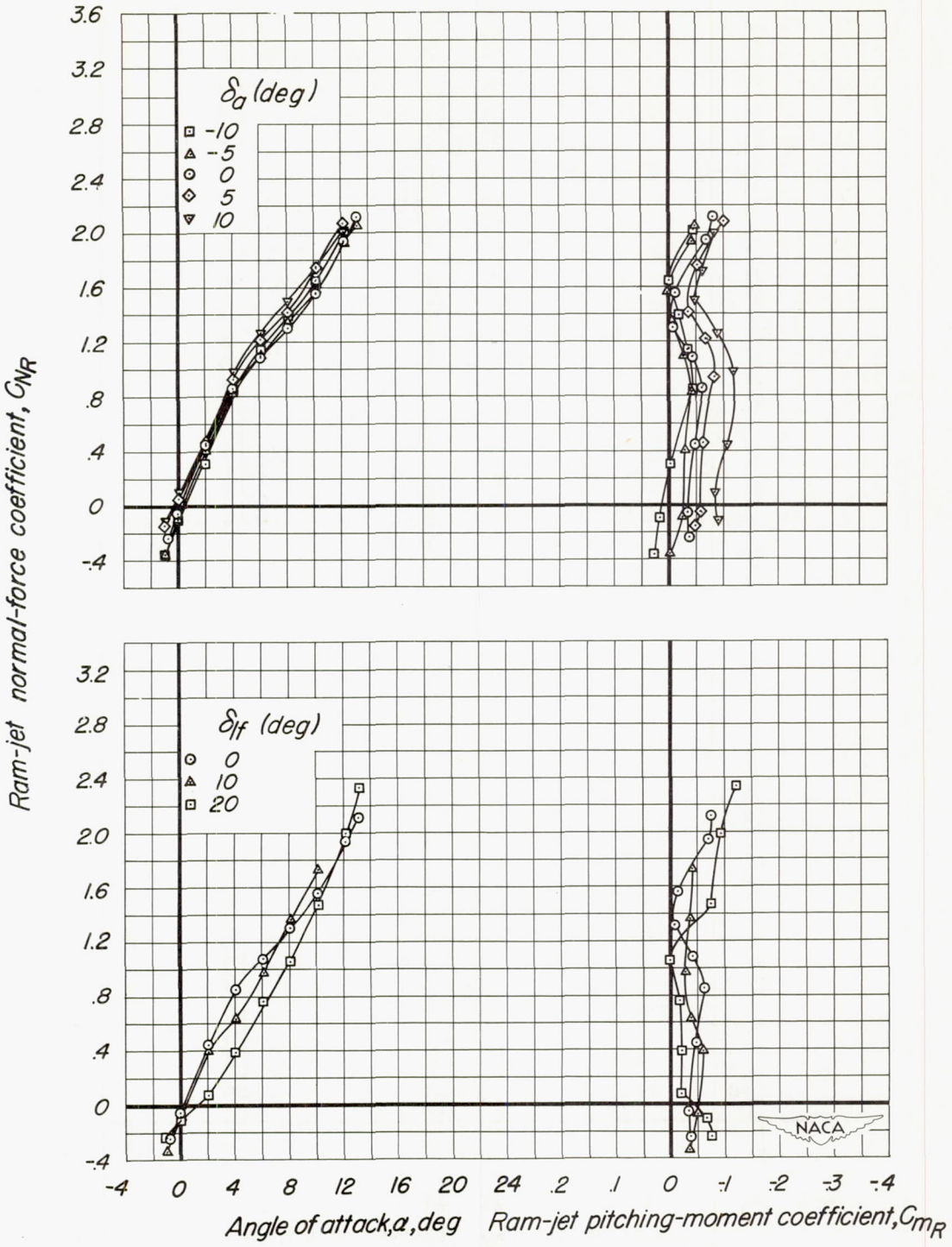

(f) Mach number, 0.90.

Figure 25.—Continued.

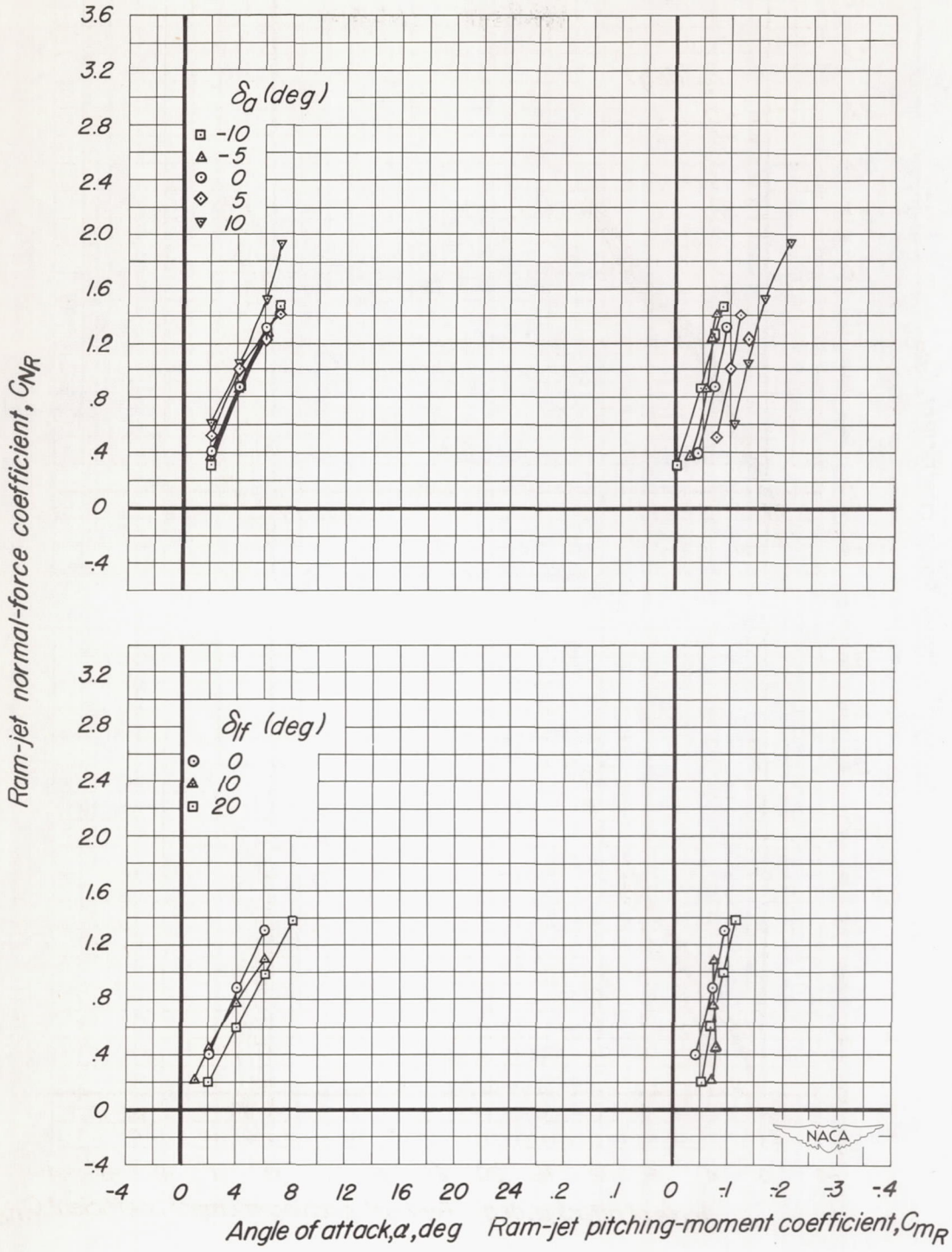

(g) Mach number, 0.925.

Figure 25.- Concluded.

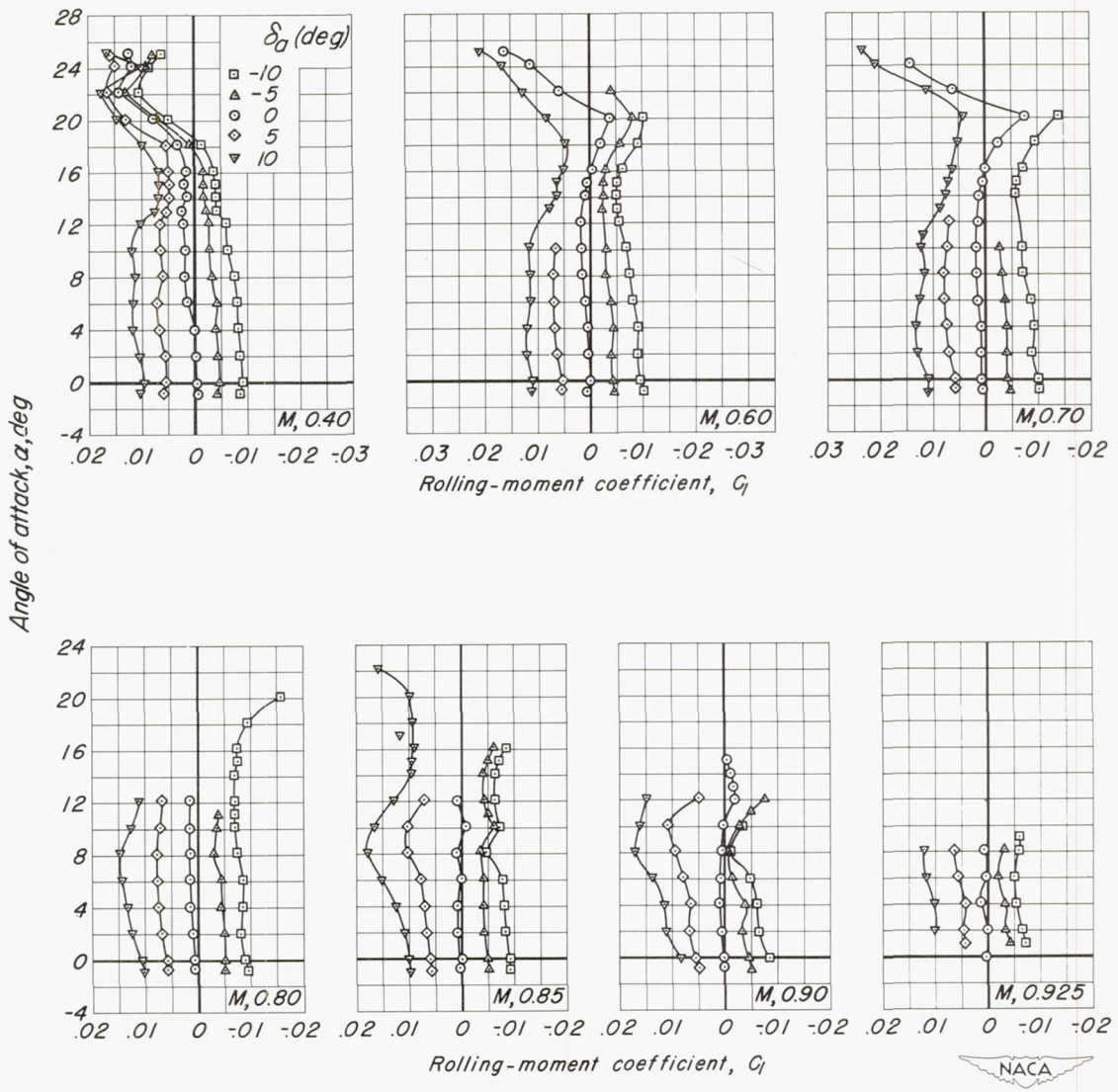

Figure 26.—The rolling-moment characteristics of the X-3 model. δ_{lf}, 0°; i_t, -2°

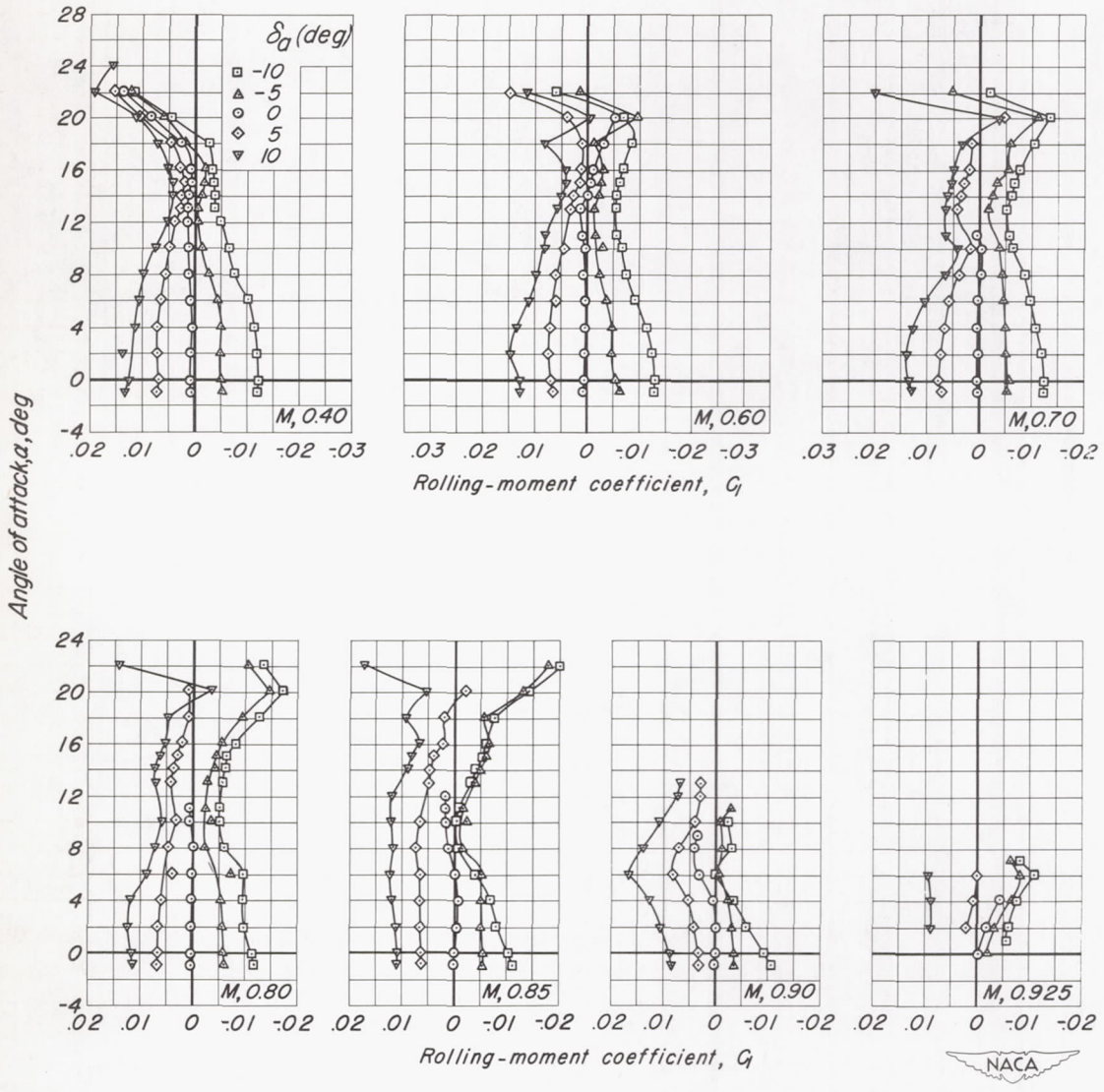

Figure 27.– The rolling-moment characteristics of the X-3 model with the wing-tip tanks. δ_{lf}, 0°; i_t, -2°.

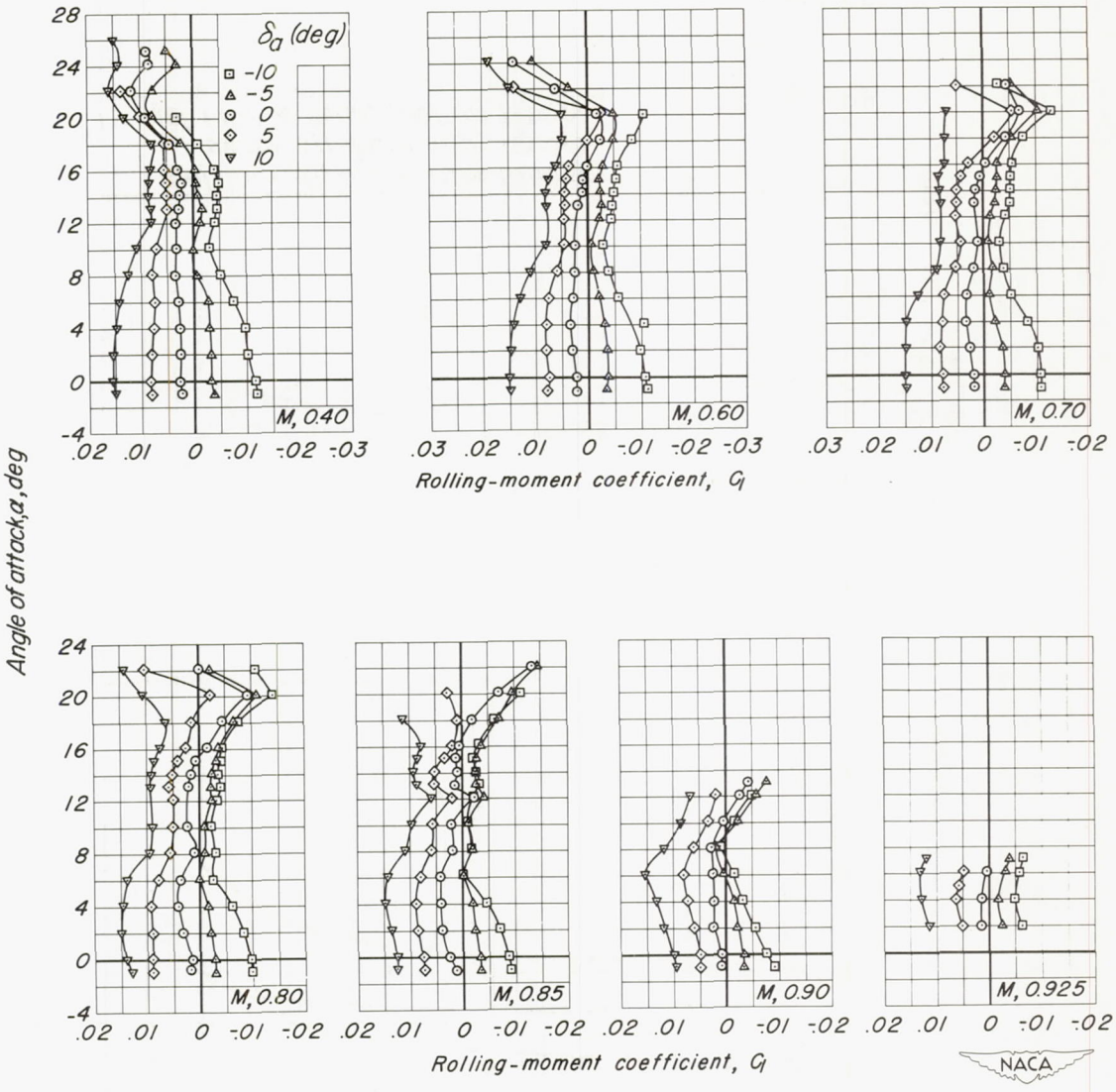

Figure 28.– The rolling-moment characteristics of the X-3 model with the wing-tip ram jets. δ_{lf}, 0°; i_t, -2°.

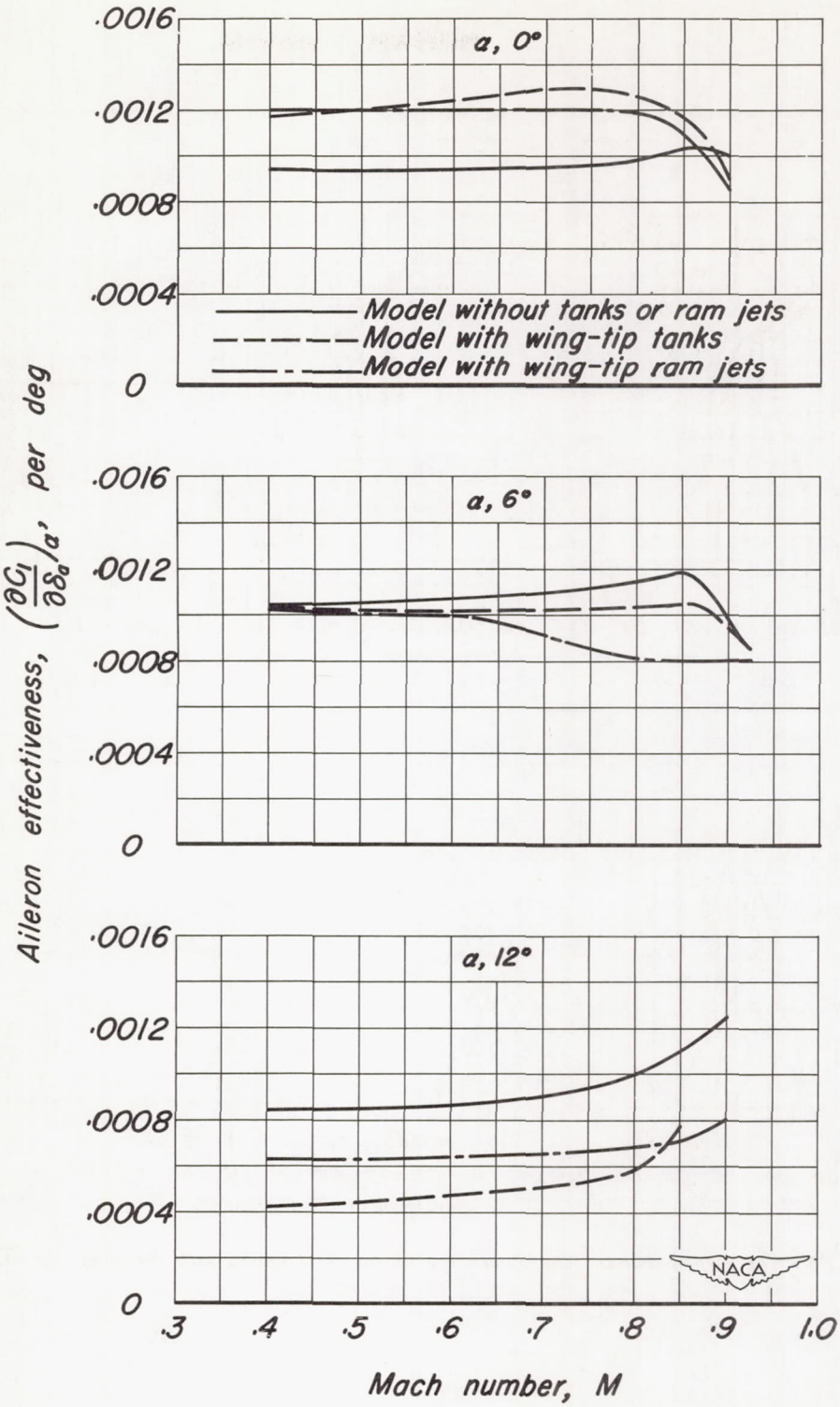

Figure 29.– The effectiveness of the left aileron on the X-3 model. δ_{lf}, 0°; i_t, -2°.

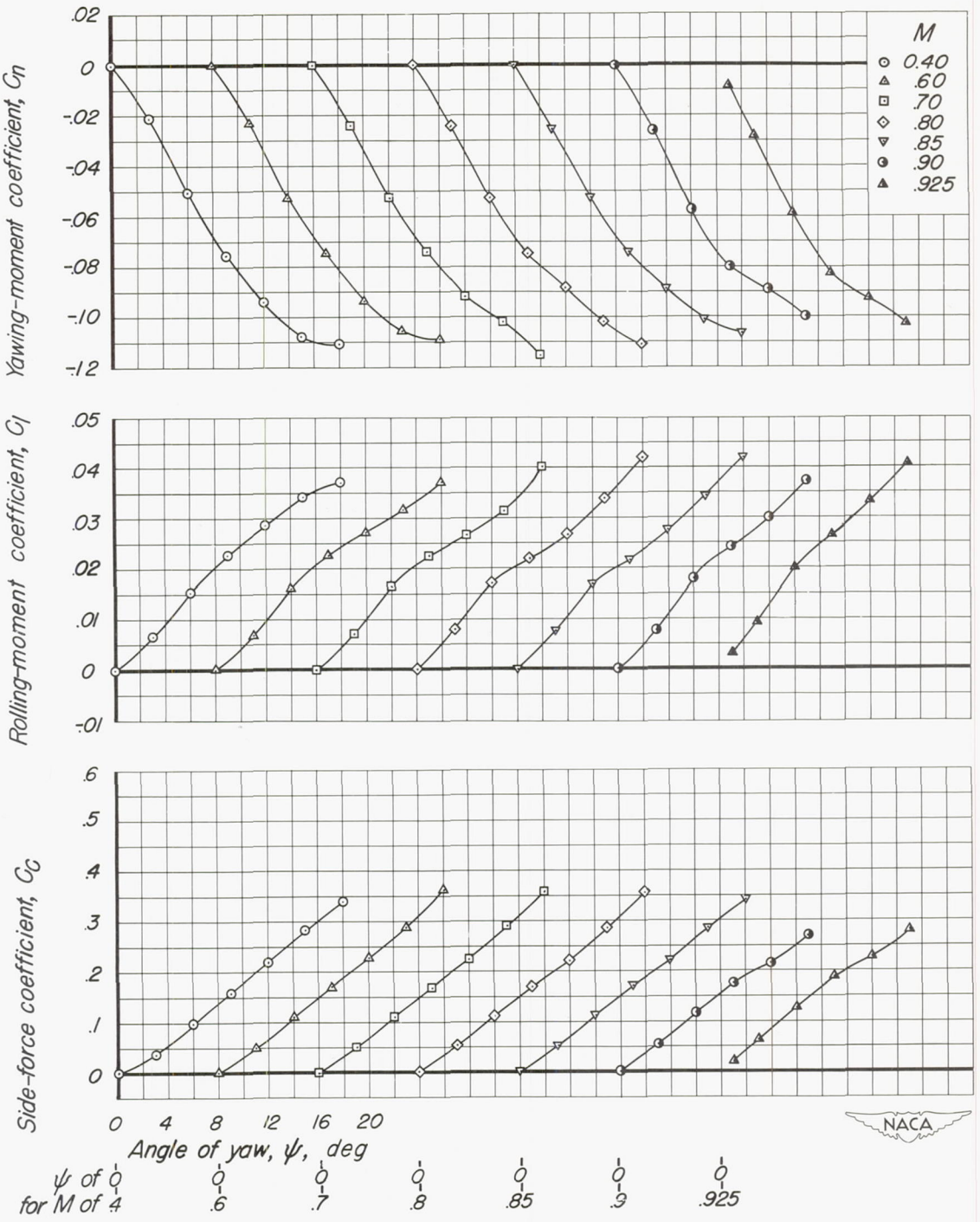

Figure 30.– The yawing-moment, rolling-moment, and side-force characteristics of the X-3 model with the underwing tanks. δ_{lf}, 0°; i_f, -2°; α, 0°.

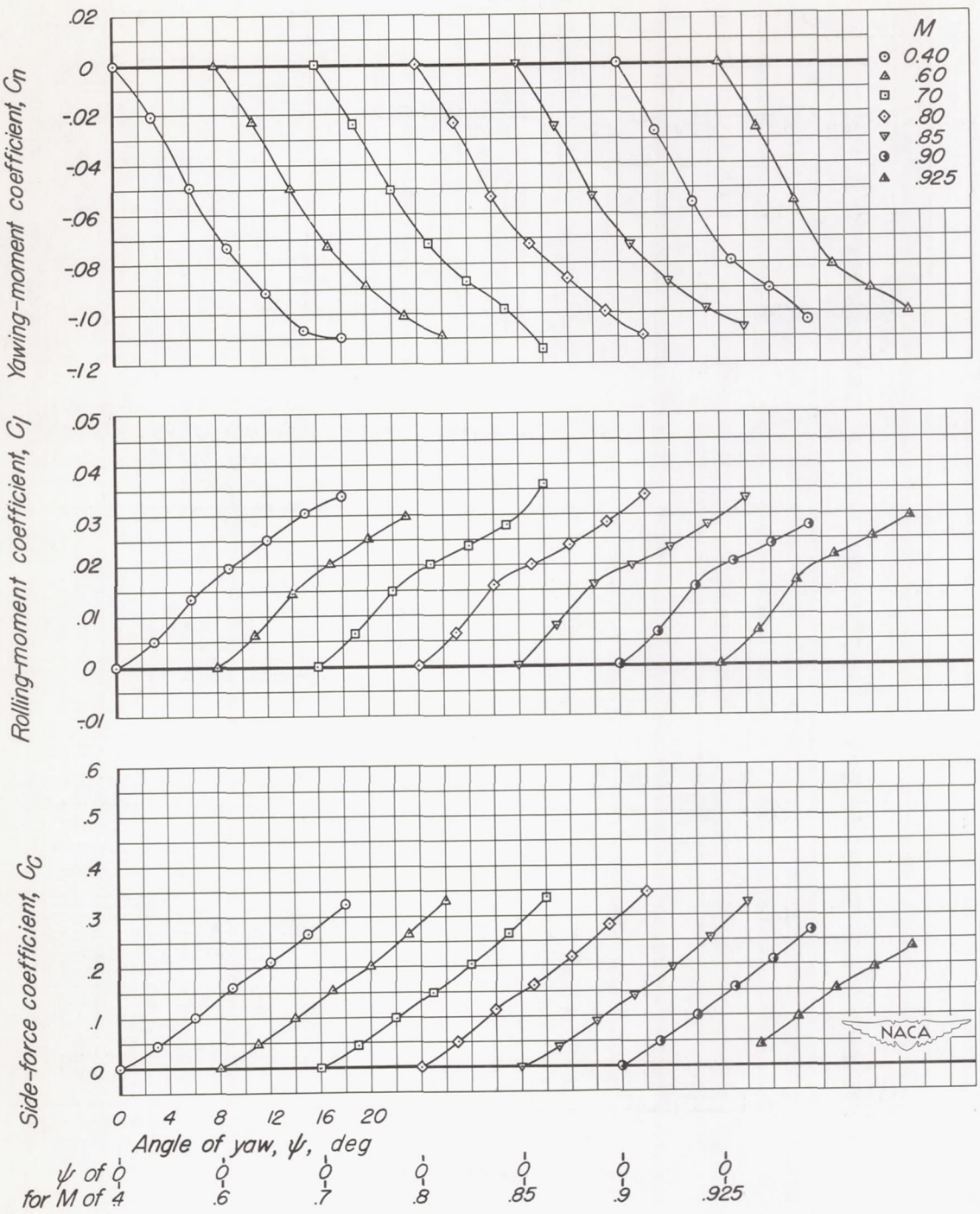

Figure 31.— The yawing-moment, rolling-moment, and side-force characteristics of the X-3 model with the wing-tip tanks. δ_{lf}, 0°; i_t, -2°; α, 0°.

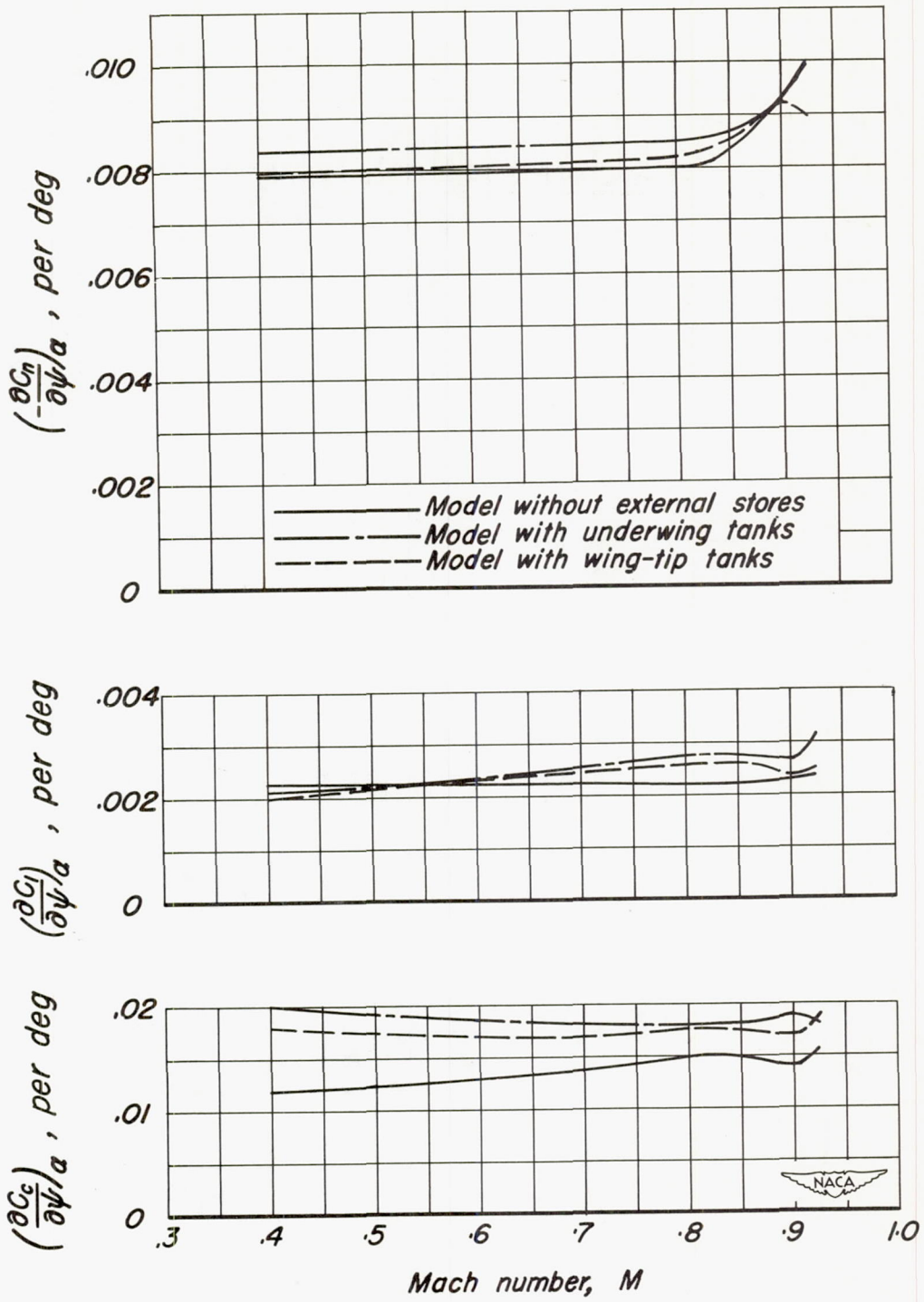

Figure 32.— The effect of external stores on the directional- and lateral-stability parameters and the side force due to yaw of the X-3 model.

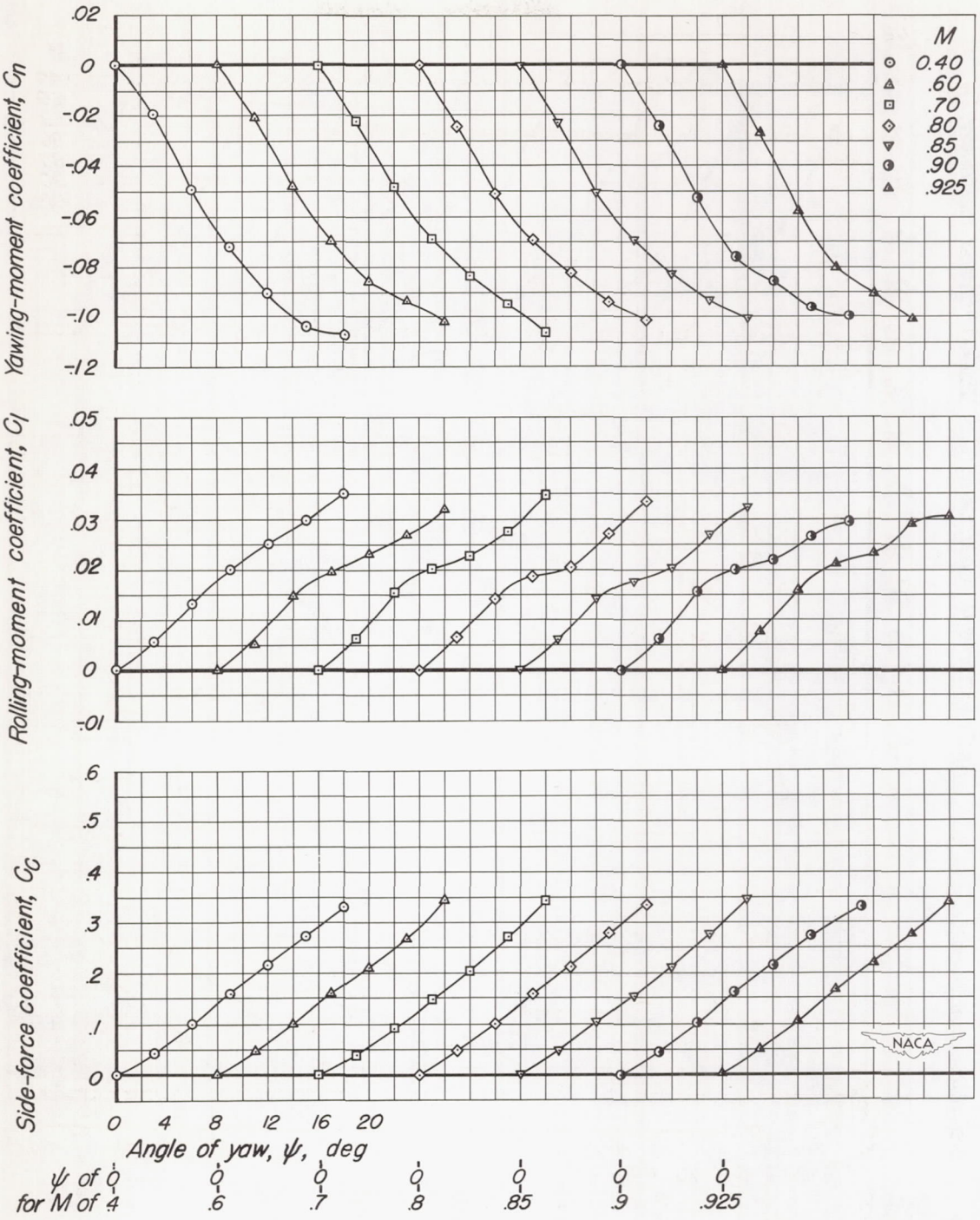

Figure 33.– The yawing-moment, rolling-moment, and side-force characteristics of the X-3 model with the wing-tip ram jets. δ_{lf}, 0°; i_t, 2°; α, 0°.

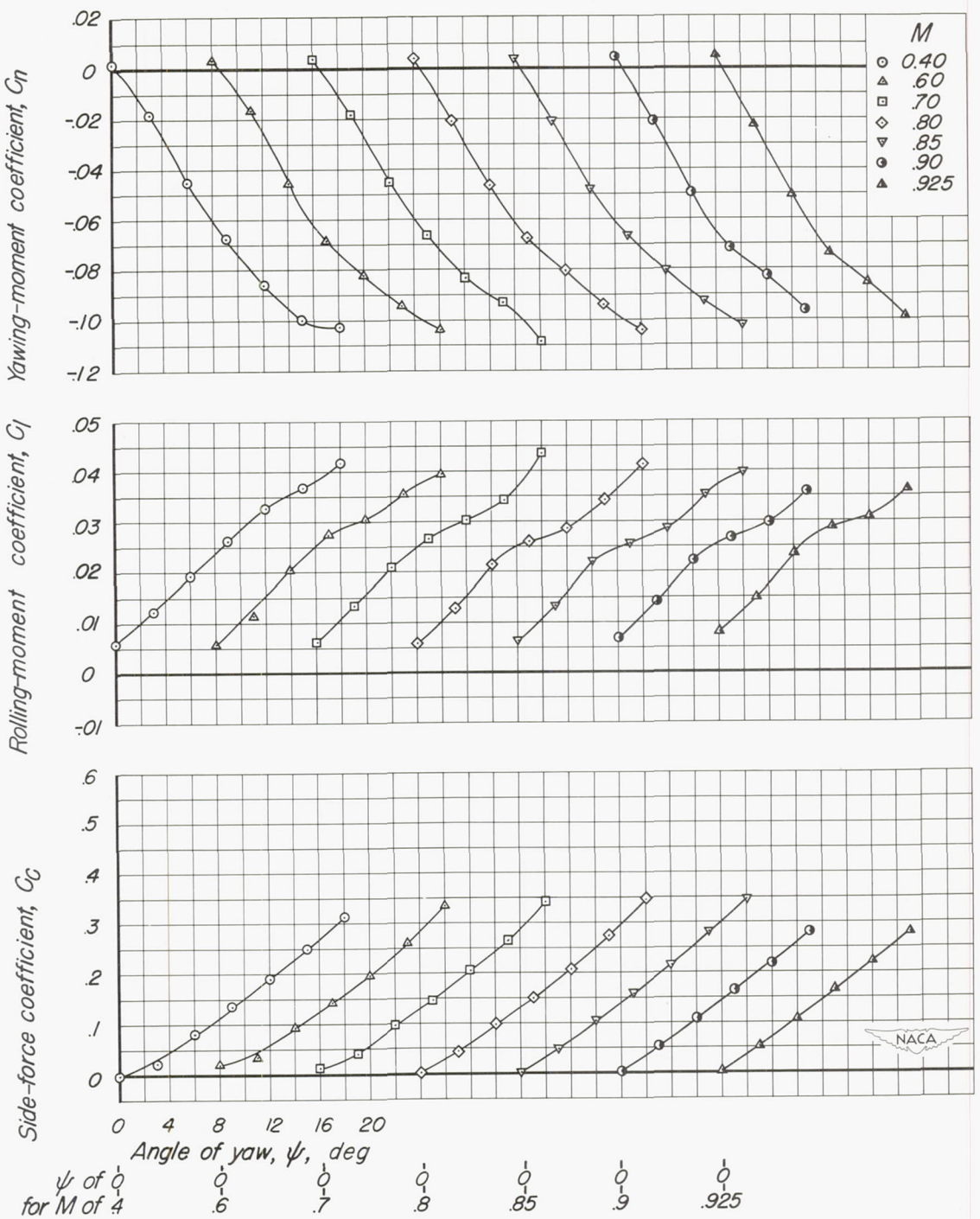

Figure 34.– The yawing-moment, rolling-moment, and side-force characteristics of the X-3 model with the right wing-tip ram jet. δ_{lf}, 0°; i_t, -2°; α, 0°.

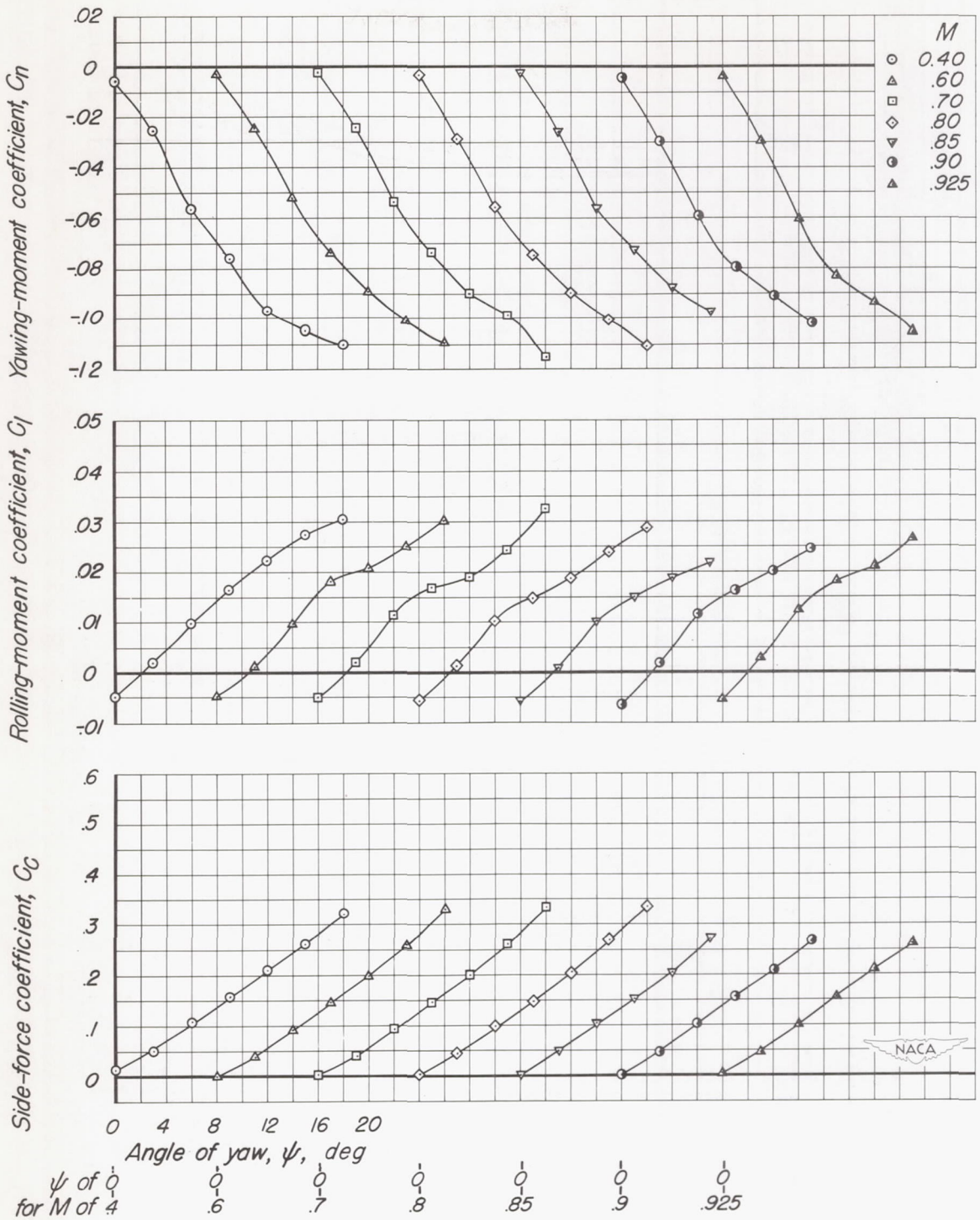

Figure 35.– The yawing-moment, rolling-moment, and side-force characteristics of the X-3 model with the left wing-tip ram jet. δ_{lf}, 0°; i_t, -2°; α, 0°.

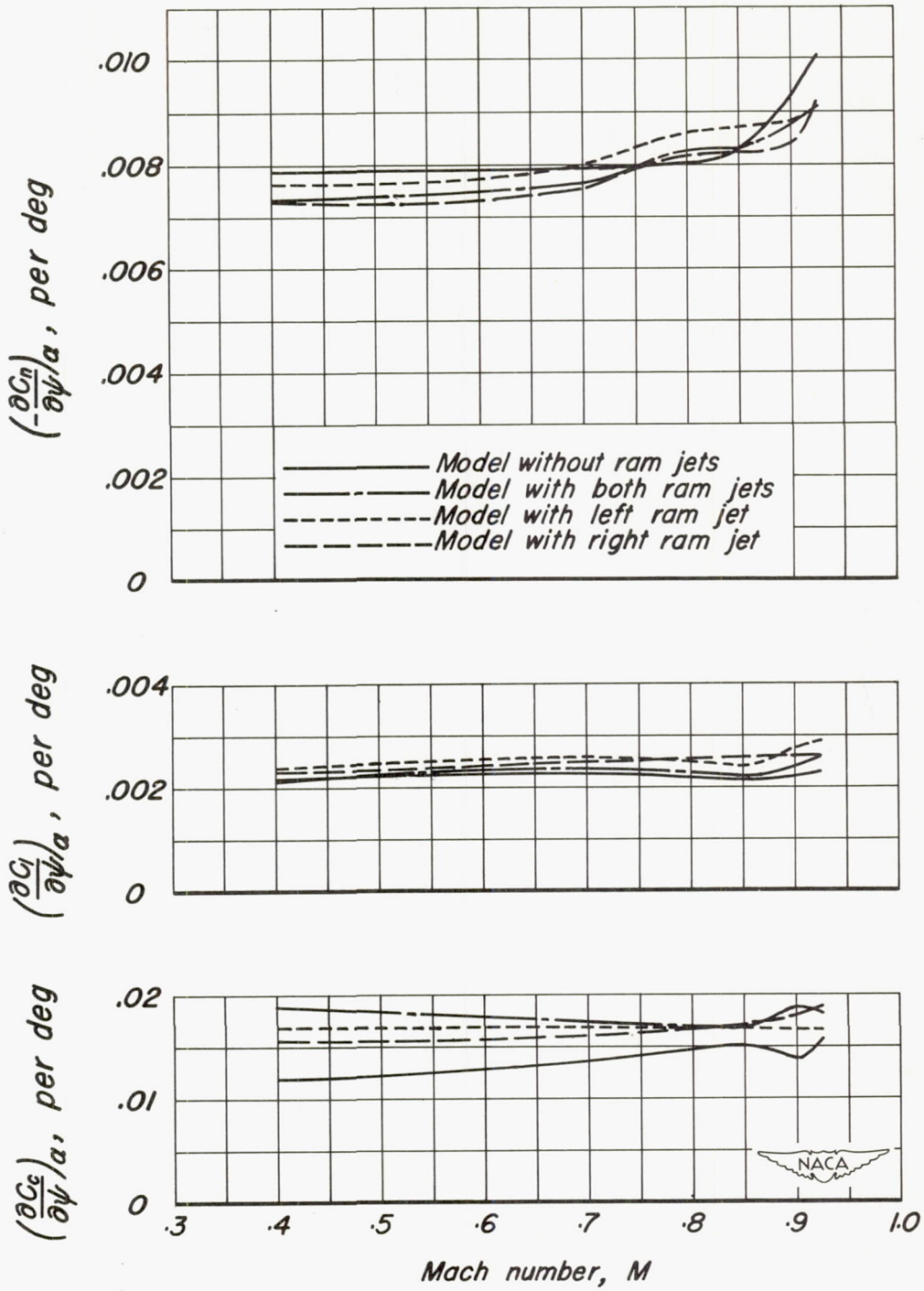

Figure 36.— The effect of the ram jets on the directional- and lateral-stability parameters of the X-3 model. δ_{lf}, 0°; i_t, -2°.